X-661-72-152

PREPRINT

NASA TM X- 65903

A STUDY OF 2-20 keV X-RAYS FROM THE CYGNUS REGION

RICHARD D. BLEACH

JUNE 1972

GSFC — GODDARD SPACE FLIGHT CENTER

GREENBELT, MARYLAND

A STUDY OF 2-20 KEV X-RAYS FROM THE CYGNUS REGION*

by
Richard David Bleach

Dissertation submitted to the Faculty of the Graduate School
of the University of Maryland in partial fulfillment
of the requirements for the degree of
Doctor of Philosophy
1972

*Supported in part by NASA Grant NGL 21-002-033

ABSTRACT

Two rocket-borne proportional counters each with 650 cm^2 net area and 1.8° x 7.1° FWHM rectangular mechanical collimation surveyed the Cygnus region in the 2-20 keV energy range on two separate occasions. X-ray spectral data gathered on September 21, 1970 from discrete sources in Cygnus are presented. The data from Cyg X-1, Cyg X-2, and Cyg X-3 have sufficient statistical significance to clearly indicate mutually exclusive spectral forms for the three. Upper limits are presented for x-ray intensities above 2 keV for Cyg X-4 and Cyg X-5 (Cygnus Loop).

A search was made on August 9, 1971 for a diffuse component of x-rays > 1.5 keV associated with an interarm region of the galaxy at galactic longitudes in the vicinity of 60 degrees. A statistically significant excess associated with a narrow disk component was detected. The angular extent of this component has a most probable value of 2 degrees and may be as large as 7 degrees at 90% confidence. The best fit spectrum yields an intensity of 2.9 photons $(cm^2\text{-sec-ster})^{-1}$ over the 2 - 10 keV range. The 3σ upper limit to any emission (e.g. iron line) in a 1.5 keV band centered at 7 keV from galactic latitudes $|b| \leq 3.5$ degrees is .3 photons $(cm^2\text{-sec-ster})^{-1}$. Several possible emission models are discussed, with the most likely candidate being a population of unresolvable low luminosity discrete sources.

ACKNOWLEDGMENTS

I wish to thank Dr. Frank B. McDonald, my thesis advisor, for giving me the opportunity and necessary support to conduct this research at Goddard Space Flight Center as well as Dr. Howard Laster, Chairman of the Department of Physics and Astronomy at the University of Maryland, who approved this research position.

I am most indebted to Dr. Elihu Boldt who has consistently and patiently directed the course of my thesis and my graduate studies in astrophysics. Special thanks go to Dr. Stephen Holt and Dr. Peter Serlemitsos for their assistance in planning and constructing the experiments and interpreting the data. I am grateful to Dr. Reuven Ramaty for interesting and helpful discussions.

Messrs. F. Birsa, C. Glasser, and M. Ziegler have provided invaluable technical support leading to the success of the experiments. I also thank the sounding rocket group at Goddard Space Flight Center and the launch crew at White Sands Missile Range for their cooperation. S. Brown and D. Arbogast have given generous assistance in preparing the accelerator experiments used to calibrate the detectors.

I thank Messrs. A. Thompson, H. Trexel, and F. Shaffer for their drafting skills and P. Resch for painstakingly typing this manuscript with the aid of N. Stevenson, R. Ramberg and B. Shavatt.

Finally, I would like to thank my wife, Gail, for helping to make this goal possible.

TABLE OF CONTENTS

LIST OF TABLES

FIGURE CAPTIONS

Figure Page

CHAPTER I

INTRODUCTION

A. General

For nearly a decade the photon energy range from 1 to about 500 keV has been detected from celestial sources situated outside the solar system. Many of the discrete sources are concentrated near the plane of our galaxy, while an isotropic diffuse component of x-ray radiation appears to cover the entire sky.

The relationship of discrete x-ray sources to other stellar objects is still a question that remains to be resolved. The apparent increase in the number of such objects near the galactic plane suggests that galactic sources such as supernovae remnants, old novae, high temperature stars, pulsars, and binary systems are likely candidates. While some x-ray sources are known to be supernovae remnants (e.g. the Crab Nebula) and others binary systems (e.g. Cygnus X-2), it is possible that x-ray objects represent a peculiar variety of any of the objects mentioned. Recently, pulsars such as the one observed in the core of the Crab Nebula (which emits pulses of radiation in the radio through x-ray band at intervals of about 33 milliseconds) have aroused interest in compact objects called neutron stars, which could be responsible for the observed pulsations. Neutron stars are composed mainly of neutron-rich nuclear matter, have small radii ($\sim$ 10 km), have high density ($\sim 10^{15}$ gm/cm^3), and can have huge magnetic fields ($\sim 10^{14}$ gauss) capable of accelerating particles to relativistic velocities. With the continual discovery of

new pulsars, unique objects have been found. The discrete x-ray source Cygnus X-1 has been observed (Oda et al., 1971; Holt et al., 1971) to be pulsating at irregular intervals with periods ranging from about 73 milliseconds to several seconds. In addition, no known supernova remnant surrounds it. Whether this object is a neutron star or an even further collapsed stage called a "black hole" (an object making its presence known only by its gravitational field) is a question requiring theoretical breakthroughs in particle physics as well as further spectral observations.

The diffuse isotropic background seen by all celestial x-ray experiments is perhaps of even more cosmological significance than the understanding of discrete sources. In both cases the same high-energy process may be involved; however, it is quite likely that the photons comprising the universal 2.7°K blackbody radiation originated with the birth of our universe some 10^{10} years ago and are seen today as x-rays after being inverse Compton scattered by extragalactic electrons.

Our own galaxy, the Milky Way, is a convenient local laboratory for investigating high energy processes referred to above, and at x-ray wavelengths (< 10 Å) most of the galaxy can be probed. Emission from hot plasmas on the order of 10^7 °K including thermal bremsstrahlung, recombination, and line radiation can be studied in discrete sources. The search for diffuse x-ray emission from processes such as inverse Compton and synchrotron radiation involving ultrarelativistic electrons provides information on the distribution of these particles in the galaxy. Non-thermal bremsstrahlung involving suprathermal charged particle collisions with ambient electrons is a mechanism which heats up the interstellar medium. For protons with kinetic energies on the

order of tens of MeV, comparison of x-ray emission with calculated and observed ionization rates sets limits on the particle population. The spectra of these mechanisms as well as their temporal variations at photon energies exceeding a few keV allows direct observation of some of the most powerful energies sources known, and in conjunction with measurements from other parts of the electromagnetic spectrum, x-rays can be a useful tool in studying the structure of our galaxy and universe.

B. Purpose

Since 1962, at least five discrete x-ray sources have been located in the Cygnus-Orion spiral arm of our galaxy. These sources have been observed on an irregular basis since 1962 from both rocket, balloon, and satellite experiments and have displayed a variety of intensities and spectral shapes as a group as well as individually. The first part of this thesis is devoted to a study of these discrete objects in the energy range 2 - 20 keV, placing the emphasis on model fits to the spectra of sources observed in a rocket flight launched September 21, 1970.

Between galactic longitudes 45^{o} - 70^{o} and at galactic latitude 0^{o} there was a lack of any discrete sources above a sensitivity of .02 photons $(cm^2\text{-sec})^{-1}$ at energies greater than 2 keV based on 3σ background statistics from the data of the 1970 flight. Investigations by Kerr and Westerhout (1965), using radio observations of the hyperfine transition line in neutral hydrogen at 21 cm, have shown the region of galactic longitude $45^{o} \leq \ell \leq 70^{o}$ to be an interarm region of our galaxy. Since then, Shane and Bieger-Smith (1966) using 21 cm data found neutral

hydrogen with radial velocities larger than expected from galactic rotation at $\ell = 63.0^{o}$ and $b = 0^{o}$. Katgert (1968) has identified this excess with a local neutral hydrogen ring structure 4^{o} in diameter centered at $\ell = 61.5^{o}$ and $b = -0.3^{o}$. This interarm region provides the motive for the second part of this thesis which concerns itself with the detection of a diffuse galactic component in the x-ray range above 2 keV. Several theories are investigated as an explanation for such an excess.

C. Previous Discrete Source Observations

On June 18, 1962 the first celestial x-rays were observed from rocket-borne Geiger counters flown by Giacconi et al. (1962). Subsequent rocket flights by the same group in October of 1962 and June of 1963 indicated that the source of some of the celestial x-rays was in the Cygnus constellation. Bowyer, Byram, Chubb, and Friedman (1965) reported seeing two x-ray sources in the Cygnus region in June and November of 1964 which were later identified as Cygnus XR-1 and Cygnus XR-2. In the same year, Fisher, et al. (1966) saw a single source in the Cygnus constellation. Rocket flights by the Naval Research Laboratory in 1965 and 1966 revealed a total of four Cygnus sources as well as a fourfold change in intensity in the Cygnus XR-1 spectrum below 10 keV as reported by Byram, Chubb, and Friedman (1966). Since then, variability in the intensity of Cygnus XR-1 has been verified by a number of observers whose results extend over 1 - 300 keV energy range. A comprehensive survey of this variability has been compiled by Dolan (1970) who finds that above 20 keV a period of almost 3 days between the maxima in intensity is the best result obtainable with inconclusive statistics. Below 20 keV

the only good evidence for variability that existed up to now were the N.R.L. results mentioned above.

The UHURU x-ray satellite launched in December of 1970 has recently observed Cygnus X-1 in the 2 - 20 keV range with surprising results. Not only does the object appear to have short term variations in strength on the order of tens to hundreds of milliseconds (Oda et al. (1971) as confirmed by Holt et al. (1971), but its intensity as well as spectral shape have changed over longer periods of observation by UHURU.

In October 1966, A.S.E. launched a rocket containing proportional counters sensitive to the energy range 2 - 20 keV and obtained results concerning three sources in the Cygnus region. Their energy resolution was sufficient enough (21% at 5.9 keV) to discriminate between acceptable spectral shapes more accurately than previous data permitted. Acceptable fits for both power law and exponential functions for Cygnus X-1, Cygnus X-2, and Cygnus X-3 were found as well as limits on the amount of low energy x-ray absorption by interstellar matter. When extrapolated to higher energies these results are found to be compatible with the balloon results of Haymes (1968) and Peterson (1968) for Cygnus X-1 and Rocchia et al. (1969) for Cygnus X-3. In 1967, Giacconi et al. (1967a) proposed an optical identification of Cygnus X-2 which is believed to be a binary system, one component being a G type subdwarf. In September 1967, N.R.L. was also able to obtain an exponential fit to the Cygnus XR-2 spectra in the 1.5 - 13 keV range. This fit, however, produced a temperature larger than the limit given by Gorenstein et al. (1967).

The Cygnus Loop or Veil Nebula is believed to be a supernova remnant which exploded about 10^4 years ago and has been observed both

optically by Parker (1967) and in the radio band by Minkowski (1968). The latter measurement shows the source to have an apparent angular diameter of about 3°. Recently, x-ray surveys of this object were made by Grader et al. (1970) and Gorenstein et al. (1971) which indicate that it is the same as the source Vul XR-1 observed by N.R.L. in 1964-65. The Grader experiment covered an energy range from .2 to 10 keV while the Gorenstein result was sensitive from .16 to 1.2 keV. Both flights saw results only in the energy range less than 1.5 keV, and both sets of data could be fitted with exponential models. A power law also gave an acceptable fit to the Grader results. In addition, Gorenstein et al. (1971) has shown evidence that line emission from O VIII was present at .65 keV which favors the exponential model. The source size in x-rays from the Gorenstein result appears to be approximately the same as the optical and radio diameters and of uniform intensity.

D. Previous Diffuse Galactic Source Observations

In June 1968, Cooke et al. (1969) launched a rocket experiment which surveyed the galactic plane in the region $\ell = 220^{\circ} - 350^{\circ}$. Their initial results indicated an excess of x-rays coming from the galactic plane in the 1.4 - 18 keV energy range as compared with the all sky background in the same energy range. This excess varied with galactic longitude ranging from a minimum of 0.3 photons cm^{-2} sec^{-1} rad^{-1} near galactic longitude 220° to a maximum of about 3 times this value at galactic longitude 350°. A subsequent flight in April 1969 covering approximately the same region of the sky revealed that up to 90% of the excess in the region $\ell > 290^{\circ}$ could be explained by contributions from known discrete sources in Centaurus. At smaller galactic longitudes

observed by Cooke (1971) the x-ray source associated with the Gum Nebula remnant could account for the observed excess as outlined by Ramaty et al. (1971).

The OSO III satellite yielded data from which Schwartz (1969) obtained spectral information for the diffuse galactic component. This measurement shows that an excess was observed only in the 7.7 - 12.5 keV range using data from galactic longitudes ℓ = 120° - 160° and ℓ = 220° - 240°. The latter range of longitudes contains portions of the Gum Nebula while the former range contains several possible supernovae remnants.

Recently Bunner et al. (1971), Hayakawa et al. (1970), and Shukla et al. (1971) have made measurements of the soft diffuse x-ray component at energies less than 1 keV which include observations of the galactic plane. These data show an excess above the extragalactic background at energies less than 300 eV where local phenomena unfortunately are difficult to account for when extracting the true galactic intensity. It is interesting to note, however, that the 1969 Bunner flight showed no excess in the energy range 500 to 1000 eV.

Other observations of the galactic plane at energies greater than 20 keV have been obtained by Vette et al. (1970), Clark et al. (1968), and Bleeker and Deerenberg (1970) which place upper limits as well as a 100 MeV data point on the galactic x-ray and γ-ray intensity.

E. Discrete Source Theories

The transformation of the basic processes which produce x-rays into a discrete source model poses a difficult problem given the data now available. For this reason current models are probably representative of an ideal situation rather than a real one. At the same time, however,

it is instructive to fit observed spectra with idealized models because certain processes may dominate in an x-ray source.

The two general classes into which x-ray sources can be grouped are (1) thermal emitters and (2) non-thermal emitters. In the former class, the source is composed of particles which exist in equilibrium states along with photons which may or may not have a black-body distribution while the latter class includes all non-equilibrium processes.

1. Thermal sources. Thermal objects emitting x-rays are thought to be hot plasmas with temperatures on the order of 10^7 ^oK. Depending on the optical thickness of such a source the object may be characterized as a black-body, "optically thick", or "optically thin" source.

The blackbody source has infinite optical thickness (i.e. photons and particles have reached energy equilibrium) the differential energy spectrum assuming no interstellar absorption is given by:

$$I_\nu = \frac{2\,h\nu^3}{c^2}\,[\exp(h\nu/kT) - 1]^{-1} \quad \frac{\text{ergs}}{\text{cm}^2\text{-sec-ster-Hz}} \qquad (1)$$

where

h = Planck constant

ν = photon frequency

k = Boltzmann constant

T = temperature of source in ^oK

The emission from such a source peaks at an energy $h\nu \approx 2.8$ kT.

An "optically thick" source has a finite optical depth and photons can be electron-scattered, free-free absorbed, and photoelectrically absorbed after they are emitted. For a given temperature, the continuum

of an "optically thick" source is softer than that of a blackbody since photons escaping from an "optically thick" source have not been scattered as much in energy space. Figure 1 illustrates this effect for the three classes of thermal emitters mentioned above. Calculations by Loh and Garmire (1971) have shown a flattening of a given free-free emission spectra as well as line broadening and line intensity reduction as a result of electron scattering. Angel (1969) has also reported that the spectral line intensities of Kα iron emission are reduced by 90% for plasma densities on the order of $N_e \simeq 10^{16}$ and optical depths of 10 or more. The problem of radiation escaping from plasmas of different optical depths has also been treated by Felten and Rees (1972) who find that for optical thicknesses ranging from 2 - 200 there exists a transition region where the energy flux of the observed radiation becomes proportional to the photon energy. At lower energies the shape is the standard Raleigh-Jeans limit proportional to ν^2 while at larger energies the spectrum takes the shape of thermal bremsstrahlung emission.

In the case of an "optically thin" thermal source, the plasma is of low enough density so that radiation escapes without interaction in the source. The first models of such a source were made in connection with the solar corona by Elwert (1954) and Seaton (1964). These results were elaborated upon by Tucker (1966). Since then, cosmic abundances of heavy elements such as iron have been further studied by Goldberg (1960) and Nussbaumer and Swings (1970) from line emission in the sun's photosphere, by Bertsch et al. (1969) from cosmic rays, by Pottach (1968) from the solar corona, and by Urey (1967) from meteorites. The abundances of iron relative to hydrogen from the above results range from 4×10^{-6} to 5×10^{-5}. The ionization equilibria have also been recalculated by

Jordan (1970) for heavy elements such as iron. Appendix A shows a calculation of x-rays that are emitted from an "optically thin" plasma at temperatures greater than 20 x 10^6 ^oK which uses the above data to determine the continuum as well as iron line emission expected from such a model.

As a simple approximation to the Tucker model an exponential function with a constant Gaunt factor is often used to express the continuum radiation arising from the bremsstrahlung mechanism. This function gives the steepest spectra for a given temperature of all thermal models discussed, and thus provides an upper limit to a temperature for a thermal source model.

Since thermal spectra can vary in shape based, to a large extent, on optical depth, it is also important to consider constraints imposed by emission from other parts of the object's electromagnetic spectrum before forming models from x-ray data alone.

2. Non-thermal sources. The second class of discrete source models includes all processes where interacting particles, or photons, or electromagnetic fields are in non-equilibrium conditions. A review of some of the more important processes which can produce x-rays follows.

Synchrotron radiation

For a given source function of particles N (particles/erg-cm^2) (from here on only electrons are considered unless otherwise noted) and a magnetic field H, the total power emitted (I_ν) in a given direction from a source of small angular size is

$$I_\nu = \frac{\sqrt{3}\, e^3}{mc^2} \iint N(H \sin\theta)\, F\, dE\, dr \quad \frac{\text{ergs}}{\text{cm}^2\text{-sec-ster-Hz}} \qquad (2)$$

where I_ν is the energy flux emitted from the sum of the two polarization

modes, θ is the pitch angle of the electron with respect to the magnetic field, ν is the frequency of the emitted photon and

$$F = \nu/\nu_c \int_{\nu/\nu_c}^{\infty} K_{5/3}(\eta)d\eta \tag{3}$$

$$\nu_c = \frac{3e\ H \sin\theta}{4\ \pi\ mc} \left(\frac{E}{mc^2}\right)^2 \tag{4}$$

where

e = charge of an electron

m = mass of an electron

E = energy of the electron

c = speed of light

$K_{5/3}$ = modified Bessel function of order 5/3 and the integration dE is over energy and the integration dr is along the line of sight from the observer in the source.

For different electron distributions various spectral shapes arise. For example, if the electrons are monoenergetic and the magnetic field is uniform then equation (2) yields

$$I_{\nu_o} = \frac{\sqrt{3}\ e^3}{mc^2} (H \sin\theta)\ F \int N\ dr \quad \frac{\text{ergs}}{\text{cm}^2\text{-sec-ster}} \tag{5}$$

If a power law energy distribution of electrons of the form $N = K\ E^{-\Gamma}$ (particles/erg-cm^3) and a uniform magnetic field (in gauss) is used then:

$$I_\nu = \frac{e^3}{mc^2} \left(\frac{3e}{4\pi\ m^3\ c^5}\right)^{(\Gamma-1)/2} a(\Gamma) K R H^{(\Gamma+1)/2} (\nu)^{-(\Gamma-1)/2} \tag{6}$$

$$= 1.35 \times 10^{-22}\ a(\Gamma)\ K R H^{(\Gamma+1)/2} \left(\frac{6.26 \times 10^{18}}{\nu}\right)^{\frac{(\Gamma-1)}{2}}$$

where

R = extent of emission region in line of sight in cm.

$a(\Gamma)$ is of the order .1 for $1.5 \leq \Gamma \leq 5$,

which is a power law in photon energy with an index that can be expressed in terms of the index of the electron distribution.

Other spectral shapes which include breaks or knees can occur if the magnetic field is allowed to depend on position and the electron distribution is allowed to vary in time. Tucker (1966) has investigated some of these situations, and Manley and Olbert (1969) have obtained exponential shaped synchrotron spectra with the injection of monoenergetic electrons up to a certain energy followed by a sharp cutoff above that energy.

Inverse Compton scattering

For photon energies much less than 500 keV the Thompson scattering cross-section is applicable for photons scattered by high energy electrons. The power transferred to photons via this effect is

$$\frac{dE}{dt} \cong c\,\sigma_T\,\bar{n}_{ph}\,\overline{\Delta E} \qquad (7)$$

where

σ_T = Thompson scattering cross section

$\bar{n}_{ph}$ = average number of photons per unit volume

$\overline{\Delta E} = 4/3\,\bar{\epsilon}\,(E/mc^2)^2$ = mean energy transferred (8)

$\bar{\epsilon}$ = mean photon energy

E = incident electron energy

Equation 7 remains valid so long as $(E/mc^2)^2\,(\bar{\epsilon}/mc^2)^2 \leq .25$. For a 1 eV optical photon this corresponds to an electron energy of $E \approx 10^{11}$ eV.

The standard approach is to assume a blackbody distribution of photons in order to derive the differential photon energy spectrum. The average blackbody photon energy is $\bar{\epsilon} \approx \alpha kT$ where $\alpha \approx 2.7$, k = Boltzmann constant, and T = temperature. If a power law energy spectrum of electrons $N = KE^{-\Gamma}$ (particles/erg-cm^3) is used then

$$I_\nu \cong \iiint N \, dE \, dr \int \bar{n}_{ph} \, \overline{\Delta E} \, \sigma_T \, c \, dE \qquad (9)$$

The third integral in equation 9 may be evaluated if we make the approximation that the Thompson cross section becomes large only at the average energy of the blackbody photon distribution. Thus equation 9 becomes

$$I_\nu \cong 2/3 \, b(\Gamma) \, \sigma_T \rho \, (mc^2)^{1-\Gamma} \, (4/3 \, \alpha kT)^{(\Gamma-3)/2} \, KR(R\nu)^{-(\Gamma-1)/2} \qquad (10)$$

$$= 4.12 \times 10^{-47} \, (1.6 \times 10^{-3})^{-(\Gamma-1)/2} \, KR[10^{-2.962\Gamma} \, b(\Gamma)] T^{(\Gamma+5)/2} \, (h\nu)^{-(\Gamma-1)/2}$$

where

$b(\Gamma)$ is on the order of 1 for $1 \leq \Gamma \leq 3.5$

ρ = photon energy density

which is the same power law in photons as obtained with synchrotron radiation using the same initial power law electron energy distribution.

The ratio of the x-ray intensities from the Compton and synchrotron processes is found from equation 2 and 9. For a power law spectrum of particles,

$$\frac{I_\nu \text{ synch}}{I_\nu \text{ comp}} \cong 1.5 \, \frac{H^2}{8\pi \, \bar{n}_{ph} \, \alpha \, kT} \left(\frac{1.8 \times 10^4 \, T}{H} \right)^{3-\Gamma/2} \qquad (11)$$

where

H is in gauss

T is in ^oK.

Previous attempts by Gould (1965) to use equation 11 in order to explain x-rays arising from the same electron population have been unsuccessful.

Non-thermal Bremsstrahlung

For the case of cosmic ray collisions with unionized atoms, the interaction which produces practically all the radiation is the Coulomb interaction of the charged incident particle with the nuclei of the target atom. The atomic electrons, on the other hand, will absorb most of the energy lost by the incident particle so that with non-relativistic incident particles the collision losses dominate over the radiative losses as shown by equation 12.

$$\frac{\Delta E \text{ rad.}}{\Delta E \text{ coll.}} \cong \frac{4}{3\pi} \frac{(z_i^2 Z)}{137} \frac{m_i}{M} \beta^2 \frac{1}{\ell n(\beta q)} \qquad (12)$$

where z_i = charge on incident particle in units of electron charge

Z = charge on target particle in units of electron charge

m_i = mass of incident particle

M = mass of target particle

$\beta = \frac{v}{c}$; ratio of the velocity of incident particle to the velocity of light

β_q = ratio of the maximum to minimum impact parameter = $\frac{\gamma^2 M v^2}{\langle h\nu \rangle}$

for $v << c$ Equation 12 becomes small and radiation losses are negligible.

In the case of relativistic particles

$$\frac{\Delta E \text{ rad.}}{\Delta E \text{ coll.}} \cong \frac{4\gamma}{3\pi} \left(\frac{z_i^2 Z}{137}\right) \frac{M}{m_i} \frac{\ell n \left(\frac{\lambda 192 m_i}{Z^{1/3} M}\right)}{\ell n (\beta q)} \qquad (13)$$

where λ is a factor of the order of unity which expresses the range of impact parameters on this semiclassical expression and γ is the Lorentz factor. Heitler (1954) has made a determination of λ from detailed quantum mechanical calculations.

In the 2-20 keV x-ray band it is the non-relativistic incident particles which are of interest despite the small radiation yield because these particles radiate a greater percentage of their energy loss into the 2-20 keV photon range than higher energy particles. An approximate expression for the photon energy emitted in non-relativistic bremsstrahlung is

$\langle h\nu \rangle \simeq E/2$ where E is the incident particle's kinetic energy.

The quantum mechanical cross section for non-relativistic bremsstrahlung is given by Heitler (1954)

$$(h\nu)\sigma_b = \frac{16Z^2e^2}{3\hbar c}\left(\frac{z^2e^2}{m_i^2}\right)^2 \frac{1}{\beta^2} \ln\left[\frac{\left(\sqrt{E} + \sqrt{E-h\nu}\right)^2}{h\nu}\right] \qquad (14)$$

the energy loss rate is given by

$$\frac{d}{dh\nu}\left(\frac{dE}{dt}\right) = v\sigma_b \langle h\nu \rangle n \qquad (15)$$

where n = density of radiating particles

The radiation source function (q) is

$$(h\nu)q = \int \frac{d}{dh\nu}\left(\frac{dE}{dt}\right) \frac{dN}{dEdV} dE \quad \frac{ergs}{cm^3\text{-sec-erg}} \qquad (16)$$

where $\frac{dN}{dEdV} = \frac{particles}{erg\text{-}cm^3}$

using Eq. (14) and (15) in Eq. (16), we get

$$(h\nu)q = \frac{8 Z^2 z_i^4 e^6 n}{3 c^2 m_i} \int_{h\nu}^{\infty} \ln\left[\frac{\left(\sqrt{E} + \sqrt{E-h\nu}\right)^2}{h\nu}\right] \frac{\beta}{E} \frac{dN}{dEdV} dE \qquad (17)$$

If we let $J = \beta c \frac{dN}{dEdV} = AE^{-\Gamma}$ (particles/cm^2-sec-ster-erg) be a power law distribution in the measured flux[1] then equation (17) becomes

$$(h\nu)q = \frac{8}{3}\frac{Z^2 z_i^4 e^6 n}{c \quad m_i} f(\Gamma)\, A\, h\nu^{-\Gamma} \tag{18}$$

$$\text{where } f(\Gamma) = \int_0^1 X^{\Gamma-1} \ell n\left[\frac{1+\sqrt{1-X}}{\sqrt{X}}\right]^2 dx \tag{19}$$

$$\text{and } X = \frac{h\nu}{E} \tag{20}$$

for $0.5 < \Gamma < 5$

$$f(\Gamma) \approx \Gamma^{-1.6}$$

It is necessary to emphasize that all the mechanisms listed above involve only steady state homogeneous conditions. No provision has been included for the time evolution of particle distributions, plasma effects, anisotropies, and acceleration of particles, all of which may be necessary to derive detailed source models. Thus the formulas above are starting points for spectral modeling rather than models in themselves.

F. Diffuse Galactic Source Theories

If the assumption is made that the galactic disk x-rays in the range 1-20 keV as reported by several authors previously mentioned are diffuse in nature as opposed to contributions from unresolved discrete sources, then several processes are possible. Boldt (1970) has investigated non-thermal bremsstrahlung radiation arising from knock-on

---

[1] ($\frac{dN}{dEdV}$ and J have the same spectral shape for ultra-relativistic particles ($\beta \approx 1$) so that for inverse Compton and synchrotron spectral shapes the results are independent of whether $\frac{dN}{dEdV}$ or J is used)

collisions of subrelativistic cosmic rays with the atomic electron of interstellar HI. The emissivity of this hydrogen can be calculated with the aid of a disk model shown in Figure (2) where θ_g is the angular thickness of the disk and θ_d is the FWHM of the detector. An approximate formula for the emissivity (η) which assumes 100% response over the FWHM of the detector, cylindrical collimation, and $\theta_d \leq \theta_g$ is given by

$$\eta = \frac{4\pi I}{N}\left[1 + \ell n\left(\frac{\theta_d}{\theta_g}\right)\right]^{-1} \frac{ev}{sec\text{-}Hatom} \qquad (21)$$

where I = integral energy flux $eV(cm^2\text{-}sec\text{-}rad)^{-1}$

N = columnar hydrogen density H atoms/cm^2

Using a flat energy spectrum of I = .15 $keV(keV\text{-}cm^2\text{-}sec\text{-}rad)^{-1}$ in the energy band $1.5 < h\nu < 12.5$ keV based on the Schwartz (1969) and Cooke (1969) measurements, $\theta_d = 4°$, corresponding to the Cooke experiment collimator, and $\theta_g = 2°$ corresponding to the HI disk where $N = 7.3 \times 10^{20}$ H atoms cm^{-2} (McGee & Murray 1961) in the direction $\ell \approx 300°$, equation (21) yields

$$\eta = 1.2 \times 10^{-17}\ eV(sec\text{-}H\ atom)^{-1} \qquad (22)$$

The data from Schwartz (1969) and Bleeker and Deerenberg (1970) indicate a break in the spectrum somewhere between 10 and 20 keV. If electrons were the incident subrelativistic particles creating this bremsstrahlung radiation, their energy would be mostly restricted to the range 10-20 keV.

Since only a small fraction of the electrons' energy is radiated, the emissivity found above must be corrected by an equation similar to (12) in order to find the ionization rate of these electrons. Berger and Seltzer (1964) have compiled such tables for the radiation fraction

of the electrons' total collisional loss rate in hydrogen.

The collisional loss rate for the electron energy range 10-20 keV using the emissivity given by equation (22) has the limits

$$(\frac{dE}{dt})\text{coll.} = (18 - 32) \times 10^{-14} \text{ eV(sec-H atom)}^{-1} \quad (23)$$

The average energy loss per atom ionized in hydrogen is 36 eV. This together with $(\frac{dE}{dt})$ gives the ionization rate (ζ) per hydrogen atom.

$$\zeta = (\frac{dE}{dt})\text{coll.}/36 = (5 - 9) \times 10^{-15} \text{ (sec-H atom)}^{-1} \quad (24)$$

This result is consistent with theoretical estimates by various authors of $\zeta \simeq 10^{-15}$ (sec H atom)$^{-1}$. In addition, pulsar dispersion measures by Hjellming, Gordon, and Gordon (1969) give $\zeta \simeq (2.5 \pm 0.5) \times 10^{-15}$ (sec H atom)$^{-1}$. Intensity measurements of the Hβ hyperfine lines in hydrogen between 4862-4863 Å provide the recombination rate which for small optical depths gives a direct measure of ζ via the relation

$$\zeta = \frac{4\pi}{E_{H\beta}} \frac{F_{H\beta}}{\int n_H \, e^{-\tau_{H\beta}} \, dr} \quad (25)$$

where $E_{H\beta}$ = energy of Hβ line

$F_{H\beta}$ = observed flux

n_H = hydrogen density

$\tau_{H\beta}$ = optical depth

the integration being performed along the line of sight.

Reynolds (1970) finds that the ionization rate could be as high as 10^{-14}(sec H atom)$^{-1}$, however, the collision loss lifetime of 10-20 keV electrons given by

$$\tau_e = E_e/\dot{E}_e \quad (26)$$

where E_e = electron energy

$\dot{E}_e$ = power radiated by electrons of energy E_e

is on the order of 10^3 years (assuming an average density of $1/cm^3$ for interstellar hydrogen) which requires a compensating acceleration mechanism for replenishment of such electrons. Pickel'ner and Tsytovich (1969) have presented arguments against such a population of electrons existing.

The above discussion applies equally to a subrelativistic proton population scattered by the atomic electrons of neutral hydrogen. The numbers above remain approximately the same for protons if the β of the protons is the same as for the electrons. The corresponding proton energy is (18-36) MeV and the collision loss lifetime is $1\text{-}3 \times 10^6$ years using the same density of hydrogen atoms as before. This lifetime is consistent with estimates for the escape lifetime of cosmic rays from the galaxy which allows a spectral break of 2 at the observed energy, and at the same time, allows a continuous spectrum of protons to exist rather than the artificially introduced range of electron energies required to match observations. This is consistent with the spectra given by Schwartz (1969) and Cooke (1969).

A number of investigations have been made into the production of diffuse x-rays via the inverse Compton effect. The scattering of the universal blackbody $\sim 3°K$ radiation by electrons has been treated by Brecher and Morrison (1969) who reach the conclusion that this model is incapable of supporting even the observed extragalactic diffuse background given present electron densities.

Inverse Compton radiation from starlight requires electrons in the energy range 13-41 MeV in order to produce 2-10 keV photons. Rees and Silk (1969) have shown that the collision loss lifetime of such electrons is comparable to estimates for their confinement time in the

galaxy. For 41 MeV electrons this results in a break in the photon spectrum of 1/2 at about 10 keV. At the present time, however, this break would not be large enough to fit the observations. In addition, Hudson et al. (1971) have found that the upper limit to the intensity of electrons needed to produce the observed 12.5 keV diffuse galactic x-rays is about 3 times smaller than the number of electrons required to produce 100 MeV bremsstrahlung γ rays in the Rees and Silk (1969) model.

A galactic x-ray excess involving inverse Compton scattering of far infra-red photons (0.4-1.3 mm) by GeV electrons has been proposed by Shen (1969), Cowsik and Pal (1969), and Ipavich and Lenchek (1970). If the power law of electrons as given by Anand et al. (1968) ($\frac{dN}{dE} = 126\ E^{-2.62}$ electrons $(m^2\text{-sec-ster-GeV})^{-1}$) is used, the resulting differential photon energy spectrum has an index of 1.81, a value which is considerably flatter than the upper limit of 3.2 found by Schwartz (1969). Bleeker and Deerenberg (1970) considered energy limits on monoenergetic infra-red photons to derive photon spectra and their results are also inconsistent with observations.

A population of weak unresolved sources has been investigated by Setti and Woltjer (1970) and Ryter (1970) as a means of producing the observed galactic excess. The Ryter model assumes the unresolved sources of the same luminosity class as the resolved sources are uniformly located at distances greater than a characteristic distance (d) which can be calculated from the observed strengths of resolved sources and the observed galactic excess in a given region of the galactic plane. Using the Seward (1970) catalog of known x-ray sources and the Cooke (1969) results, Ryter obtains a value for $d \geq 10$ kiloparsecs in the $\ell = 250° - 350°$ region of the plane.

In addition, Ilovaisky and Ryter (1971) have asserted that the soft x-ray galactic excess at about 300 eV could be accounted for by either known or unknown galactic supernovae remnants. In particular the observations of Bunner et al. (1971) and Hayakawa et al. (1970) previously mentioned include galactic plane regions where supernovae remnants are found. The region of the Cooke (1969) measurements contains the Vela supernova remnant, and the Schwartz (1969) results also include possible supernovae regions. Until better x-ray spectra of such objects are obtained it is difficult to make positive identifications with such objects.

The following chapter explains the physical design of the proportional chambers and the accompanying electronic systems. Chapter III covers the methods of data analysis used to interpret the data, while Chapter IV outlines the general features of the two rocket flights. Results of both flights are presented individually in Chapter V and a discussion of these results is found in Chapter VI. Appendix A involves an explanation of the spectral models used in the data analysis as well as a detailed calculation of radiation from a hot "optically thin" plasma. Appendix B outlines an attempt to calibrate the detectors with a continuous energy source of x-rays produced via the thin-target bremsstrahlung mechanism.

CHAPTER II

DESCRIPTION OF THE DETECTORS

A. Proportional Chambers

The x-ray detectors consist of two multi-anode, multi-layer aluminum gas proportional chambers pressurized to slightly more than one atmosphere. One detector contains a mixture of 90% argon, 10% methane and the other a mixture of 90% xenon, 10% methane. Rectangular mechanical collimators made of copper-plated stainless steel define the acceptance angles of incident radiation and are used to support the thin aluminized mylar or kapton windows which confine the gas to the chamber. Figure 3 shows a schematic design of the counter and Table 1 gives the detector specifications for each flight.

The multi-anode proportional chambers described above are the result of efforts by the Goddard Space Flight Center X-Ray Group to produce an x-ray proportional counter which will 1) efficiently collect electrons within a large gas volume, 2) reduce internal background to a minimum, 3) maintain sufficiently long gas stability in order to obtain good energy resolution, 4) perform independent measurements of observed radiation within one chamber, 5) be as compact in design as possible. Each anode is enclosed by a square array of ground wires which defines a distinct element of the chamber as shown in Figures 4 and 5. This arrangement provides an electric field of sufficient strength so that the electrons inside the gas reach the anode quickly and have path lengths small enough to prevent the production of negative ions.

Internal background reduction is accomplished by use of electronic logic as follows:

1. A requirement is made so that one and only one of a group of adjacent elements can show a valid signal at any one time.

2. All elements which are adjacent to the walls of the chamber are grouped into a single output which is used in anticoincidence with the rest of the chamber.

The above requirements prevent Compton electrons which are produced in the walls of the counter and which contribute most of the internal background from producing a valid x-ray event. The only wall area left unprotected against such a process is the end walls of the counter where the ground wires and anodes are attached. The detector has purposely been constructed long and narrow in order to keep this end wall area to a minimum.

Frequently the gas in proportional counters becomes contaminated with impurities from the walls of the counter or from small gas leaks. This contamination in turn leads to gain changes in the charge output from events occurring in the counter and finally to the degradation of the energy resolution of the counter. To keep this contamination to a minimum the technique of baking and evacuating the assembled chamber at a temperature of about 80°F for approximately 24 hours is employed before introducing gas into the chamber. Since the counters are contained in a single chamber any gain shifts from the effects mentioned above will show up in all layers thereby facilitating the use of correction factors to the original calibrations.

The multilayered construction of the chambers (4 layers in the xenon counter and 5 layers in the argon counter) permits each layer to

be analyzed independently of the others. This arrangement gives consistency measurements between layers as well as isolating higher energy parts of the spectrum as one analyzes the deeper layers. Figure 6 shows the quantum efficiencies of each layer of the detectors.

B. Collimation

Each of the detectors has its acceptance angle defined by a grid of rectangular mechanical collimators which have a 1.8° FWHM response in the width and a 7.1° FWHM response in the length of the collimator face as shown in Figures 7 and 8. The collimators are made of stainless steel tubing which are copper plated to prevent fluorescent radiation from iron in the stainless steel. The effective solid angle subtended by each collimator is 3.9×10^{-3} steradians. Both collimators have their look axes aligned to within 6 arc minutes. As an added protection against charged particle effects, the sides of the detector were plated with tin and the collimator side was covered with a thin layer of copper.

C. The Electronic Circuitry

Excluding the anticoincidence elements, the eight anodes in each layer of the chamber are divided into two groups of four anodes each such that adjacent elements never belong to the same group as shown in Figure 4 (bottom). The four layered detector thus has eight distinct groups plus an anticoincidence group all of which have separate high voltage connections through load resistors and high voltage feedthroughs. The three layered detector has six groups plus an anticoincidence group.

The outputs of each of the two groups of anodes from a given layer pass through the primary windings of separate pulse transformers and are

then summed at the input of a charge sensitive amplifier. A flow diagram of the signal is shown in Figure 9. The separate pulse transformer outputs are later used in the logic circuits shown in Figure 10, to reveal a coincidence between two or more groups in the chamber. This condition causes an event to be rejected because of reasons discussed previously.

Each individual layer analog output then passes through its own analog to digital conversion circuit (see Cancro et al., 1968) which pulse height analyzes the signal and places it into one of 127 channels if the upper and lower threshold energy requirements are met. A block diagram of this logic is shown in Figure 10. In addition;

1. All events above lower threshold and below upper threshold which have no coincidence among different layers are counted in scalar II (see Figure 11).

2. Events in a given layer which have a coincidence among adjacent elements are pulse height analyzed and counted in a mark bit.

3. All events exceeding upper threshold or which have coincidence between layers are counted in scalar I.

4. All events from a given layer below lower threshold are sampled layer by layer on a commutated basis and counted in scalar I'.

5. All rates in the anticoincidence elements are flagged when the counting rate exceeds 10^3 counts/sec. (called Flag I) and 10^4 counts/sec. (called Flag II).

D. The Telemetry Format

The data are transmitted in a pulse code modulation format at a 50.24 KHz bit rate. Digital data are retrieved in the form of frames

consisting of 64 sixteen bit binary words repeated continuously. Word one consists of a synch word and word 33 contains scalar I, scalar I', Flag I, and Flag II information. The other 62 words in a frame each contain pulse height analyzed x-ray events along with their layer identification and a flag to indicate whether a mark bit event occurred. Scalar II events are also contained in these 62 words. Figure 11 shows the readout format and timing for each frame and word within a frame.

E. Energy Calibration

Several radioactive sources were used to provide calibration points at detectable energies. These sources along with their decay modes and photon energies are listed in Table 2. The "effective energies" have been computed on the basis of a superposition of gaussian curves for line energies in Table 2 where the energy separation of various lines is too small to be resolved by the detectors.

In addition, several low energy calibration points were obtained from characteristic lines produced by thick-target bremsstrahlung (similar to the procedure described in Appendix B) with electrons incident on various target materials listed in Table 3. In order to minimize absorption of these low energy photons, the region between the photon source and the detector was evacuated. After subtraction of the continuum this procedure provided energy resolution data as well as calibration points down to the lower threshold energy of the detectors.

The calibration procedure just described revealed several nonlinearities in the energy response of the system. A typical calibration curve of the photon energy vs. pulse height channel number shown in Figure 12 illustrates that for channel numbers smaller than 11 the

response is non-linear. This behavior was verified by use of a variable pulse height, pulse rate generator which revealed that most of the non-linearity occurred in the analog to digital converter with the remainder divided between the various pre and post amplifier sections. There also exists a slight distortion of the calibration curve when count rates on the order of a few thousand counts/sec. are present. This phenomenon is due to a baseline shift in the voltage of the analog signal when many pulses overlap due to large count rates. For count rates observed in the flight experiments, however, this effect was negligible. The non-linear calibration curve was incorporated into the analysis of each channel of data.

Finally, an attempt was made to provide a continuous energy calibration of the system using photons produced by thin-target bremsstrahlung with electrons incident on .1 mil aluminum targets. The experimental spectrum agreed with the theoretical Kirkpatrick-Wiedmann (1945), Motz and Placious (1958) cross sections at energies above 5 keV but at lower photon energies were in disagreement with predicted values. A summary of this method of calibration is given in Appendix B.

CHAPTER III

ANALYSIS OF DATA

A. Spectral Analysis Procedure 1

Sources for which sufficient statistics exist are spectrally analyzed layer by layer by folding a theoretical model through the response function of the detector and comparing the results with the data using a chi square test described below for goodness of fit. The response function is represented by the integral transforms

$$\left(\frac{dn}{dE}\right)_E = \exp(-\mu_w(E')\chi_w)[1 - \exp(-\mu_g(E')\chi_g)]$$

$$\left\{ \int_o^\infty \left[1 - \sum_{n\ell,n'\ell'} P_{n\ell,n'\ell'}(E')\right] J(E') \frac{\exp\left[-\frac{(E-E')^2}{\sigma^2(E')}\right]}{\sigma(E')\sqrt{\pi}} dE' \right. \tag{27}$$

$$\left. + \sum_{n\ell,n'\ell'} \int_o^\infty P_{n\ell,n'\ell'}(E')\, J(E') \frac{\exp\left[-\frac{(E + E_{n\ell}^{n'\ell'} - E')^2}{\sigma^2(E' - E_{n\ell}^{n'\ell'})}\right]}{\sigma(E' - E_{n\ell}^{n'\ell'})\sqrt{\pi}} dE' \right\}$$

where $J(E')$ = theoretical differential photon spectrum

$P_{n\ell,n'\ell'}(E')$ = fluorescence x-ray escape probability for a transition from atomic levels $n'\ell'$ to $n\ell$

$\sigma(E')$ = energy resolution of the detector

$\left(\frac{dn}{dE}\right)_E$ = resulting differential spectrum at energy E

$\mu_g(E')$ = absorption coefficient for the gas fill at energy E' (gm/cm^2)

$\mu_w(E')$ = absorption coefficient for the detector window at energy E'

χ_w = thickness of window (cm^2/gm)

χ_g = thickness of gas layer (cm^2/gm)

and the integration is performed over all energies E'. Since the detector pulse height analyzes the x-rays into 127 channels, the differential spectrum $(\frac{dn}{dE})_E$ is then summed over the width of each energy channel.

$$N(E_i) = \int_{E_i-\frac{\Delta E_i}{2}}^{E_i+\frac{\Delta E_i}{2}} (\frac{dn}{dE})_E \, dE \qquad (28)$$

where $N(E_i)$ is the counts received in each energy channel of width ΔE_i.

In practice, the computer evaluates equations 27 and 28 in small enough increments so that the error in not going to a smaller increment is less than 1%.

The response function of the detector in terms of equation 27 is described as follows with parameters listed in Table 3.

Window Attenuation. Radiation coming into the detector from a source must pass through the interstellar medium and the detector window which confines the gas. The absorption of photons in the window occurs via the photoelectric effect and has an energy dependence proportional to $E^{-8/3}$ except for discontinuities at the absorption edges of the atoms. The term $\exp(-\mu_w(E')\chi_w)$ in equation 27 gives the number of photons transmitted through the detector window and the layers of gas on top of the layer being analyzed. Values for absorption coefficients were taken from Storm and Israel (1967).

Detector Efficiency. After passing through the detector window, the main energy loss mechanism for kilovolt x-rays is the photoelectric effect. The number of photons absorbed in such a process is given by $[1 - \exp(-\mu_g(E')\chi_g)]$ and represents the efficiency of the detector at energy E'.

Fluorescent Escape Radiation. X-rays exceeding the energy of an absorption edge of the counter gas can generate characteristic fluorescent radiation which may escape from the counter. The probability $P_{n\ell,n'\ell'}$ for radiation traveling along the z axis and escaping from a rectangular box detector with height z can be calculated from equation 29.

$$P_{n\ell,n'\ell'}(E') = \frac{1}{4\pi B}\int_o^z \exp\left[-\mu_g(E')z\right]\mu_g(E')f_n g_{n\ell,n'\ell'}dz \int \exp\left[-\mu_g(E_{n\ell,n'\ell'})|r|\right] dx\, dy\, d\Omega \tag{29}$$

where $B = \int \exp\left[-\mu_g(E')z\right]\mu_g(E')\, dx\, dy\, dz$ (30)

f_n = fluorescent yield of atomic shell n

dx,dy,dz = differentials of the coordinates of the fluorescent x-ray relative to the detector

$|r|$ = distance of the wall of the counter to the point of production of the fluorescent x-ray

$g_{n\ell,n'\ell'}$ = transition probability from atomic levels of $n'\ell'$ to $n\ell$

$E_{n\ell,n'\ell'}$ = energy of fluorescent x-ray

$d\Omega$ = solid angle of detector seen by escaping x-ray.

Equation 29 simplifies for the case of a semi-infinite counter to the following form

$$P_{n\ell,n'\ell'}(E') = \frac{1}{2}f_n g_{n\ell,n'\ell'}\left[1 - \frac{\mu_g(E_{n\ell,n'\ell'})}{\mu_g(E')}\ell n\left(1 + \frac{\mu_g(E')}{\mu_g(E_{n\ell,n'\ell'})}\right)\right] \tag{31}$$

Equation 31 is valid for the K edge in the argon counter and the L edges in the xenon counter since photons near the absorption edges are almost totally absorbed. For the K edges of xenon this is not true, but the efficiency of the gas at energies near the K absorption edge is small and the effect of using equation 31 rather than 29 is approximately the same.

Energy Resolution. When x-rays interact photoelectrically in a gas, statistical fluctuations in the number of ion pairs produced are coupled with fluctuations in the gas multiplication process as well as electron collection efficiency. These factors contribute to a spread in pulse height for a given event. In addition, electronic components generate random noise which add to this spread. All of these factors can be approximated by one expression which takes the form of a Gaussian curve.

$$R(E,E') = \frac{1}{\sqrt{\pi}\,\sigma(E')} \exp\left[-(E-E')^2/\sigma^2(E')\right] \qquad (32)$$

where $\sigma^2(E')$ can be written in a power series expansion

$$\sigma^2(E') = A + BE + CE^2 + \ldots\ldots \qquad (33)$$

In practice, all coefficients in equation 33 are small except for B at energies greater than 2 keV.

Escape Due to Electron Path Lengths. If the path lengths of the electrons which have been ionized are greater than the dimensions of a single element in the chamber, some of the incident photon's energy will be deposited in a neighboring element and will be anticoincidenced. Since this affects the probability for absorption, a suitable correction factor must be added to the efficiency of the gas. A relevant parameter is the range of a particle in the absorbing medium (i.e., the distance

a particle can travel before losing all its kinetic energy). For non-relativistic particles the range is proportional to the kinetic energy squared. The probability that an electron will escape from the element can therefore be expressed as $P_e = (1 - \alpha E^2)$ where α is an experimentally determined coefficient listed in Table 4.

Fluorescent Radiation from Ambient Material. Just as fluorescent radiation can be generated in the gas of the detector, it may also occur as a result of photons interacting with any material which the counter is made of. The principal contribution to this effect is the brass mechanical collimators which contain copper and nickel which fluoresce at energies 8.1 and 7.6 keV respectively. These probabilities incorporated in the second term of equation 27 are both energy and solid angle dependent and have been experimentally determined using a diffuse x-ray source produced by thick target bremsstrahlung (similar to the proceeding described in Appendix B) with 80 keV electrons.

B. Spectral Analysis Procedure 2

Sources which have differential spectral data comparable to 3σ above background have been analyzed less rigorously than procedure 1. First, equation 28 was evaluated for each layer in a detector using an input spectral shape resembling the data and normalized to 1 photon per energy channel. This gave approximate efficiencies for each energy channel. Second, data from different layers in each counter were summed. In the argon counter, all four layers were summed. In the xenon counter, layer 1 was used from 2 to 9.3 keV, layers 1 + 2 were used from 9.3 to 11.0 keV, and all layers were used at energies greater than 11.0 keV based on useable gas efficiency. Finally, data from both counters were

summed using the appropriate layers and corrected to a true incident flux by dividing by the sum of the efficiencies found in step 1. As an example, consider data from an energy channel i from the first and second layers of xenon and all four layers of argon. The corrected spectrum is given by:

$$N(E_i) = \frac{N_T(E_i)}{Eff_T(E_i)} \quad \text{counts in ith energy bin} \tag{34}$$

where

$$N_T(E_i) = N_{X1}(E_i) + N_{X2}(E_i) + N_{A1}(E_i) + N_{A2}(E_i) + N_{A3}(E_i) + N_{A4}(E_i) \tag{35}$$

$$Eff_T(E_i) = Eff_{X1}(E_i) + Eff_{X2}(E_i) + Eff_{A1}(E_i) + Eff_{A2}(E_i) + Eff_{A3}(E_i) + Eff_{A4}(E_i) \tag{36}$$

The subscripts in the summation refer to individual layers of the detectors. The resulting differential spectrum can then be compared using a chi-square test described below to various spectral shapes and equation 34, is reevaluated by an iterative procedure using the best fit from the chi-square test and recalculated efficiencies.

C. The Chi-Square Test

In order to determine which spectral models were consistent with the data, Pearson's (1900) Chi-Square test was used. This test uses the fact that the quantity

$$\mu = \sum_{i=1}^{k} \frac{(F_i - N_i)^2}{\sigma_i^2} \tag{37}$$

has approximately a χ^2 distribution with the number of degrees of freedom

equal to the minimum number of channels i needed to determine $\sum_{i=1}^{k} N_i$

where: F_i = expected number of counts in the ith energy channel

N_i = observed number of counts in the ith energy channel

σ_i^2 = variance of the expected counts in the ith energy channel

k = number of channels.

The values of μ when related to the chi-square probability distribution for a given number of degrees of freedom express the probability that upon repeating the experiment a larger value of μ would be obtained. This means that for values of μ with very small or very large probabilities the model can be rejected. The arbitrary criterion used to determine the range of acceptable spectral models was $.1 \leq P \leq .9$ where P is the chi-square probability. Values of P for different degrees of freedom are tabulated in Abramowitz and Stegun (1964) and the IBM/360 Scientific Subroutine Package.

In general, the models require that the F_i's be a function of several variables such as absorption coefficients, spectral indices, and normalization constants. This requires the solution of a multi-dimensional weighted least square fit where all parameters are simultaneously varied in order to obtain an absolute minimum chi-square. The limits on the parameters are then defined by contours in the multi-dimensional space.

We have chosen to restrict the number of independent parameters by requiring that for a given spectral index the normalization constant be determined by the total number of counts in the spectrum. In addition, since the interstellar absorption is negligible above 5 keV, best fits above 5 keV were used to determine the model to which an

absorption parameter was later added. Thus, only one approximately independent parameter was varied for each evaluation of chi-square.

The determination of the variance σ_i^2 in the expected value F_i requires an analysis of the error in the weighted least squares fit prescribed by equation 37. In practice, however, σ_i^2 is comparable to the variance in the observed counting rate when there is a reasonable fit to a model. Therefore, we choose σ_i^2 equal to the variance in the observed counts. In general, the evaluation of σ_i^2 involves the summing of errors from the total counts observed from a source and the subtraction of background counts observed for a different length of time. The general expression for σ_i^2 is thus:

$$\sigma_i^2 = N_i + \left(\frac{T_1}{T_2}\right)^2 B_i \tag{38}$$

where N_i = observed total counts received in the ith energy channel before background subtraction

T_1 = time spent collecting data N_i

B_i = observed total background counts received in the ith energy channel

T_2 = time spent collecting data B_i

The assumptions on N_i for use in the above test are:

1. each and every count is placed into one and only one channel i
2. N_i should be large; a rule of thumb is that $N_i \geq 5$ (especially if the number of degrees of freedom is ≤ 5).

In practice, energy channel widths are chosen so that at least nine total counts were present in a particular channel before background subtraction. This requirement was chosen as being indicative

of a 3σ effect. Where the errors were large compared to the data after background subtraction or where the net counts in a particular channel were less than zero additional lumping of channels occurred following a rule of thumb that the size of each bin in energy space was as large or larger than the preceding bin on a logarithmic scale. This latter procedure resulted in the error for each bin being approximately the same.

D. Spatial Analysis of Data

As in the spectral case, a spatial model for a source can be folded into the detector response function to give the expected counting rate as a function of the look direction of the detector axis. The general response function for a collimator is given by:

$$dn = \int_E \int_A \int_\Omega J(\theta, \varphi, E) \cos|(\theta-\theta')| da\, d\Omega\, dE \qquad (39)$$

where $J(\theta, \varphi, E)$ = intensity of the source as a function of coordinates in some spherical reference system and as a function of photon energy

$da \cos|(\theta-\theta')|$ = projected area of the detector on a plane perpendicular to the direction θ

θ = angle of source in a spherical reference system

θ' = look angle of detector axis in a spherical reference system

E = energy of the incident radiation

$d\Omega$ = solid angle subtended by the area $da \cos|(\theta-\theta')|$

For the special case of radiation coming into a rectangular collimator with dimensions w by d and height h from a spherical

coordinate system where w is parallel to polar latitude (b) and d is parallel to azimuthal longitude (ℓ) equation 39 can be written

$$\frac{dn}{dE} = \int_{b'-\theta^1_{max}}^{b'+\theta^1_{max}} J(b, \ell, E) \cos(b-b') \, wd \left[1 - \frac{\tan|b-b'|}{\tan(\theta^1_{max})}\right] \qquad (40)$$

$$\int_{\ell'-\theta^2_{max}}^{\ell'+\theta^2_{max}} \left[1 - \frac{\tan|\ell-\ell'|}{\tan(\theta^2_{max})}\right] \cos(b) \, db \, d\ell$$

where $\theta^1_{max} = \tan^{-1} \frac{h}{d}$

$$\theta^2_{max} = \tan^{-1} \frac{w}{d}$$

Using equation 37 we can perform chi-square tests in a fashion similar to the spectral analysis described above in order to check the acceptability of spatial models (e.g. Figure 13) with the data. In this case, N_i in equation 37 becomes the number of counts observed in a spatial interval i, F_i is the expected number of counts from integrating equation 40 over a spatial interval i and $\sigma_i^2 = F_i$.

CHAPTER IV

THE FLIGHT EXPERIMENTS

Table 1 lists relevant information concerning flights 13.07 and 13.08. Aspect information was gathered from star field photographs using two 35 mm. Nikon F cameras operated asynchronously with 2.6 sec exposures so that no two frames coincided. The positional error from such analysis is estimated to be about .2°.

Pre and post flight energy calibration was obtained with an Fe^{55}(5.9 keV) source mounted on the inside of mechanical doors which covered the detectors before and after the flight targets were observed. These sources were used to verify the results of earlier ground based calibrations.

The extragalactic diffuse background spectrum obtained from 61 sec. of data from flight 13.08 with the detectors pointing at galactic latitudes greater than 3.5° is presented in Figure 14.

Internal background information was obtained from flight 13.08 with 20 sec. of data collected while the detectors were pointed earthward and an additional 20 seconds while the doors were closed and atmospheric absorption above 2 keV was negligible. The latter measurements were used to determine internal background above about 10 keV since the earth's atmosphere itself is a source of hard x-rays.

A summary of results is presented in Table 5.

CHAPTER V

RESULTS

A. Flight 13.07

The aspect solution for the portion of the flight in which the Cygnus sources were scanned is shown in Figure 15 and a counting rate profile is presented in Figure 16. Energy spectra for Cygnus X-1, Cygnus X-2, and Cygnus X-3 were obtained as well as upper limits for Cygnus X-4 and Cygnus X-5 (Cygnus Loop). The spectra cover an energy range of 2-15 keV from the top layer of each detector while lower layers provided additional information in the 15-20 keV band. These usable energy ranges were determined after the discovery of leaky linear gates in the analog circuitry which caused spectral distortion of energy channels above 15 keV triggered by low energy events. Since few low energy events penetrate to the lower layers of the detectors, these layers were not distorted above 15 keV to any great extent and were used for analyzing spectra above this energy.

Background subtraction was obtained from approximately 20 seconds of data gathered when the detectors were looking at the Cygnus Loop which was not observed above 2 keV.

Limits on the spectral parameters are based on the 90% confidence limits (unless otherwise noted) of the chi square distribution described in Chapter III. In addition, all spectra were examined for line emission with negative results. The upper limits to iron line emission

in a 1 keV band centered at 7.0 keV for all sources was about 20% of the continuum. This result is in general agreement with line emission from an "optically thin" hot plasma with universal abundances as shown in Figure 17. Luminosities are given for sources in the energy range 2-15 keV unless otherwise noted.

Cygnus X-1. Cygnus X-1 was observed for approximately six seconds during the flight. After background subtraction approximately 1900 net counts occurred in the 2-15 keV range in the first layer of the xenon detector and approximately 1300 net counts were collected from the same energy range in the first layer of the argon detector. This represents a source to background strength of 20:1 in the xenon first layer and 10:1 in the argon first layer. The spectra were then compared with exponential, power law, blackbody, and "optically thin" isothermal plasma models by use of the chi square test discussed previously. Only a power law gave an acceptable fit. The spectrum is of the form:

$$\frac{dN}{dE} = 7.4\ ^{+2.4}_{-1.3}\ E^{-(2.6\pm.3)}\ \frac{\text{photons}}{\text{cm}^2\text{-sec-keV}} \qquad (41)$$

as shown in Figure 18. We are reasonably confident that this soft new spectrum (in contrast to Gorenstein et al., 1967) does not arise from a systematic effect in our experiment, since both the xenon and argon filled detectors (as well as the argon layers individually) are in agreement with this spectrum. The UHURU satellite has recently analyzed spectra from Cygnus X-1 with indices greater than 2 (Giacconi, personal communication, 1971), and balloon measurements in September 1970 (Matteson and Peterson, personal communication, 1970) are consistent with the softer spectrum of Cygnus X-1 up to 100 keV (see Figure 19).

During the time of observation Cygnus X-1 showed temporal variations on time scales of 100 milliseconds and greater (Holt et al.,1971) while the UHURU satellite has seen variations on smaller time scales (cf. Oda et al., 1971). The variability of Cygnus X-1 in strength and spectral shape are additional evidence for the non-thermal nature of the object.

Although the spectra of Cygnus X-1 was consistent with no interstellar absorption, the Brown and Gould (1970) results were tested in conjunction with the best power law fit above 5 keV where interstellar absorption is small. We obtain an upper limit of 5×10^{21} H atoms/cm^2 in the line of sight. It is interesting to note, however, that a minimum chi square was reached with 1.2×10^{21} H atoms/cm^2 which is in close agreement with 1.6×10^{21} H atoms/cm^2 calculated by Gursky et al. (1971).

In order to compare the distance of Cygnus X-1 with other authors (c.f. Ilovaisky, 1970; Gursky, 1971) the temperature brightness profiles of Muller and Westerhout (1957) from 21 cm. neutral hydrogen emission were used in conjunction with the Schmidt (1965) model of the rotating galaxy (see Appendix A), to give 5×10^{21} H atoms/cm^2 out to a distance of about 7 kpc in the direction of Cygnus X-1. These numbers are consistent with Lindblad's (1965) optical depth profiles for the same region.

Using an exponential model of gas density versus height above the galactic plane discussed in Appendix A, an upper limit of 7 kpc is found for the distance to Cygnus X-1 while our best fit gives a distance of about 1 kpc which is in good agreement with the distance found by Gursky et al. (1971). If Gaussian distribution of hydrogen density versus

height above the galactic plane is used (see Appendix A) the best fit gives about .7 kpc.

Assuming the above distances to Cygnus X-1 we calculate the x-ray luminosity at the source in the band 2-15 keV to be 4.9×10^{37} ergs/sec. for 7 kpc, and 1.0×10^{36} ergs/sec. for 1 kpc.

Cygnus X-2. In four seconds approximately 750 net counts were collected in the xenon first layer 2-15 keV range after subtracting background in a fashion similar to that for Cygnus X-1. The corresponding number for the argon first layer was approximately 450 net counts.

The energy spectrum of this source was consistent with an exponential fit given by:

$$\frac{dN}{dE} = 1.4 \pm .3 \exp(-E/4.5 \pm .7)/E \quad \frac{\text{photons}}{\text{cm}^2\text{-sec-keV}} \tag{42}$$

as shown in Figure 20.

In addition, a blackbody model and an "optically thin" hot plasma model (see Appendix A) gave slightly less acceptable fits than the exponential. The best temperatures for these fits are 1.3 keV and 2.8 keV respectively.

Finally, a power law fit could not be reconciled at all with our spectrum. Both counters agreed in the results listed above and data from the second layer in each counter indicates virtually no counts above 15 keV which agrees well with the thermal spectrum obtained below 15 keV found by us as well as other observers (c.f. Gorenstein et al., 1967) as shown in Figure 21.

Although the above fits are consistent with no interstellar absorption, the Brown and Gould (1970) results give an upper limit of

2.1×10^{22} H atoms/cm^2 with a temperature of 4.0 keV from an exponential model normalized to data above 5 keV. The minimum chi square with absorption included was obtained with 5×10^{21} H atoms/cm^2 while 21 cm. emission from the Muller and Westerhout (1957) profiles indicate approximately 1.3×10^{21} H atoms/cm^2 out to a distance of 5 kpc using the Schmidt (1965) model.

Since optical measurements by Kraft and Demoulin (1967) indicate that Cygnus X-2 is at a distance of about 600 parsecs the excess absorption observed in the x-ray spectrum could be due to self absorption in the source.

If the best absorption fit is used to evaluate the optical depth of the source at a given energy, then information on the scale size and electron density of the emitting region can be obtained. At 2 keV the optical depth using the best fit with interstellar absorption is .4. If most of this result is due to absorption within the source then for electron densities less than about 10^{24} cm^{-3} the photoelectric effect in the K shell of neon and magnesium hydrogenic ions is the major source of photon absorption at 2 keV in a hot plasma with universal abundances. Using the ionization equilibria of Tucker (1966) at a plasma temperature of 4 keV and the K shell photoelectric absorption cross section given by Heitler (1954), the photoelectric opacity at 2 keV is:

$$\kappa_{abs} \cong 10^{-25} N_X \qquad (43)$$

where N_X = electron number density.

Since the photons are electron scattered as they escape, the Thompson cross section can be used for 2 keV photons to give the electron scattering opacity.

$$\kappa_{esc} = 6.7 \times 10^{-25} N_X \tag{44}$$

Comparing equations 43 and 44 we see that photons are electron scattered about 7 times before being photoelectrically absorbed. This result allows neutron diffusion theory to be used (c.f. Davison, 1957) to calculate an optical depth given by:

$$\tau = (3 \kappa_{abs} \kappa_{esc})^{1/2} R_X \tag{45}$$

where R_X is the scale size of the source. At 2 keV and an optical depth of .4 equation 45 gives

$$N_X \cong 10^{24} R_X^{-1} \tag{46}$$

In order to obtain a second equation that may be solved simultaneously with equation 46, we use the bremsstrahlung emission formula (see equation 69 Appendix A) to get

$$\frac{\langle N_X^2 \rangle R_X^3}{d^2 T^{1/2}} \approx I \tag{47}$$

where I = intensity of radiation received from the source
in ergs/cm^2-sec-erg

d = distance to the source in cm.

T = temperature of the source in °K

Using a distance of 600 parsecs and a temperature of about 50 million degrees gives

$$\langle N_X^2 \rangle R_X^3 \cong 10^{58} \tag{48}$$

Solving equations 46 and 48 we obtain

$R_X = 10^{10}$ cm. as a lower limit to the size of the emitting region and $N_X = 10^{14}$ cm^{-3} as an upper limit to the electron density.

The luminosity of Cygnus X-2 at the source assuming a distance of 600 parsecs is 2.5×10^{35} ergs/sec.

Cygnus X-3. Cygnus X-3 was observed for approximately 4 seconds with approximately 800 net counts less background in the 2-15 keV range from the xenon 1st layer and 480 counts less background from the argon 1st layer.

The spectrum was tested with both thermal and power law models, all of which gave unacceptable χ^2 fits using the 90% confidence levels. Furthermore, the data have high enough statistical significance to exclude a power law or thermal continuum absorbed by cold interstellar matter using the Bell and Kingston (1967) or Brown and Gould (1970) results.

The minimum chi square for any model used was:

$$\frac{dN}{dE} = 87\ f(E, Eo)\ E^{-3.9}\ \frac{\text{photons}}{\text{cm}^2\text{-sec-keV}} \qquad (49)$$

where f(E, Eo) denotes the Brown and Gould (1970) interstellar opacity at a characteristic energy of 4.0 keV which corresponds to 1.6×10^{23} H atoms/cm^2 in the line of sight.

Figure 22 shows the spectrum of Cygnus X-3 including a feature at approximately 3.5 keV which is possibly due to absorption. The only element with an absorption edge near this energy having a significant universal abundance is argon. If we increase the universal abundance of argon to 10^{19} argon atoms/cm^2 in the line of sight and keep the other parameters in equation 49 except the normalization constant fixed,

the 90% confidence level in the chi square test is barely reached.

Since the argon counter itself has an absorption edge at 3.2 keV, data from this counter gave little additional information about such an absorption feature. Additional data must be gathered to determine if the feature is statistically significant.

Above 15 keV, data from the lower layers of both counters indicate a hardening of the spectra which is consistent with balloon results (see Figure 23).

Cygnus X-4. This source, reported by Giacconi et al. (1967b) at a strength of approximately .19 keV $cm^{-2}sec^{-1}$ in the energy range 2-5 keV, was not detected above a level of .04 keV $cm^{-2}sec^{-1}$ in the same energy range. This upper limit represents 3σ statistics on the counting rate at the time we passed over the reported position (Giacconi et al. 1971) of Cygnus X-4, and also is approximately 1% of our observed intensity for Cygnus X-1.

Cygnus X-5. We did not observe the Cygnus Loop above 10^{-2} photons $cm^{-2}sec^{-1}$ above 2 keV. This upper limit represents 3σ statistics assuming a source of uniform surface brightness coincident with radio supernova remnant. This result implies agreement with a thermal model for the sources (c.f. Tucker 1971) since the power law fit of Grader et al. (1970) would have been seen at about an order of magnitude above our upper limit while their thermal fit corresponding to a temperature of 400 eV would be below our threshold of detectability.

B. Flight 13.08

Spatial Profile. Data from four successive scans across the galactic plane along the 1.8 degree collimation direction at longitude 61.8° were folded into 1 degree bins in galactic latitude shown in Figure 24. These data come from a portion of the galactic plane where no discrete sources were observed with 99% confidence for a flux of .03 photons $(cm^2\text{-sec})^{-1}$ above 2 keV anywhere in the region $45° \leq \ell \leq 70°$ or .02 photons $(cm^2 sec)^{-1}$ above 2 keV for a source at a given position in the same region based on 3σ statistics on the estimated background from flight 13.07. In addition, there were two measurements of the diffuse cosmic background made at galactic latitudes $|b| \gtrsim 8$ degrees which were included in the profile.

Separation of the data into one degree bins in galactic latitude was chosen on the basis of a trial and error procedure designed to bring out maximum structure in the profile without being statistics limited. A chi square test using the mean counting rate as a model showed that the data are inconsistent with statistical fluctuations to a confidence level greater than 99%. A least squares fit to a two parameter point source model of the form:

$$N_i = A + Bf_i \tag{50}$$

where N_i = total counts in the ith bin

A = diffuse non-disk background counts in the ith bin

B = total observed source counts

f_i = fraction of total counts from a point source expected in the ith bin

showed that a point source at b = 0° could be excluded to a χ^2 confidence level of 92% while a point source at any other latitude gives a poorer fit. This result agrees with data obtained in flight 13.07 where the same portion of galactic plane was examined with the 1.8° collimator scanning in galactic longitude. Figure 25 shows the counting rate profile of flight 13.08 using the same data included in the spatial profile in Figure 24. At longitudes from about 53° - 62° our detectors were pointed at about b = -.5° and counting rates were at least 20 percent larger than the peak counting rate in Figure 24. This gives us further reason to believe that a single discrete source is not the entire cause of the effect we observe.

Recently, the UHURU satellite has detected a discrete variable x-ray source at ℓ = 68.45°, b = 1.68° with a maximum strength of about 12% of Cygnus X-2 (cf. Giacconi 1971). Although we would have seen such a source in flight 13.07 it is possible that this variable source might contribute to our current result. A two parameter least squares fit of the form given by equation 50 to a point source at the position and maximum strength reported by UHURU can be excluded to a χ^2 confidence level greater than 99%; however, we found that a superposition of a diffuse disk model (discussed below) and a discrete source at the position and strength observed by UHURU attributes 4 counts/sec to the b = 1-2 degree bin of Figure 23.

With regard to possible x-ray emission from an extended object seen by Katgert (1969) at 21 cm wavelengths, we can rule out any major contribution to our effect from this source on the basis that flight 13.07 would have observed this object at almost the same sensitivity as flight 13.08. Since the object is believed to be the remnant of multiple

supernova explosions and is approximately 10^6 years in age, it seems likely that the hard x-ray emission has long since disappeared.

If the data are due to a diffuse galactic emission, then the spatial profile in Figure 24 can be fitted to determine the angular size of the model. A linearized two dimensional chi square test to a uniform disk model (see Figure 2) was made for models with angular thickness (θ_g) ranging up to 8°. The results in Figure 26 show that a line source could barely be excluded at the 90% confidence level while disks with $\theta_g > 7°$ can be excluded with confidence levels > 90%. It is interesting to note that there exists a broad minimum in Figure 26 which correlates well with the angular thickness of the HI disk at galactic longitude 61.8° shown in Figure 27. For $\theta_g \simeq 2$ degrees an intensity of 2.9 photons $(cm^2\text{-sec-ster})^{-1}$ over a 2-10 keV band is obtained when data collected from $3.5° \leq b \leq 8°$ are subtracted from data where $b \leq 3.5°$ and renormalized to the count rate at $b = 0°$.

Spectra. The galactic disk energy spectrum was constructed from four successive scans across the plane by subtracting data where $|b| > 3.5°$ from data where $|b| \leq 3.5°$ a dividing point chosen on the basis of the FWHM response of our collimators to a disk model with $\theta_g \approx 2°$ as shown in Figure 24b. The data were then renormalized as discussed above. In addition, 12 seconds of data from longitudes 53° to 61.8° and latitude -.5° were included since no discrete sources were found in this region from flight 13.07 or UHURU results. The total net counts from both counters (approximately 400 in the energy range 2-30 keV) were grouped into five energy bins of approximately equal logarithmic size with the third bin purposely center at about 7.1 keV

C.2

corresponding to the K edge of iron. The spectrum was then analyzed according to spectral analysis procedure 2 and is present in Figure 28. We note that the spectrum exhibits a lack of counts in the energy bin 6 to 9.3 keV. This feature occurs at energies which include both the Kα emission and K absorption edge of iron. Above 12 keV the galactic excess became less than 1σ above background.

The data were then checked for spectral shape by comparing them with a uniformly emitting disk model described as follows.

$$I_b = \frac{1}{4\pi} \int_o^{N_H} \frac{q}{n_H} e^{-\mu r} dr + I_B e^{-\mu N_H} \text{ photons}(\text{cm}^2\text{-sec-kev-ster})^{-1} \quad (51)$$

where I_b = galactic disk spectrum at galactic latitude b

I_B = isotropic extragalactic background spectrum

$$\propto E^{-1.4} \frac{\text{photons}}{\text{cm}^2\text{-sec-ster-keV}}$$

q = photon source function $(\text{cm}^3\text{-sec-keV})^{-1}$

n_H = interstellar hydrogen density (H atoms/cm^3)

μ = absorption coefficient due to interstellar gas

N_H = columnar density (H atoms/cm^2) of the emitting region along the line of sight given by N_H = constant for $|b| \leq \theta_g/2$ and $N_H \propto \csc |b| > \theta_g/2$

The first term on the right in equation 51 represents the disk which is attenuated by cold interstellar matter and the second term on the right in equation 51 represents the attenuated extragalactic diffuse background.

A chi square test was made using equation 37 and the data to determine acceptable spectral indices and temperatures for several choices of N_H, assuming q to be in the form of a power law ($q = K(h\nu)^{-\Gamma}$) or an exponential ($q = K \exp(-h\nu/kT)/h\nu$).

From the 21 cm. data compiled by Daltabuit (1970) shown in Figure 27 and observations of Burton (1970), values of N_H were to lie between $1\text{-}3\times10^{22}$ H atoms/cm^2 at 61.8° and b = 0°. Brown and Gould (1970) absorption coefficients were used with the addition of iron absorption whose abundance was determined from Nussbaumer and Swings (1970) as 3.1×10^{-5} that of hydrogen.

The range of values for (q) which give acceptable χ^2 fits for a power law are

$$q = (8.5^{+3.8}_{-1.9}) \times 10^{-21} E^{-(2.8\pm.5)} \frac{\text{photons}}{\text{cm}^3\text{-sec-keV}} \qquad (52)$$

The corresponding fits to an exponential form are

$$q = (5.6^{+6.7}_{-1.9}) \times 10^{-21} \exp\left(-\frac{E}{2.1^{+1.4}_{-\ .8}}\right)/E \frac{\text{photons}}{\text{cm}^3\text{-sec-keV}} \qquad (53)$$

The above values were computed on the basis of a disk with $\theta_g = 2°$ and an interstellar hydrogen density of .7 H atoms/cm^3. Approximately the same goodness of fit was achieved for either model. We can also set a 3σ upper limit of .3 photons (cm^2-sec-ster)$^{-1}$ to any emission within a 1.5 keV bin centered at 7 keV (e.g. iron line) from the galactic disk at latitudes $|b| \leq 3.5°$. Such narrow band emission could be produced by charge exchange between stopping energetic iron nuclei and neutral H atoms, resulting in ultimate capture of electrons to the K shell (c.f. Silk and Steigman, 1969). If we assume that every iron atom now in the interstellar gas emitted two K x-rays (c.f. Ramaty et al., 1971) within the galactic lifetime, then the time averaged line intensity would be comparable to this upper limit.

Inverse Compton Model. The range of acceptable power law indices indicates that inverse Compton produced x-rays are not the dominant effect in our galactic disk spectrum. This applies to the electron spectrum given by Anand et al. (1968) for electron energies in the range of about 5 to 200 GeV which give a photon spectral index of 1.8 as well as the low frequency radio synchrotron ($< 10^2$MHz) results of Alexander et al. (1969) as interpreted by Goldstein et al. (1970) for electron energies 200 MeV to several GeV which give a photon spectral index of 1.4.

We can, however, calculate upper limits to the fraction of our effect due to 2.7°K blackbody photons undergoing Compton collisions. Using the power law spectrum given by Anand et al. (1968) we find, using equation 10 in Chapter 1, that the photon spectrum is given by

$$I(h\nu) = 9.0 \times 10^{-26} T^{3.8} (h\nu)^{-1.8} R \ \frac{\text{photons}}{\text{cm}^2\text{-sec-ster-keV}} \qquad (54)$$

where T = blackbody photon temperature in °K.

$h\nu$ = photon energy in keV

R = emitting region in cm. along the line of sight

Using T = 2.7°K and R = 17 kpc equation 54 gives $I(h\nu) = .01 - .003$ $\frac{\text{photons}}{\text{cm}^2\text{-sec-ster-keV}}$ at 5 and 10 keV respectively which is 6% and 9% of the flux given by our hardest acceptable power law fit at these energies. The Goldstein et al. (1970) electron spectrum produces a photon spectrum given by

$$I(h\nu) \approx 7.1 \times 10^{-26} T^{3.4} (h\nu)^{-1.4} R \ \frac{\text{photons}}{\text{cm}^2\text{-sec-ster-keV}} \qquad (55)$$

and using the same analysis as above we find that the fraction of our

results at 5 and 10 keV is 6% and 11% respectively. In either case the predicted flux is small enough so that the 3σ upper limit to the data in our energy channel 9 to 17 keV requires an energy density (ρ) of about $7 eV/cm^3$ in microwave radiation after removing the temperature dependence on ρ and assuming a temperature of 2.7°K. This upper limit is much larger than the $4.3\ eV/cm^3$ upper limit obtained by Hudson et al. (1971).

Synchrotron Emission Model. Another possible production mechanism for the observed galactic excess is synchrotron emission from ultra-relativistic electrons radiating in the interstellar magnetic field (Freitas Pacheco, 1970). The electron energies required to produce 2-30 keV x-rays in an interstellar magnetic field of 3×10^{-6} gauss range from about $2\text{-}7 \times 10^5$ GeV. At these energies we extrapolate from observations at lower electron energies given by choosing a spectral index of 2.6 to give an electron spectrum of $I_e(E) = 63.1\ E^{-2.6}$ electrons $(m^2\text{-sec-ster-GeV})^{-1}$ above 10^3 GeV. This corresponds to a photon spectrum of

$$I(h\nu) = 3.9 \times 10^{-22}\ R(h\nu)^{-1.8}\ \frac{\text{photons}}{cm^2\text{-sec-ster-keV}} \qquad (56)$$

in a field of 3 μ gauss and yields about 8 times the flux of our hardest power law fit at 10 keV using 17 kpc for R.

If we assume, however, that the electrons are uniformly produced in time and space then a break of one unit in the electron spectrum could be expected at an energy corresponding to the electron confinement time in the galaxy. Assuming a lifetime of about 10^6 years puts the break at about 10^3 GeV. The resulting synchrotron flux using the analysis above is then consistent with our spectral index of 2.3 but gives only 3% of

the observed flux. If we choose the electron energy at which the break must occur in order to match our data we find that this energy is about 6×10^4 GeV corresponding to an electron lifetime of about 10^4 years in a field of 3μ gauss.

Based on an estimate of a supernova rate of 1 per 100 years in the galaxy, only about 10^{-2} supernovae would have occurred on the average in the direction of our observation in 10^4 years. It appears then that a uniform supply of electrons is not forthcoming from such sources.

Upper limits to electron fluxes from air shower measurements given by Kamata et al. (1968) at energies of about 10^{13} eV also yield small synchrotron fluxes which are about an order of magnitude below our results.

Suprathermal Proton Model. If a population of non-relativistic protons were responsible for the observed galactic excess then equation 21 allows us to calculate the ionization rate in the interstellar medium. Using equation 18 as the photon source function for non-relativistic bremsstrahlung due to a power law spectrum of particles, a transformation to the proton rest frame allows one to calculate the radiation from such a process. With this transformation equation 18 becomes

$$(h\nu)q = (8\,\alpha\,\sigma_T\,Mc^2)\; f(\Gamma) n\, A\left(\frac{M}{m}\,h\nu\right)^{\Gamma-1} \quad \frac{\text{keV}}{\text{keV-cm}^3\text{-sec}} \qquad (57)$$

where α = fine structure constant

σ_T = Thompson cross section

$f(\Gamma)$ is defined in equation 19 with $x = \frac{M}{m}\frac{h\nu}{E}$

M = proton rest mass

m = electron rest mass

n = number density of hydrogen plus electrons

A = normalization constant for the differential energy spectrum of protons

The integral energy loss function for all suprathermal protons above energy $E_o = (\frac{M}{m})\ h\nu_o$ is

$$Q(E_o) = 4\pi \int_{E_o}^{\infty} AE^{-\Gamma} \frac{dE}{dx}\, dE \tag{58}$$

where $$\frac{dE}{dx} = \frac{1}{\beta c}\frac{dE}{dt} = (\frac{M}{2E})^{1/2}\ \frac{dE}{dt} \tag{59}$$

from Hayakawa and Kitao (1956).

$$-\frac{dE}{dt} = 1.46 \times 10^{-12}(n_H + 4n_e)E^{-0.3}\ \frac{\text{MeV}}{\text{nucleon-sec}} \tag{60}$$

The ionization rate is given by

$$\zeta = \frac{Q(E_o)}{n_H\ q_o} \tag{61}$$

where q_o = average energy loss per ionization = 36 eV for hydrogen (Dalgarno & Griffing, 1958). Combining equations 52, 57, 58, 59, and 60, equation 61 becomes

$$\zeta = \frac{4\pi\ cn_H\ (h\nu_o)^{.2}(h\nu)^{\Gamma+1}\ q}{N_H(n_H + n_e)\ (\Gamma-.2)}\ (\text{sec-H atom})^{-1} \tag{62}$$

where $c = 1.14 \times 10^{+7}$

n_e = number density of electrons

and $4n_e$ was neglected in equation 60 because the energy loss depends only on the hydrogen density.

Using equation 52 and 62 we find that for $h\nu_o$ = 2 keV $\zeta = (1\text{-}7) \times 10^{-13}(\text{sec-H atom})^{-1}$ with the limits defined by the limits in equation 52.

For the exponential spectrum given by equation 53 a photon source

function corresponding to equation 57 was derived assuming mono-energetic photons of energy kT and was used to evaluate ζ. The result was $\zeta = 8\text{x}10^{-14}(\text{sec-H atom})^{-1}$.

In fact, $8\text{x}10^{-14}(\text{sec-H atom})^{-1}$ represents a lower limit to the ionization rate because an exponential fit to our data shows that the photon energy spectra turns over at about 2 keV or slightly higher than our detector threshold. This means that the ionization is due to protons of energy $E_o \geq (\frac{M}{m})h\nu_o$ where $h\nu_o \approx 2$ keV, allowing us to use 2 keV as the lower energy limit in equation 62 without seriously underestimating the ionization contribution from protons with energies less than that corresponding to $h\nu_o = 2$ keV. Since the ratio of bremsstrahlung to collision losses in the interstellar hydrogen gas is a function of particle velocity, independent of charge, the above results are the same for all cosmic ray particles with velocities equal to the protons discussed here.

Transition Radiation. Johansson (1971) has suggested that transition radiation produced during the traversal of relativistic charged particles through interstellar grains could be an important source of cosmic x-rays. Ramaty and Bleach (1972) have investigated this proposition in light of the known theory of transition radiation (Garibyan, 1960; Bass and Yakovenko, 1965), and the astrophysical information on interstellar grains, soft x-rays, and low energy cosmic rays with the conclusion that for grain sizes on the order of 10^{-5} cm. the maximum energy at which appreciable radiation occurs is about 150 eV. Since the maximum energy at which radiation is produced is directly proportional to the size of the grain it appears that x-rays in the kilovolt range are not produced by this mechanism unless grain sizes are much larger. Even if one allows

for large grain sizes the energy density in cosmic rays required to produce the observed galactic excess seen by Bunner et al. (1971) (which is 16 times larger at 260 eV than our photon source function predicts using the steepest power law fit) is prohibitively large.

Unresolved Sources. Using the model of Ryter (1970) outlined in Chapter I, we can determine the distance beyond which unresolved sources exist in the disk. An average of Ryter's apparent flux per radian from observed x-ray sources in the region $120° \leq \ell \leq 30°$ shows that our observed galactic excess is only about 2% of this flux. According to Figure 2 in Ryter (1970) the distance beyond which unresolved sources lie is about .8 of the extent of the galaxy in our direction of observation. If all x-ray objects seen by UHURU in the 1971 catalog (Giacconi et al., 1971) in the longitude range $30° \leq \ell \leq 130°$ and $|b| \leq 15°$ are used (excluding the strong source Cygnus X-1) to construct a FWHM thickness of the disk assuming absolute value in galactic latitude for source positions, then our detector would have observed a disk with a FWHM of $> 14°$ in resolved sources. If unresolved sources of this type formed the basis for the Ryter model then this size for an unresolved disk component would be inconsistent with our spatial profile.

If we assume that a new class of low luminosity x-rays sources exist such that there are enough of them to justify the use of the volume emissivity q found above, then the distance beyond which unresolved sources of a single luminosity lie can then be calculated as follows:

Let: $2R_D$ = diameter of the disk

$2R_o$ = thickness of the disk

R_s = distance beyond which unresolved sources lie

L = luminosity of one source (ergs/sec)

I = threshold sensitivity of the detector (ergs/cm^2-sec)

n = volume density of sources

N = number of observed sources of luminosity L

N_T = total number of sources of luminosity L in the galaxy

q = volume emissivity of the disk (ergs/cm^3-sec)

Providing that $R_s \leq R_o$ we have the following relations

$$nL = q \tag{63}$$

$$N = n \frac{4}{3} \pi R_s^3 \tag{64}$$

$$L = 4 \pi R_s^2 I \tag{65}$$

$$N_T = 2 \pi (R_D)^2 R_o n \tag{66}$$

Equation 64 is valid as long as $R_s \leq R_o$. Combining the above equations we find

$$N = \frac{R_s q}{3I} \tag{67}$$

Using the q found from our best power law fit to the galactic spectrum, $R_s = R_o$ from our best fit to the profile in Figure 24 and I = threshold sensitivity of the UHURU satellite $\simeq 5 \times 10^{-11}$ergs/cm^2-sec, we find $20 \leq N \leq 30$ depending on the value of $R_D (10 \leq R_D(\text{kpc}) \leq 17)$ which was used to find R_o.

Based on the sky survey of UHURU, (Giacconi et al. (1971)) we find about 37 sources at $|b| > 15°$ which includes 20 objects tentatively identified with extragalactic objects of which a dozen seem to be fairly positive identifications. This means that some 20-35 sources could be galactic if an isotropic distribution is assumed. Currently this number is in agreement with our prediction of 20 to 30 resolvable galactic sources of one low luminosity class on the order of 10^{32} ergs/sec.

CHAPTER VI

DISCUSSION

A. Discrete Sources

Cygnus X-1. Cygnus X-1 appears to be a compact non-thermal emitter with temporal variations in intensity and spectral shape ranging from hundreds of milliseconds to about 1 year over the x-ray band 2-100 keV. At the present time, there is little evidence for suggesting correlations between temporal variations at photon energies above 20 keV with softer x-ray photons (c.f. Matteson, 1971), implying that different regions in the source produce photons of different energies or that emission mechanisms may vary within the source. Matteson (1971) has also investigated several models of x-ray emission from Cygnus X-1. These include the eclipsing binary star model suggested by Dolan (1970, 1971), the thermal bremsstrahlung model proposed by Sartori and Morrison (1967), the synchrotron model proposed by Manley and Olbert (1969), and the stellar accretion model suggested by Prendergast and Burbidge (1968). None of the above models are capable of explaining all the x-ray observations; however, the Dolan (1970, 1971) model suggests a collapsed stellar object as one component of the binary system while the Manley and Olbert (1969) model extrapolated to radio frequencies using pre-1970 data in the 1-10 keV x-ray band agrees with the Hjellming and Wade (1971) radio flux at 2695 MHz. The optical flux

predicted using the above extrapolation corresponds to about a 15th magnitude object. Bolton (1972) and Hjellming and Wade (1972) have concluded that the variable (~ 9th magnitude) star HDE 226868 is closely coincident to the radio source position, however, a 15th magnitude red star also lies within the x-ray error box (Giacconi et al., 1971). The limits (1-7 kpc) for the distance to Cygnus X-1 make this source the most powerful of the discrete Cygnus X-ray emitters.

Cygnus X-2. Cygnus X-2 is believed to be a binary star system at a distance of about 600 parsecs radiating via thermal emission. Our observations are consistent with this interpretation in that no rapid temporal variations of the type observed from Cygnus X-1 were seen, and our calculated density of electrons (~ 10^{14}cm^{-3}) and size (~ 10^{10} cm.) of Cygnus X-2 would indicate a stellar-like object. In the 2-20 keV range a source temperature of kT=4.5 keV is found which, when extrapolated to the optical band, is capable of accounting for only 25% of the observed flux (Cathey and Hayes, 1968) suggesting different emission components for the two regimes. At energies above 20 keV upper limits to the flux (Webber and Reinert (1970), Overbeck and Tananbaum (1968 a, b) indicate a variable high energy component may be present in the spectrum.

Cygnus X-3. Cygnus X-3 is a puzzling phenomena at this time. First, it cannot be exactly like Cygnus X-2 because it has been observed at energies greater than 30 keV (Matteson and Peterson, personal communication, 1970) and is observed to be considerably harder than thermal above about 10 keV in our experiment as well. Second, there

are no rapid temporal fluctuations as in the case of Cygnus X-1. Third, the spectrum is different from the other two sources. Whether this arises because of self-absorption in the source or by absorption from cold interstellar matter is unknown at present. Radio observations by Wendker (1970) of the Cygnus-X complex show the source G 80.0+0.8 (with an angular diameter of 16 arc minutes) to lie within the x-ray error box given by Giacconi et al. (1971). One possibility is that Cygnus X-3 is the source of excitation for such an object.

Cygnus X-4. Our upper limit to the flux of Cygnus X-4 is consistent with observations by Giacconi et al. (1967b) indicating that this object emits only soft x-rays.

The Cygnus Loop. Our upper limit to the flux from the Cygnus Loop indicates that an extended soft thermal source associated with the supernova remnant is an adequate representation.

A.S.E. 1954+31. This object should have been observable at a strength of approximately 20% of the maximum reported from UHURU but was not seen in our September 1970 experiment. It is possible that this variable source was observed in our August 1971 flight.

B. The Galactic Disk

The excess of 2-30 keV x-rays observed at longitude 61.8° in the galactic plane enables us to place restrictions on the size and source mechanisms if the observed effect is assumed to be the result of a diffuse galactic emission.

With regard to the angular size we can say that disks thicker than about 7 degrees (corresponding to about 1 kpc based on 10 kpc in the line of sight) are improbable and particle or stellar populations with thicknesses larger than this do not contribute significantly to our observations. Furthermore, the x-ray excess appears to lie symetrically on either side of the galactic plane (to within statistics) indicating a somewhat uniform effect. For these reasons a disk shaped model shown in Figure 2 was chosen for the geometry which contained the emission with the best fit to such a disk being about 2° in angular thickness.

Inverse Compton radiation proved unsuccessful in explaining our results. Our acceptable spectral indices are incompatible with either the Anand et al. (1968) results for electron energies between 5 and 200 GeV or the Alexander et al. (1969); Goldstein et al. (1970) results for electron energies from about 200 MeV to several GeV. Secondly, the 2.7°K blackbody radiation is capable of accounting for only a few percent of our observed spectrum with a 3σ upper limit of about 7 ev/cm^3 as the energy density in the microwave region.

Synchrotron losses from galactic electrons in a magnetic field of a few microgauss could explain the observed photon flux if the interstellar electron spectrum observed at several hundred GeV is extrapolated to 10^6 GeV. The photon spectral index produced by such electrons is, however, incompatible with our 90% confidence limits. If we allow for a break of unity in the interstellar electron spectrum at 10^3 GeV corresponding to a confinement lifetime of about 10^6 years

then we find consistency with our observed spectral shape but with a photon flux amounting to only a few percent of our data. Upper limits given by Kamata et al. (1968) on 10^4 to 10^5 GeV electrons from air shower measurements also fall an order of magnitude below our observed flux. A break in the interstellar electron spectrum at an energy of about 6×10^4 GeV corresponding to a lifetime of 10^4 years would account for our results via the synchrotron mechanism but we have no reason for expecting such a break. The radiative lifetime at this energy is about 1.5×10^4 years, during which time we would expect $< 10^{-1}$ galactic supernovae in our field of view.

Since our best fit to the size of the disk is approximately the same as the thickness of neutral hydrogen in this region the suprathermal model discussed by Boldt (1970) was investigated and found to consistently require ionization rates ranging from a few times to an order of magnitude larger than observed or predicted by theoretical models. The only justification for such a model would be to assume compact "hot" regions where such large ionization rates could exist.

We have investigated transition radiation as a means of explaining our effect because of the recent article by Johanssen (1971) suggesting that relativistic charged particles passing through interstellar grains could produce hard x-rays, at the energies of interest. Ramaty and Bleach (1972) have found, however, that because of the small size of the grains (about 10^{-5} cm) transition radiation could not be produced in any significant quantity above photon energies on the order of 100 to 200 eV.

The result of many unresolved low luminosity discrete sources is capable of producing the effect we observe. Assuming that this sample is composed of sources of a single luminosity, then there must be a sufficient number in order to justify the use of our source function (q) throughout the disk. For objects with intrinsic luminosities greater than about 10^{36} ergs/sec, our integral source function of about 7×10^{-30} ergs/cm^3-sec (2-10 keV) implies that less than 10^2 such sources could comprise a disk population. Our detectors have sufficient sensitivity, however, to measure most of these sources as discrete.

A galactic model has been suggested by Ryter (1970) in which the disk is composed of resolved discrete x-ray sources out to a distance (d) in the plane of the disk and unresolved sources of the same luminosity class at distances greater than d. When applied to our results, this model yields a distance (d) greater than 80 percent of the disk's extent in the plane. Since the angular extent of the disk using the above distance is approximately the same for both resolved and unresolved sources we have attempted to compare the angular size of our disk with a disk composed of already resolved sources from the UHURU catalog (c.f. Giacconi et al., 1971). The resolved galactic sources found in the region $30° \leq \ell \leq 330°$, excluding sources of strength $> 10^{-1}$ Tau X-1, would produce an effective disk brightness with angular extent $\geq 10°$ based on absolute values of galactic latitude for source positions. Since this result exceeds our 90% confidence limit to the angular extent of the disk, we conclude that unresolved

x-ray sources with intrinsic luminosities similar to previously resolved low latitude sources probably cannot by themselves adequately describe our effect.

Our upper limit of 7° for the angular extent of the diffuse emission corresponds to a galactic disk thickness of 1.2 kpc for a distance to the edge of the plane equal to 10 kpc. We note that the UHURU catalog (Giacconi et al., 1971) includes isotropically distributed objects of relatively weak flux, some of which might be low luminosity sources within the galaxy. The limiting sensitivity of UHURU to sources as distant as 0.6 kpc corresponds to an intrinsic luminosity of $\sim 10^{33}$ ergs/sec. In this case, when UHURU completes a full sky survey with its limiting sensitivity, it should detect an isotropic distribution of ≤ 60 sources of intrinsic luminosity $\leq 10^{33}$ ergs/sec., while the unresolved sources of the same population in the disk at distances greater than 0.6 kpc could produce our observed excess.

In conclusion, we have reason to believe that all but unresolved low luminosity sources are unlikely or negligible contributors to our observed galactic excess. Further improvements in detector sensitivity and observation time in the succeeding generations of satellite experiments will make possible measurements of the other mechanisms previously mentioned as diffuse contributors to galactic x-ray emission. These observations, for example, could be important tools in studying the galactic distribution of electrons and other charged particles.

More frequent x-ray observations of the discrete sources in the Cygnus region will permit temporal variations to be carefully studied

in regard to correlating low and high energy x-ray data with other radiation from these sources. It will then be possible to construct detailed models of these discrete x-ray objects.

APPENDIX A

SPECTRAL MODELS

Chapter I describes x-ray production mechanisms which have various spectral shapes. In particular, the inverse Compton and synchrotron processes usually produce power law spectra of the form $\frac{dN}{dE} \propto K\, A\nu^{-\Gamma}$ while thermal sources generally have spectra resembling an exponential shape. In 1966 Tucker calculated the radiation from a hot tenuous plasma with temperature on the order of 10^7°K. The following is a recalculation of such radiation using ionization equilibrium of Jordan (1970), the abundance of Nussbaumer and Swings (1970) for iron, the temperature averaged Gaunt Factors of Karzas and Latter (1961), the abundances of Brown and Gould (1970), and ionization equilibrium of Tucker (1966) for other elements. Oscillator strengths for iron line emission were taken from Chapman (1969) and Allen (1963).

Line emission was calculated only for the $1S^1 1S$ - $1S2P^1 P$ transition in FeXXV and FeXXVI because of its suitable energy for detection in our experiments. FeXXV has resonance, intercombination, and forbidden lines at 6.70, 6.68, and 6.65 keV respectively while for FeXXVI the Kα line energy is at 6.9 keV.

Line Emission. The energy released per sec per unit volume due to line emission is given by:

$$\frac{dE_{nn'}}{dt\ dV} = n_e n_i 8\pi^2\ e^4 f_{nn'} \langle g_{nn'} \rangle\ (6\pi mkT)^{-1/2}\ \exp\left(-\frac{E_{nn'}}{kT}\right)\ \frac{\text{ergs}}{\text{sec-cm}^3} \qquad (68)$$

where n_e = number density of electrons

n_i = number density of ions

$f_{nn'}$ = dipole oscillator strength of the transition from levels n to n'

$\langle g_{nn'} \rangle$ = an effective Gaunt factor taken from Regemorter (1962) and equal to about .205 for $20 < T°K < 100$ million degrees

$E_{nn'}$ = the energy of the emission line

Bremsstrahlung. The energy emitted per sec per unit volume per unit energy due to bremsstrahlung by a Maxwellian distribution of electrons interacting with ions of charge Z is given by

$$\frac{dE_{B,z}}{dtdVdE} = \sum_z n_e n_z \frac{2^4 e^6 z^2}{3^{3/2} m^2 c^3} \left(\frac{2\pi m}{kT}\right)^{1/2} \bar{g} \exp\left(-\frac{E}{kT}\right) \frac{\text{ergs}}{\text{sec-cm}^3\text{-erg}} \quad (69)$$

where $\bar{g}$ = the temperature averaged Gaunt factor of Karzas and Latter (1961)

and the summation is over all ions with charge z.

Recombination. Using the hydrogenic approximation to the recombination cross section given by Elwert (1954), the energy emitted per unit time per unit volume per unit energy due to a Maxwellian distribution of electrons being captured to a quantum level n of an ion with charge z is given by

$$\frac{dE_{r,z}}{dtdVdE} = n_e n_z 8\pi A h I_H^2 \frac{z^4}{n^3} \left(\frac{\bar{\zeta}}{2n^2}\right)\left(\frac{m}{2\pi kT}\right)^{3/2} \exp\left[-\frac{(I_{zn}-E)}{kT}\right] \frac{\text{ergs}}{\text{sec-cm}^3\text{-erg}} \quad (70)$$

where A = constant = 2.11×10^{-22} cm^2

n = the principal quantum number of the final state

$\left(\frac{\bar{\zeta}}{2n^2}\right)$ = the incompleted fraction of shell n

$I_{z,n}$ = the ionization potential of state n

For temperatures above 20 million degrees most of the atoms are completely ionized and most recombinations will be at quantum levels n = (1-2). In this case, dielectronic and higher orders of recombination can be neglected. Table 6 shows the elements and their abundances for each model. The ratio of the power in iron line emission to power in the continuum is at 1 keV band centered at 7.0 keV is shown in Figure 17, as a function of temperature.

Interstellar Absorption. At energies less than about 5 keV absorption of x-rays by the interstellar medium becomes increasingly important. Several authors have published x-ray photoelectric absorption cross sections among them are Bell and Kingston (1967) and Brown and Gould (1970). The principal contribution of the former authors was the use of a more accurate cross section for photoionization of atomic helium than had previously been used, while the latter authors used lower abundances of helium and neon.

The Bell and Kingston results give an absorption coefficient continuous in energy and represented by $\sigma(E) \propto (\frac{Ea}{E})^{8/3}$ cm^2/H atom where Ea is the e fold transmission energy. Brown and Gould's cross sections include discontinuities at the K edges of the elements so that the absorption coefficient can be represented by $\sigma(E) \propto \sum_i \sigma_i(E)\ N_i$ cm^2/H atom where σ_i is the cross section one atom of element i and N_i is the abundance of element i relative to hydrogen. Expressing the transmission of x-rays through the interstellar medium one must then add the factor $\exp(-\sigma(E)N_H)$ (where N_H is the number of neutral hydrogen atoms/cm^2 in the line of sight) to any spectral model.

An independent measurement of N_H can be found using 21 cm. hydrogen emission observations. If one assumes that the neutral hydrogen is

uniformly distributed, and "optically thin" with constant temperature T_g, then the number of hydrogen atoms/cm^2 in the line of sight is given by

$$N_H = 1.84 \times 10^{18} T_g \int_{-\infty}^{+\infty} \tau(v)dv \qquad (71)$$

where T_g = spin temperature of the hydrogen in °K

$\tau(v)$ = the optical depth

v = radial velocity of the gas relative to the observer

In practice, a velocity-distance relation is used to determine the limits of integration in equation 1. This relation can be derived from a differentially rotating galactic model discussed by Schmidt (1965) and is given by

$$v_r = R_o [\omega(R)-\omega(R_o)] \sin(\ell) \cos(b) \qquad (72)$$

where R_o = distance from the galactic center to the sun

$\omega(R)$ = angular velocity of the hydrogen at a radial distance R from the galactic center

ℓ and b = are galactic longitude and latitude respectively

v_r = velocity of hydrogen at radial distance r from the observer

The angular velocity of hydrogen $\omega(R)$ is determined from an empirical formula derived by Contopolous and Stromgren (1965) from radio observations and given by

$$\omega(R) = 67.76 + 50.06R - 4.0448R^2 + 0.0861R^3 \text{ cm/sec} \qquad (73)$$

where R is in kpc. This polynominal is applicable for $3 \leq R \leq 13$ kpc.

Thus for a given r and R_o, R can be found and used in equations 72 and 73 to find the radial velocity of the neutral hydrogen at distance r. The amount of hydrogen within a given distance r from the observer can then be calculated via equation 71.

The ratio of the amount of hydrogen found from x-ray spectra to hydrogen found from 21 cm measurements can be used to determine x-ray source distances if a model for the distribution of the gas is used.

Since the gas density drops with increasing vertical distance Z from the galactic plane the choice of either a barometric model or a gaussian model has been used in the past. Assuming a uniform density in the radial direction for a given latitude the barometric model for interstellar absorption gives

$$N_H^{ab} = n_H(0)\ Z_o \csc(b)\ [1 - \exp(-\frac{R}{Z_o \csc(b)})\ ] \qquad (74)$$

where N_H^{ab} = x-ray absorption in H atoms/cm^2

$n_H(0)$ = density of hydrogen gas in the galactic disk at b = 0°

Z_o = e-fold height in density of gas

R = distance of source

In the case of emission

$$N_H^{em} = n_H(0)\ Z_o \csc b \qquad (75)$$

since we can set R = ∞ for low latitude measurements of 21 cm emission. The ratio of equations 74 and 75 is determined from observations. For the case of a gaussian density distribution we have

$$N_H^{ab} = \int_0^R n_H(0) \exp(-\frac{r}{Z_1 \csc b})^2\ dr \qquad (76)$$

and

$$N_H^{em} = n_H(0)\frac{(Z_1 \csc b)^{1/2}\sqrt{\pi}}{2} \qquad (77)$$

where Z_1 = e-fold height of the gaussian distribution.

From Kerr and Westerhout (1965) the half density point is 110 pc. at the sun which makes Z_o = 158 pc. while for sources off the galactic plane in the direction of the galactic center for $|b| > 1^o$.

$Z_o \approx 158\ [1-(1 + 100 \tan (b))^{-1}]$ pc. (Ilovaisky, 1970) (78)

The optical depth velocity profiles were taken from Linblad (1965) where the assumed spin temperature T_g = 125°K. If the spin temperature fluctuates along the line of sight or the gas density varies so as to form optically thick regions the values of N_H^{em} could be in considerable error. If the optical depth is small, however, then the relation $T_b = T_g \tau$ where T_b is the temperature brightness is valid. In this case temperature brightness-velocity curves such as those published by Muller and Westerhout (1957) may be used in evaluating equation 71.

APPENDIX B

ENERGY CALIBRATION WITH THIN TARGET BREMSSTRAHLUNG

A continuous energy source of x-rays provides a more complete calibration of the detectors than "line" sources. A monoenergetic electron beam of 80 keV was used to produce x-rays by striking a .1 mil aluminum target (see Figure 32). The detector viewed the target at 90° to the incident electron beam and the region between the target and detector was evacuated to reduce low energy photon absorption. Since most of the electrons are scattered at small angles, the region in back of the target was extended to minimize backscattering of electrons which could ultimately enter the detector.

The theoretical non-relativistic bremsstrahlung cross section was taken from the results of Motz and Placious (1958) and is given by

$$d\sigma = A \left(\frac{Z_{eff}}{Z_{al}}\right) \left[\frac{T_o^2 + 2mc^2 T_o}{T_o + 2mc^2 T_o + (h\nu)^2}\right]^2 (1-\beta_o \cos\theta)^{-2} d\sigma_s \qquad (79)$$

where A = normalization constant due to distortion of wave functions by the Coulomb field of the aluminum nucleus

Z_{eff} = the effective atomic number for aluminum when screening is important

Z_{al} = atomic number of aluminum

T_o = kinetic energy of incident electron

mc^2 = rest mass of the electron

$h\nu$ = energy of radiated photon

$\beta_o = \frac{v_o}{c}$ for the incident electron

θ = angle at which radiation is produced relative to incident electron beam

$d\sigma$ = Sommerfeld-Kirkpatrick-Wiedmann cross section

The Sommerfeld-Kirkpatrick-Wiedmann cross section is approximated by equations 2, 8 and 9 in Kirkpatrick and Wiedmann(1945) and for our experiments $\theta = 90°$.

Comparing experimental data with equation 79 via the spectral analysis procedure 1 discussed in Chapter III and normalizing equation 79 to the total number of observed photons we find that in the energy range 5-20 keV acceptable fits occur. Below 5 keV, however, the theoretical cross-section overestimates the observations by about 30%. This is probably due to the retardation correction factor used by Motz and Placious (1958) who claim the error could be as large as a factor of 2. There are also several experimental errors which become important at low energies. First, our detector window absorption must be accounted for and second, absorption of photons escaping from the aluminum target has to be corrected for. Figure 33 gives an illustration of the theoretical and experimental spectra normalized to all data between 2 and 20 keV.

The theoretical spectrum was calculated for 80 keV electrons. Attenuation of photons with energies less than about 5 keV is due to the detector window, 5 mils of beryllium covering the detector window in order to eliminate any scattered electrons which might enter the detector, and a 1 mil mylar window separating the detector from the vacuum system in which the electrons are produced. All of the window absorption coefficients were taken from Storm and Israel (1967) and incorporated in the analysis.

REFERENCES

Abramowitz, M. and Stegun, I. E., 1964, Handbook of Mathematical Functions, (National Bureau of Standards).

Alexander, J. K., Brown, L. W., Clark, T. A., Stone, R. G., and Weber, R. R., 1969, Ap. J. (Letters) 157, L163.

Allen, C. W., 1963, Astrophysical Quantities, (Athlone Press, London).

Anand, K. C., Daniel, R. R., and Stephens, S. A., 1968, Proc. Ind. Acad. Sci. 67A, 267.

Angel, J. R. P., 1969, Nature 224, 160.

Bass, F. G., and Yakovenko, V. M., 1965, Soviet Physics Uspekki 8, 420.

Bell, K. L., and Kingston, A. E., 1967, Mon. Not. R. Astr. Soc. 136, 241.

Berger, M. J., and Settzer, S. M., 1964, Tables of Energy Losses and Ranges of Electrons and Positrons, (NASA Report SP-3012, Washington).

Bertsch, D. L., Fichtel, C. E., and Reames, D. V., 1969, Ap. J. (Letters) 157, L53.

Bleeker, J. A. M., and Deerenberg, A. J. M., 1970, Nature 227, 470.

Boldt, E., 1970, Observed Galactic Hard X-Ray Emission as an Indication for Cosmic Ray Heating of Interstellar Hl, (NASA document X-661-70-422).

Bolton, C. T., 1972, Nature 235, 271.

Bowyer, S., Byram, E. T., Chubb, T. A., and Friedman, H., 1965, Science 147, 394.

Brecher, L., and Morrison, P., 1969, Phys. Rev. Letters 23, 802.

Brisken, A. F., 1971, Line Emission from Laboratory X-Ray Sources, preprint.

Brown, R., and Gould, R., 1970, Phys. Rev. D1, 2252.

Bunner, A. N., Coleman, P. L., Kraushaar, W. L., and McCammon, D., 1971, Ap. J. (Letters) 167, L3.

Burton, W. B., 1970, Astron. and Astrophysics Suppl. 2, 261.

Byram, E. T., Chubb, T. A., and Friedman, H., 1966, Science 152, 166.

Cancro, C. A., Crockett, W. R., Garrahan, N. M., McGowan, R. G., 1968, X-Ray Experiment Electronics for High Altitude Balloon and Rocket Flights, (NASA document X-711-68-74).

Cathey, L. R., and Hayes, J. E., 1968, Ap. J. (Letters) 151, L89.

Chapman, R. D., 1969, Ap. J. 156, 87.

Clark, G. W., Garmire, G. P., and Kraushaar, W. L., 1968, Ap. J. (Letters) 153, L203.

Contopolous, G., and Stromgren, B., 1965, Tables of Plane Galactic Orbits, (NASA Institute for Space Studies, New York).

Cooke, B. A., Griffiths, R. E., and Pounds, K. A., 1969, Nature 224, 134.

Cooke, B. A., and Pounds, K. A., 1971, Nature 229, 144.

Cowsik, R., and Pal, Y., 1969, Phys. Rev. Letters 23, 1467.

Daltabuit, E., 1970, Angular Distribution of Interstellar Atomic Hydrogen, preprint .

Davison, B., 1957, Neutron Transport Theory, (Oxford: Clarendon Press, London).

Dolan, J. F., 1970, Space Science Rev. 10, 830.

Dolan, J. F., 1971, Nature 233, 109.

Elwert, G., 1954, Naturforsch 53, 637.

Felten, J. E., and Rees, M. J., 1972, Astron. and Astrophysics 17, 226.

Fisher, P. C., Johnson, H. M., Jordan, W. C., Meyerott, A. J., and Acton, L., 1966, Ap. J. 143, 203.

Freitas Pacheco, J. A. de, 1970, Astron. and Astrophysics 8, 420.

Garibyan, G. M., 1960, Soviet Physics JETP 37, 372.

Giacconi, R., Gursky, H. Paolini, F. R., 1962, Phys. Rev. Letters 9, 439.

Giacconi, R., Gorenstein, P., Gursky, H., Usher, P. D., Waters, J. R., Sandage, A., Osmer, P., and Peach, J., 1967a, Ap. J. (Letters) 148, L129.

Giacconi, R., Gorenstein, P., Gursky, H., and Waters, J. R., 1967b, Ap. J. (Letters) 148, L119.

Giacconi, R., Gursky, H., Kellogg, E., Murray, S., Schreier, E., and Tananbaum, H., 1971, The UHURU Catalog of X-Ray Sources, A.S.E. document 2855.

Goldberg, L., Muller, E. A., and Allen, L. H., 1960, Ap. J. (Suppl.) 45, 1.

Goldstein, M. L., Ramaty, R., and Fisk, L. A., 1970, Phys. Rev. Letters 24, 1193.

Gorenstein, P., Giacconi, R., and Gursky, H., 1967, Ap. J. (Letters) 150, L85.

Gorenstein, P., Harris, B., Gursky, H., Giacconi, R., Novick, R., Vanden Bout, P., 1971, Science 172, 369.

Gould, R. J., 1965, Phys. Rev. Letters 15, 577.

Grader, R. J., Hill, R. W., and Stoering, J. P., 1970, Ap. J. (Letters) 161, L45.

Gursky, H., Gorenstein, P., Kerr, F. J., and Grayzeck, E. J., 1971, Ap. J. (Letters) 167, L15.

Hayakawa, S., Kato, T., Makino, F., Ogawa, H., Tanaka, Y., and Yamashita, K., 1970, Non Solar X- and Gamma Ray Astronomy, L. Gratton, editor, (Dordrecht: D. Reidel Publishing Co.).

Haymes, R. C., Ellis, D. V., Fishman, G. J., Glenn, S. W., and Kurfess, J. D., 1968, Ap. J. (Letters) 151, L125.

Heitler, W., 1954, The Quantum Theory of Radiation, (Oxford Univ. Press, London).

Hjellming, R. M., Gordon, C. P., and Gordon, K. J., 1969, Astron. and Astrophysics 2, 202.

Hjellming, R. M., and Wade, C. M., 1971, Ap. J. (Letters) 168, L21.

Hjellming, R. M., and Wade, C. M. 1972, Nature 235, 271.

Holt, S. S., Boldt, E. A., Schwartz, D. A., Serlemitsos, P. J., and Bleach, R. D., 1971, Ap. J. (Letters) 166, L65.

Hudson, H. S., Peterson, L. E., and Schwartz, D. A., 1971, Nature 230, 177.

Ilovaisky, S. A., and Ryter, C., 1971, Astron. and Astrophysics 15, 224.

Ilovaisky, S. A., 1971, Astron. and Astrophysics 11, 134.

Ipavich, F., and Lenchek, A., 1970, Phys. Rev. D2, 266.

Johansson, S. A. E., 1971, Astrophysical Lett. 9, 143.

Jordan, C., 1970, Mon. Not. R. Astr. Soc. 148, 17.

Kamata, K., Shibata, S., Saavedra, O., Domingo, V., Suga, K., Murakami, K., Toyoda, Y., LaPointe, M., Gaebler, J., and Escobar, I., 1968, Can. Journ. Phys. 46, S72.

Karzas, W. J., and Latter, R., 1961, Ap. J. (Suppl.) 6, 167.

Katgert, P., 1969, Astron. and Astrophysics 1, 54.

Kerr, F. J., and Westerhout, G., 1965, Stars and Stellar Systems Vol V, A. Blaauw and M. Schmidt, Editors, (The University of Chicago Press, Chicago).

Kirkpatrick, P. and Wiedmann, L., 1945, Phys. Rev. 67, 321.

Kraft, R. P., and Demoulin, M. H., 1967, Ap. J. (Letters) 150, L183.

Lindblad, P. O., 1965, Bull. Astr. Inst. Netherlands Suppl. 1, 77.

Loh, E. D., and Garmire, G. P., 1971, Ap. J. 166, 301.

Manley, O. P., and Olbert, S., 1969, Ap. J. 157, 223.

Matteson, J. L., 1971, An X-Ray Survey of the Cygnus Region in the 20 to 300 keV Energy Range, Ph.D. Thesis, University of California, San Diego.

McGee, R. X., and Murray, J. D., 1961, Austr. J. of Physics 14, 260.

Minkowski, R., 1968, Rev. Mod. Phys. 30, 1048.

Motz, J. W., and Placious, R. C., 1958, Phys. Rev. 109, 235.

Muller, C. A., and Westerhout, G., 1957, Bull. Astr. Inst. Netherlands 13, 151.

Nussbaumer, H., and Swings, J. P., 1970, Astron. and Astrophysics 7, 455.

Oda, M., Gorenstein, P., Gursky, H., Kellogg, E., Schreier, E., Tananbaum H., and Giacconi, R., 1971, Ap. J. (Letters) 166, L1.

Overbeck, J. W., and Tananbaum, H. D., 1968a, Phys. Rev. Letters 20, 24.

Overbeck, J. W., and Tananbaum, H. D., 1968b, Ap. J. 153, 899.

Parker, R. A. R., 1967, Ap. J. 149, 363.

Pearson, K., 1900, Phil. Mag. 50, 157.

Peterson, L. E., Jacobson, A. S., Pelling, R. M., and Schwartz, D. A., 1968, Can. J. Phys. 46, S437.

Pikel'ner, S. B., and Tsytovich, V. N., 1969, A. J. (U.S.S.R.) 46, 8.

Pottasch, S. R., 1968, Origin and Distribution of the Elements, L. H. Ahrens, Editor, (Pergamon Press, London).

Prendergast, K. H., and Burbidge, G. R., 1968, Ap. J. (Letters) 151, L83.

Ramaty, R., Boldt, E. A., Colgate, S. A., and Silk, J., 1971, Ap. J. 169, 87.

Ramaty, R., and Bleach, R., 1972, Astrophysical Letters 11, 35.

Rees, M. J., and Silk, J., 1969, Astron. and Astrophysics 3, 452.

Reynolds, R., 1971, An Investigation Into the Optical Fluorescence of Interstellar H1, Ph.D. Thesis, University of Wisconsin, Madison.

Rocchia, R., Rothenflug, R., Boclet, D., and Durouchoux, P., 1969, Astron. and Astrophysics 1, 48.

Ryter, C., 1970, Astron. and Astrophysics 9, 288.

Sartori, L., and Morrison, P., 1967, Ap. J. 150, 385.

Schmidt, M., 1965, Stars and Stellar Systems Vol. V, A. Blaauw and M. Schmidt, Editors, (The University of Chicago Press, Chicago).

Schwartz, D. A., 1969, The Spatial Distribution of the Diffuse Component of Cosmic X-Rays, Ph.D. Thesis, University of California, San Diego.

Schwartz, D. A., Boldt, E. A., Holt, S. S., Serlemitsos, P. J., and Bleach, R. D., 1971, Nature 233, 110.

Seaton, M. J., 1964, Planet. Space Sci. 12, 55.

Setti, G. and Woltjer, F., 1970, Astrophysics and Sp. Sci. 9, 185.

Seward, F. D., 1970, An Illustrated Catalog of Cosmic X-Ray Sources, Report UCID 15622, Lawrence Radiation Laboratory, Livermore.

Shane, W. W. and Bieger-Smith, G. P., 1966, Bull. Astr. Inst. Netherlands 18, 263.

Shen, C. S., 1969, Phys. Rev. Letters 22, 568.

Shukla, P. G., and Wilson, B. G., 1971, Ap. J. 164, 265.

Silk, J., and Steigman, G., 1969, Phys. Rev. Letters 23, 597.

Storm E., and Israel, H. I., 1967, Photon Cross Sections from .001 to 100 MeV for Elements 1 through 100, Los Alamos Scientific Laboratory Report LA-3753.

Tucker, W. H., 1966, Cosmic X-Ray Sources, Ph.D. Thesis, University of California, San Diego.

Tucker, W. H., 1971, Science 172, 372.

Urey, H. C., 1967, Quart. J. Roy. Astron. Soc. 8, 23.

Van Regemorter, M. H., 1962, Ap. J. 136, 906.

Vette, J. I., Gruber, D., Matteson, J. L., and Peterson, L. E., 1970, Ap. J. (Letters) 160, L161.

Webber, W. R., and Reinert, C. P., 1970, Ap. J. 162, 883.

Wendker, H. J., 1970, Astron. and Astrophysics 4, 378.

TABLE I. Compilation of flight information.

AEROBEE 170 ROCKET FLIGHTS

G.S.F.C. FLIGHT NUMBER	13.07	13.08
FLIGHT DATE	21 SEPT. 1970 10:30 M.S.T.	9 AUG. 1971 22:30 M.S.T.
LAUNCH LOCATION	WHITE SANDS MISSILE RANGE NEW MEXICO	WHITE SANDS MISSILE RANGE NEW MEXICO
APOGEE	91 MILES	88 MILES
DETECTORS	1 ARGON — 9:1 ARGON TO METHANE AT 840mm PRESSURE 1 XENON — 9:1 XENON TO METHANE AT 840mm PRESSURE	SAME AS 13.07
COLLIMATION (FWHM)	1.8° x 7.1°	SAME AS 13.07
DETECTOR NET AREA	650 cm^2	SAME AS 13.07
DETECTOR WINDOW	1 MIL ALUMINIZED MYLAR	1 MIL ALUMINIZED KAPTON
USEABLE ENERGY RANGE	ARGON – 2 – 20 KEV XENON – 2 – 40 KEV	ARGON 1.5 – 20 KEV XENON 2 – 40 KEV
OBJECTS VIEWED	CYGNUS X-1 CYGNUS X-2 CYGNUS X-3	GALACTIC PLANE FROM ℓ = 354° TO 90° WITH LATITUDE SCAN AT ℓ = 61.8°, b = ± 7.5°

TABLE II. Photon energies of radioactive calibration sources (taken from Brisken, A. F. (1971))

RADIOACTIVE CALIBRATION SOURCES

SOURCE	DECAY MODE	$T_{1/2}$	ENERGY (KEV)	RELATIVE LINE INTENSITY	EFFECTIVE ENERGY (KEV)
$_{26}Fe^{55}$	E.C. K	2.7 Yr.	5.899 5.888 6.492	1.0 .52 .18	5.96
$_{27}Co^{57}$	E.C. γ K	270d.	14.37 6.404 6.391 7.059	1.0 1.0 .52 .19	14.37 6.47
$_{48}Cd^{109}$	E.C. K	470d.	22.163 21.990 24.942 24.912 25.455	1.0 .52 .184 .092 .029	22.58
RATIO OF L TO K ABOUT .2	L		2.984 3.151 3.346 2.978 3.235 3.204	1.0 .55 .20 .12 .085 .064	3.08
$_{56}Ba^{133}$	E.C. K	7.2 Yr.	30.973 30.625 34.987 34.920 35.896	1.0 .52 .205 .103 .074	31.72
$_{61}PM^{145}$	E.C. K	18 Yr.	37.361 36.847 42.271 42.166 43.441	1.0 .52 .216 .108 .082	38.30

TABLE III. Characteristic x-ray line energies (keV) of various materials.

CHARACTERISTIC X-RAYS FROM VARIOUS MATERIALS

TARGET MATERIAL	TRANSITION	MEAN PHOTON ENERGY	WEIGHTED AVERAGE
Al	Kα	1.487	1.487
P	Kα Kβ	2.014 2.142	2.020
S	Kα Kβ	2.307 2.468	2.317
Cl	Kα Kβ	2.622 2.817	2.636
K	Kα Kβ	3.312 3.589	3.337
Ca	Kα Kβ	3.690 4.012	3.719
Ti	Kα Kβ	4.508 4.931	4.550
Cr	Kα Kβ	5.411 5.947	5.467

TABLE IV. Parameters used in the response function of the proportional chambers.

DETECTOR RESPONSE FUNCTION PARAMETERS

DETECTOR	FLIGHT NUMBER	ENERGY CALIBRATION (KEV PER CHANNEL)	ENERGY RESOLUTION (FWHM)	ELECTRON PATH LENGTH FACTOR α	FLUORESCENT RADIATION $f_n \times g_{nln'l'}$
X^+ XENON	13.07	~.28 ABOVE 3.5 KEV	$.518\sqrt{E}$	2.45×10^{-4}	.124 FOR L X-RAYS AT 4.33* KEV .70 FOR Kα X-RAYS AT 29.7* KEV .3 FOR Kβ X-RAYS AT 33.8* KEV
	13.08	~.369 ABOVE 4.2 KEV	$.494\sqrt{E}$	1.23×10^{-4}	
A^+ ARGON	13.07	~.259 ABOVE 3.5 KEV	$.518\sqrt{E}$	2.45×10^{-4}	.12 FOR K X-RAYS AT 2.98 KEV
	13.08	~.185 ABOVE 2.1 KEV	$.494\sqrt{E}$	1.23×10^{-4}	

* WEIGHTED AVERAGE
+ FIRST LAYER

TABLE V. Summary of Results.

SUMMARY OF RESULTS

FLIGHT	OBJECTS VIEWED	BEST FIT SPECTRA AE^{-n}		$A\,EXP(-E/kT)/E$	
		A	n	A	kT (KEV)
		PHOTONS $(CM^2-SEC-KEV)^{-1}$			
13.07	CYGNUS X-1	$7.4^{+2.4}_{-1.3}$	$2.6 \pm .3$	—	—
	CYGNUS X-2	—	—	$1.4 \pm .3$	$4.5 \pm .7$
	CYGNUS X-3 *	87	3.9	—	—
13.08	GALACTIC DISC $\ell = 61.8°$	PHOTONS $(CM^3-SEC-KEV)^{-1} \times 10^{-21}$			
		$8.5^{+3.8}_{-1.9}$	$2.8 \pm .5$	$5.6^{+6.7}_{-1.9}$	$2.1^{+1.4}_{-.8}$
	DIFFUSE EXTRAGALACTIC BACKGROUND	PHOTONS $(CM^2-SEC-KEV-STER)^{-1}$			
		$8.2^{+6.0}_{-3.8}$	$1.35 \pm .4$	—	—

* AT THE SOURCE, ASSUMING 1.6×10^{23} H ATOMS / CM^2 (BROWN & GOULD, 1970) INTERSTELLAR ABSORPTION

TABLE VI. Abundances of elements used for "optically thin" plasma emission.

RELATIVE ABUNDANCE N_Z/N_H

ELEMENT	MODEL 1 (UNIVERSAL ABUNDANCE)*	MODEL 2 (TUCKER MODEL 2)	MODEL 3 (TUCKER MODEL 3)
H	1.00	0.00	1.00
He	8.32×10^{-2}	1.00	0.16
C	3.98×10^{-4}	0.25	——
N	1.12×10^{-4}	——	——
O	8.91×10^{-4}	0.50	.075
Ne	1.00×10^{-4}	0.25	——
Mg	2.50×10^{-5}	——	——
Si	3.16×10^{-5}	0.05	.062
S	2.24×10^{-5}	——	——
A	7.59×10^{-6}	——	——
Fe	3.15×10^{-5}	6.00×10^{-3}	6.00×10^{-3}

*ABUNDANCES TAKEN FROM BROWN AND GOULD (1970) WITH IRON ABUNDANCE FROM NUSSBAUMER AND SWINGS (1970) ADDED.

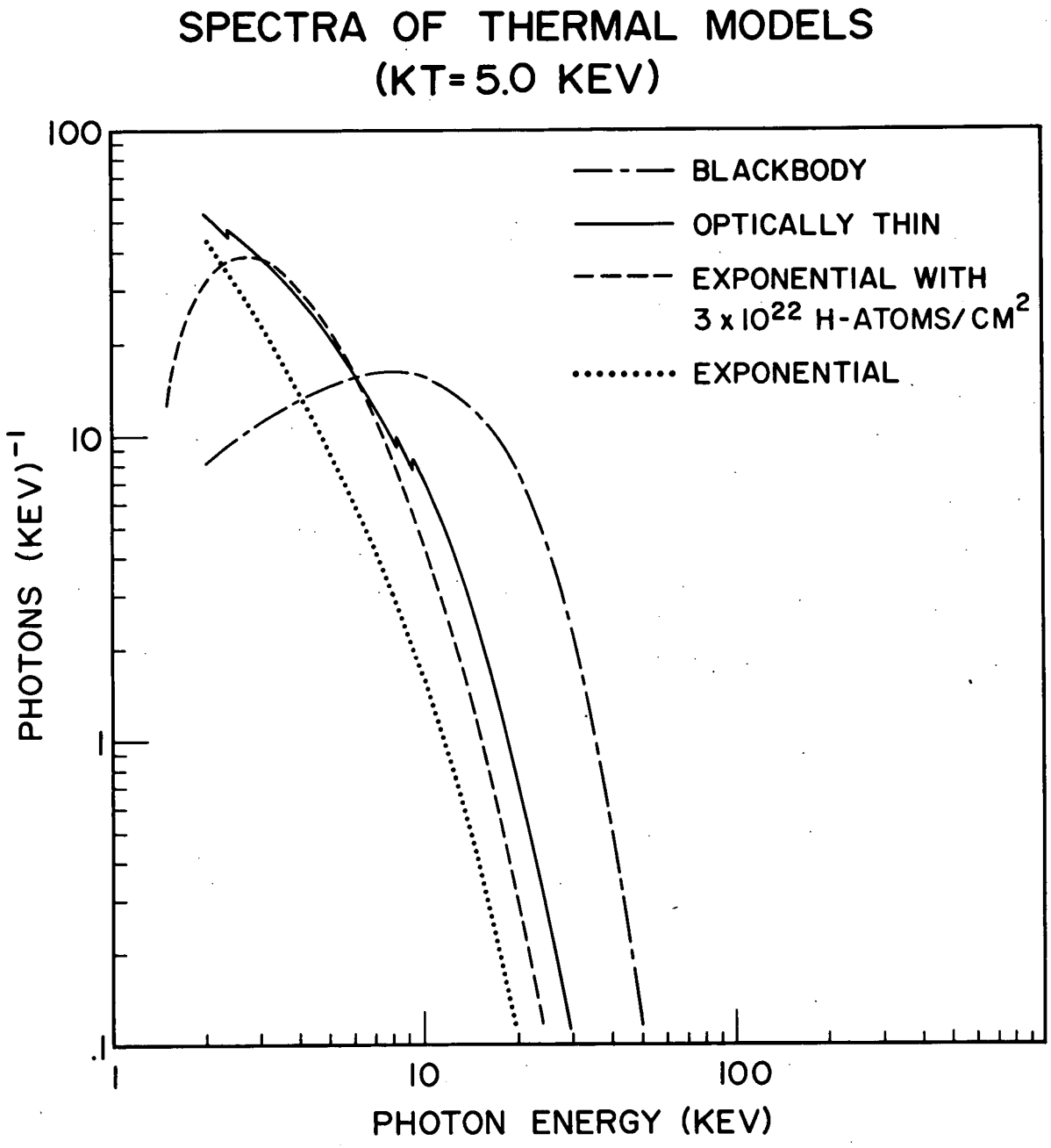

FIGURE 1 - Comparison of blackbody, "optically thin", exponential with photoelectric absorption resembling "optically thick", and exponential thermal spectra at a temperature corresponding to kT = 5.0 keV and normalized to the same number of counts between 0 and 50 keV

GALACTIC DISK MODEL

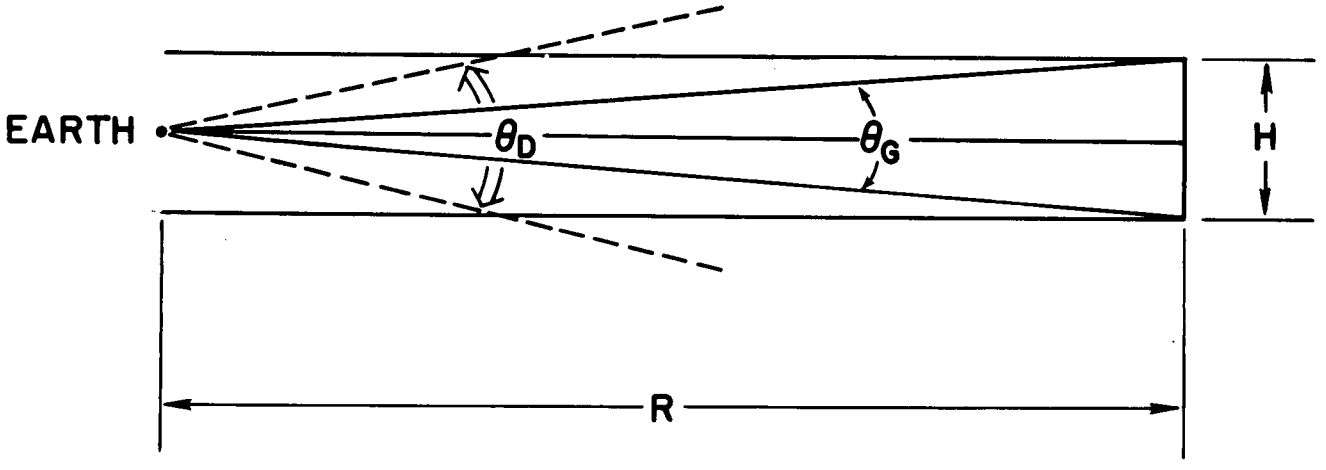

FIGURE 2 - Cross-section view of disk model with angular thickness θ_g seen by a detector with FWHM response θ_D. Thickness of the disk is H and distance from earth to the edge of the disk is R.

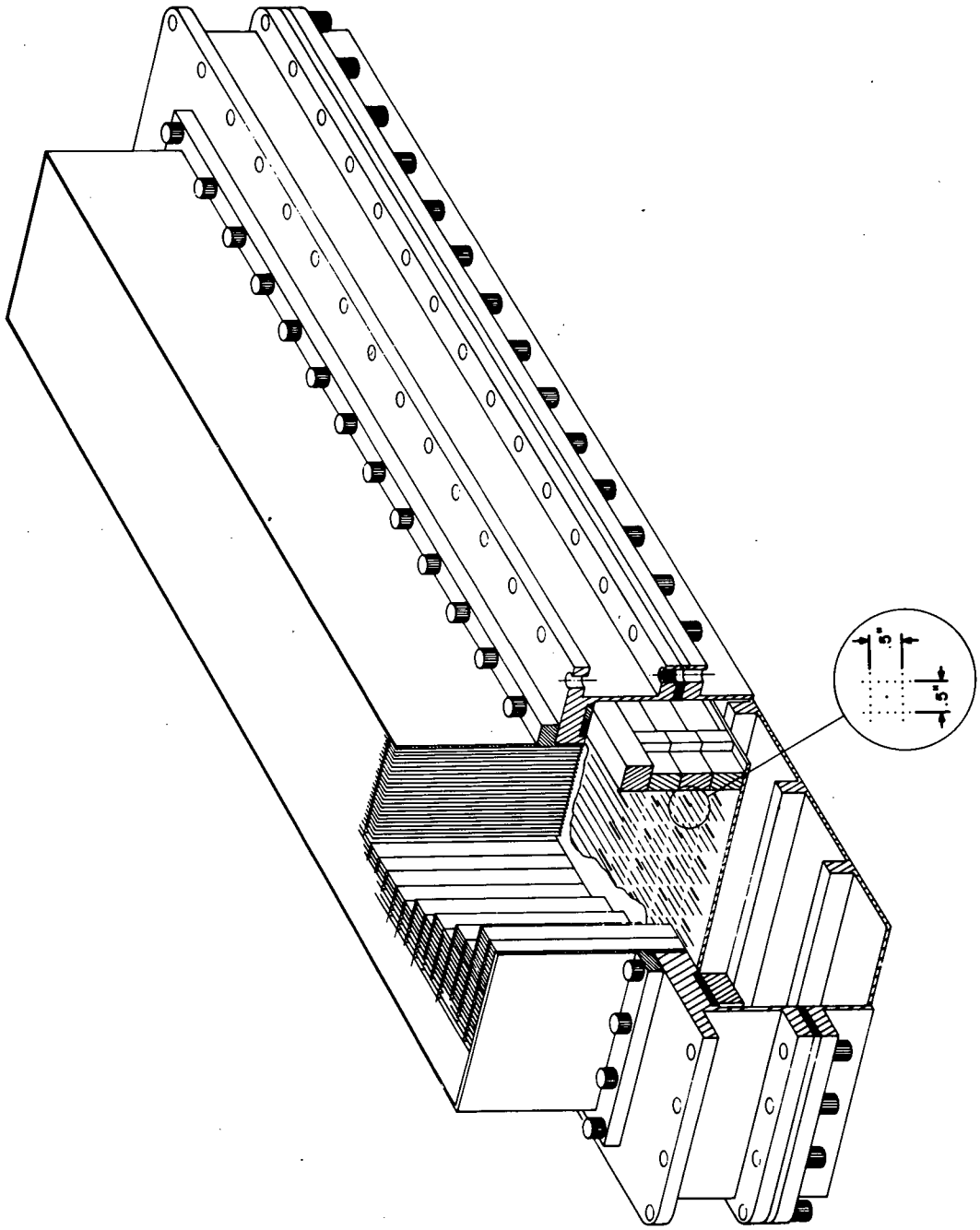

FIGURE 3 - An isometric view of the proportional chamber (not drawn to scale).

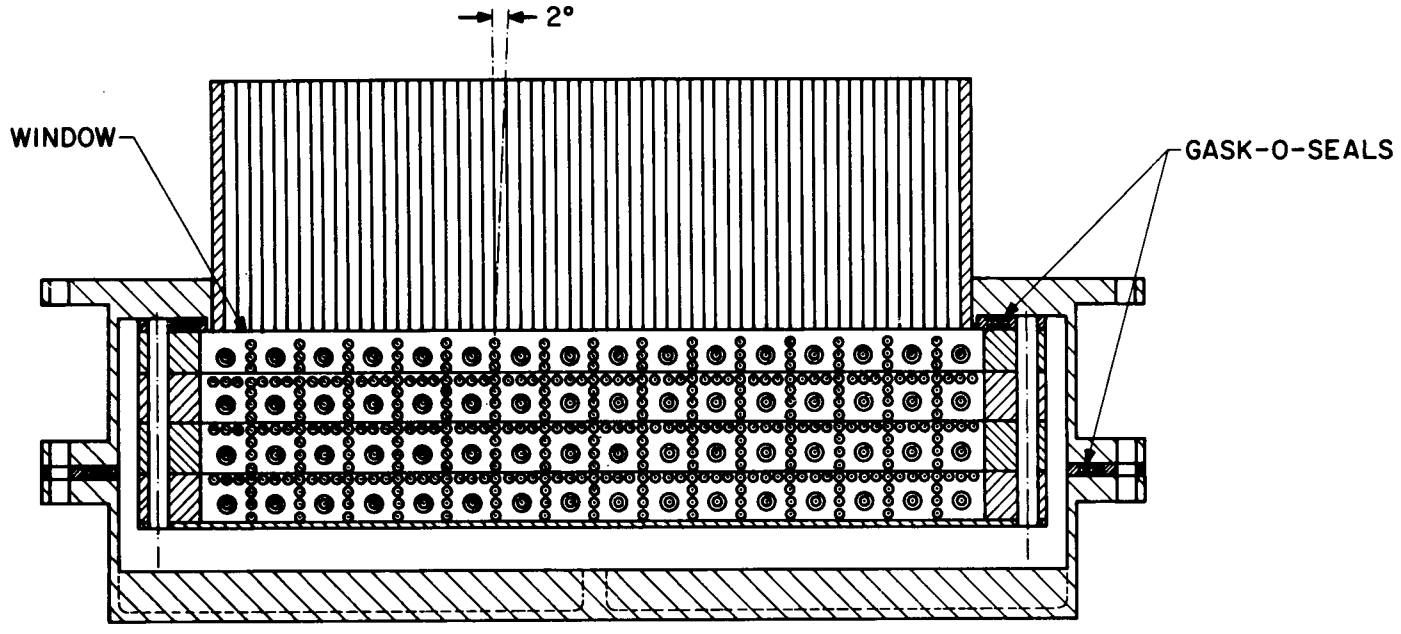

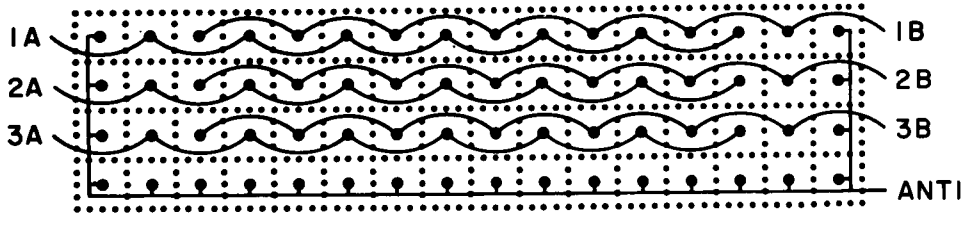

FIGURE 4 - top) Section view of the proportional chamber
bottom) Grouping of the 50 counter elements into 9 independent subgroups for background reduction purposes.

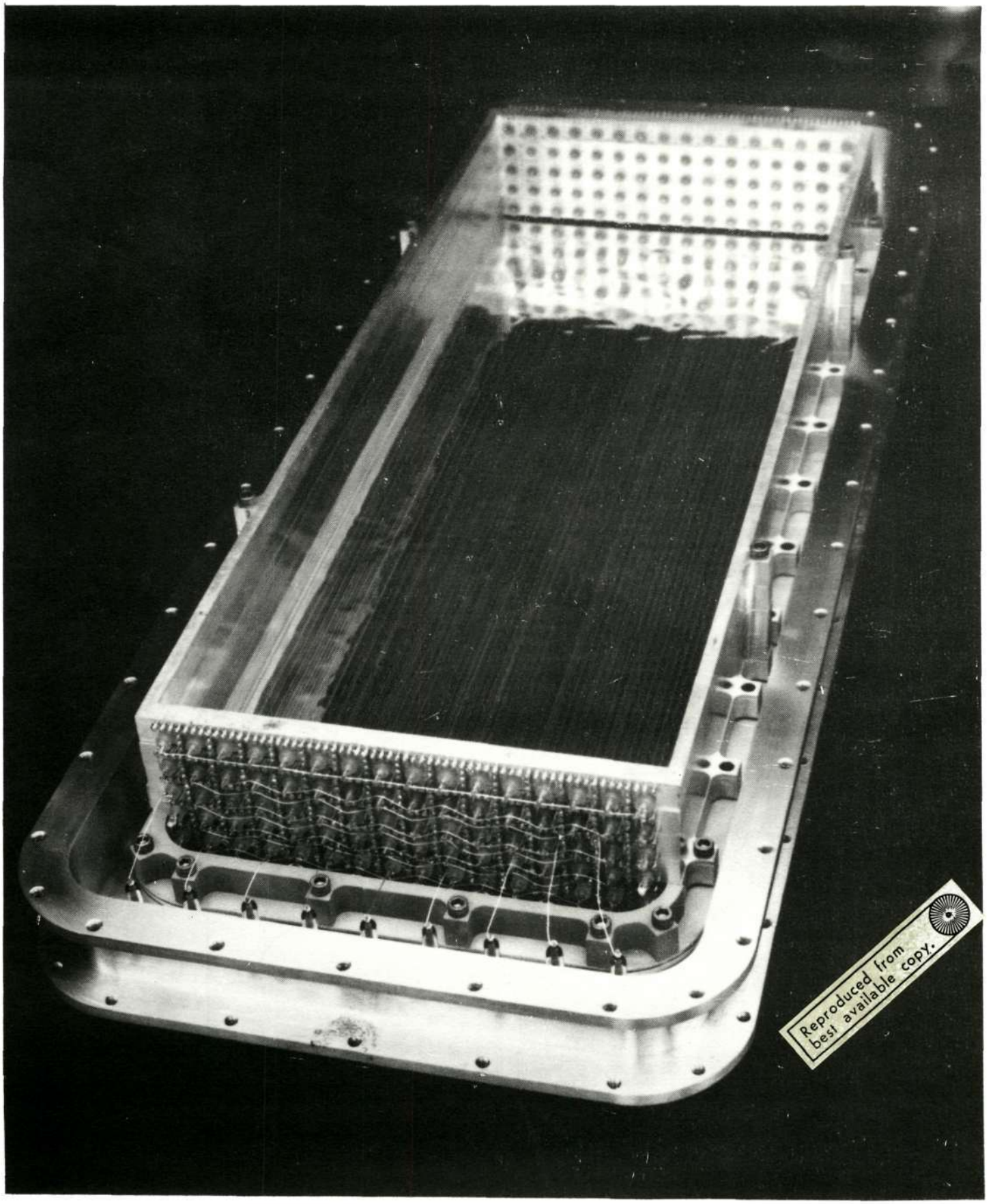

FIGURE 5 - A stack of 5 proportional chamber layers

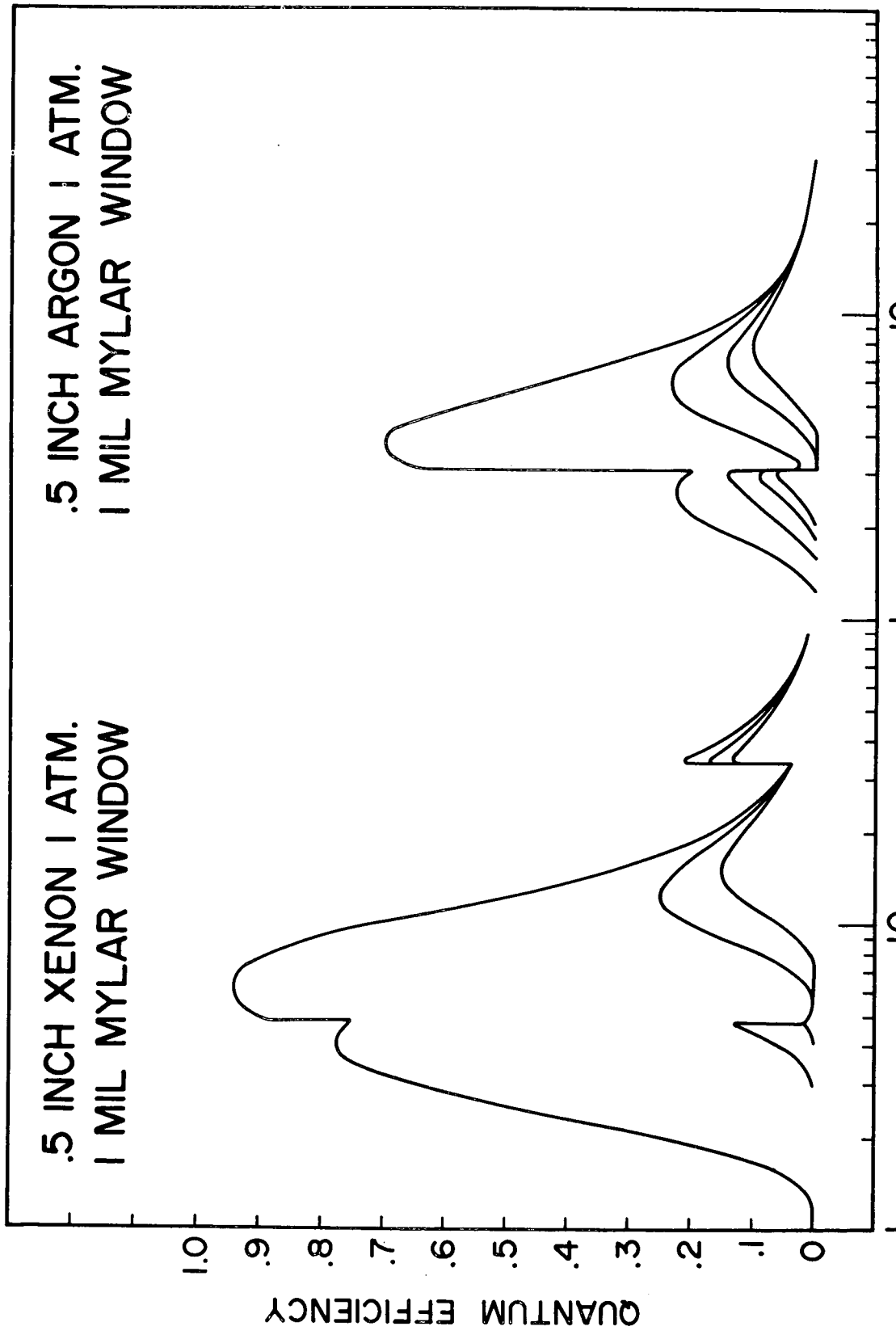

FIGURE 6 - Calculated layer efficiencies for: left) xenon chamber, right) argon chamber

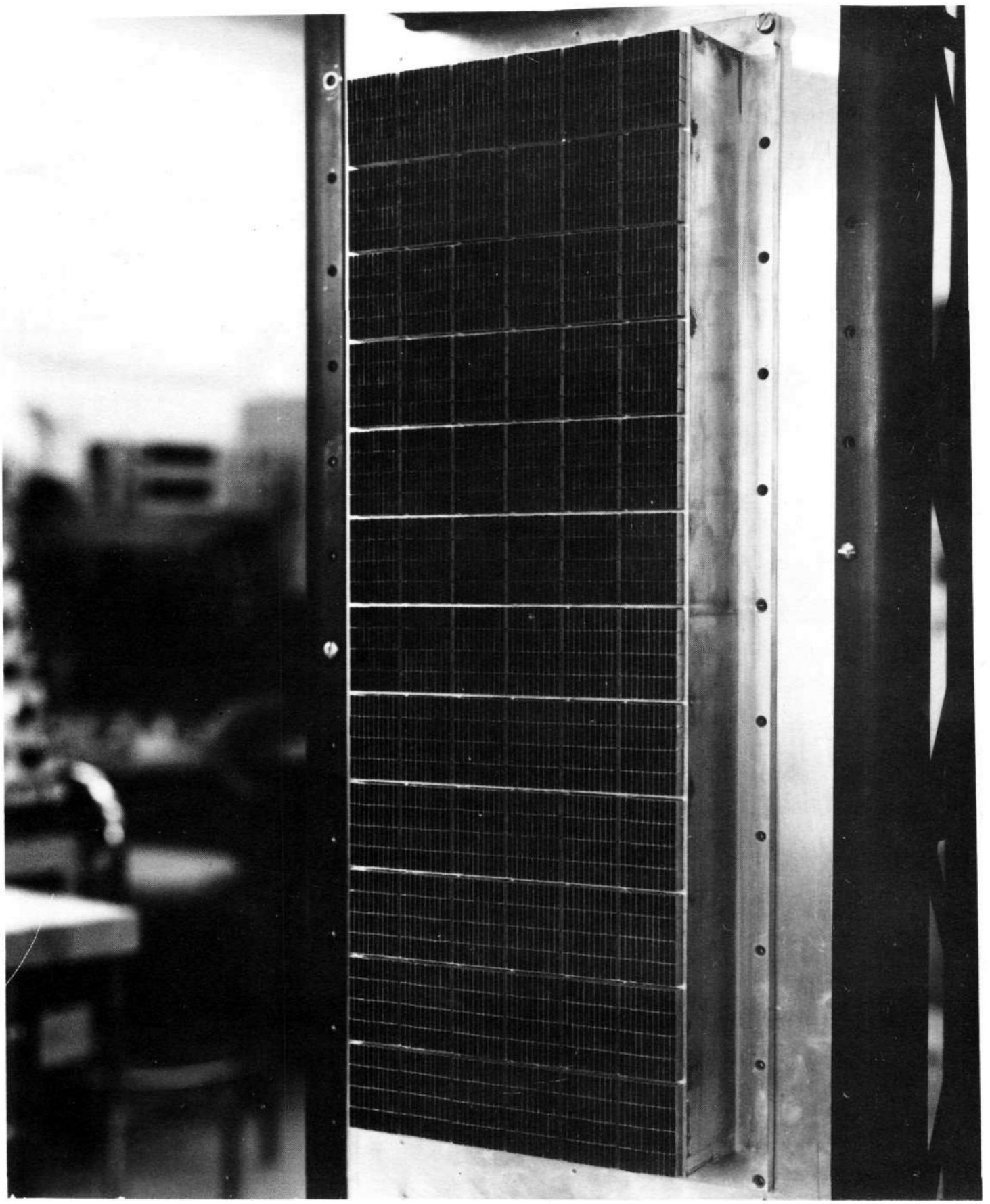

FIGURE 7 - 1.8° x 7.1° (FWHM) collimator for xenon and argon detectors

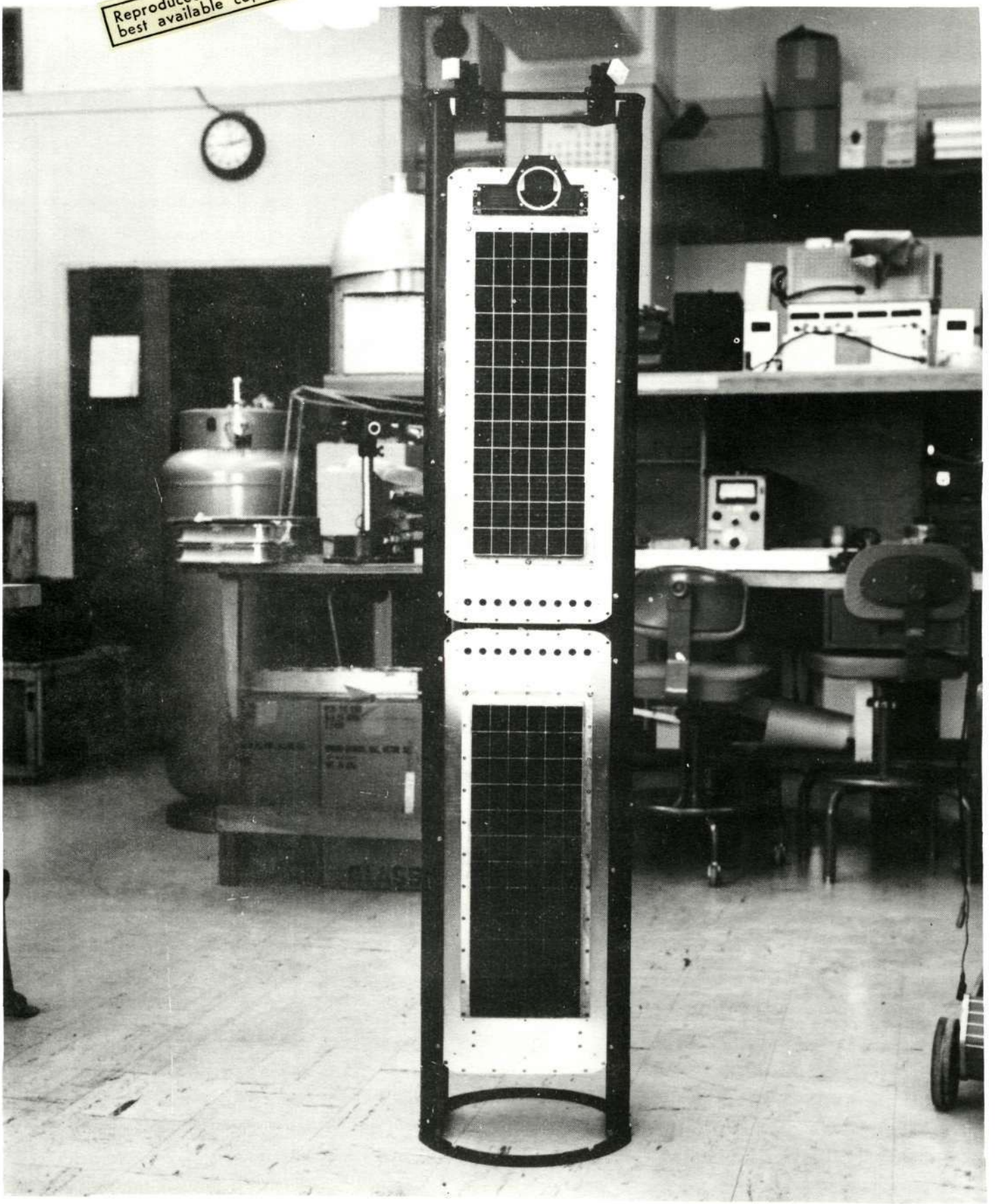

FIGURE 8 - Detectors mounted in payload frame

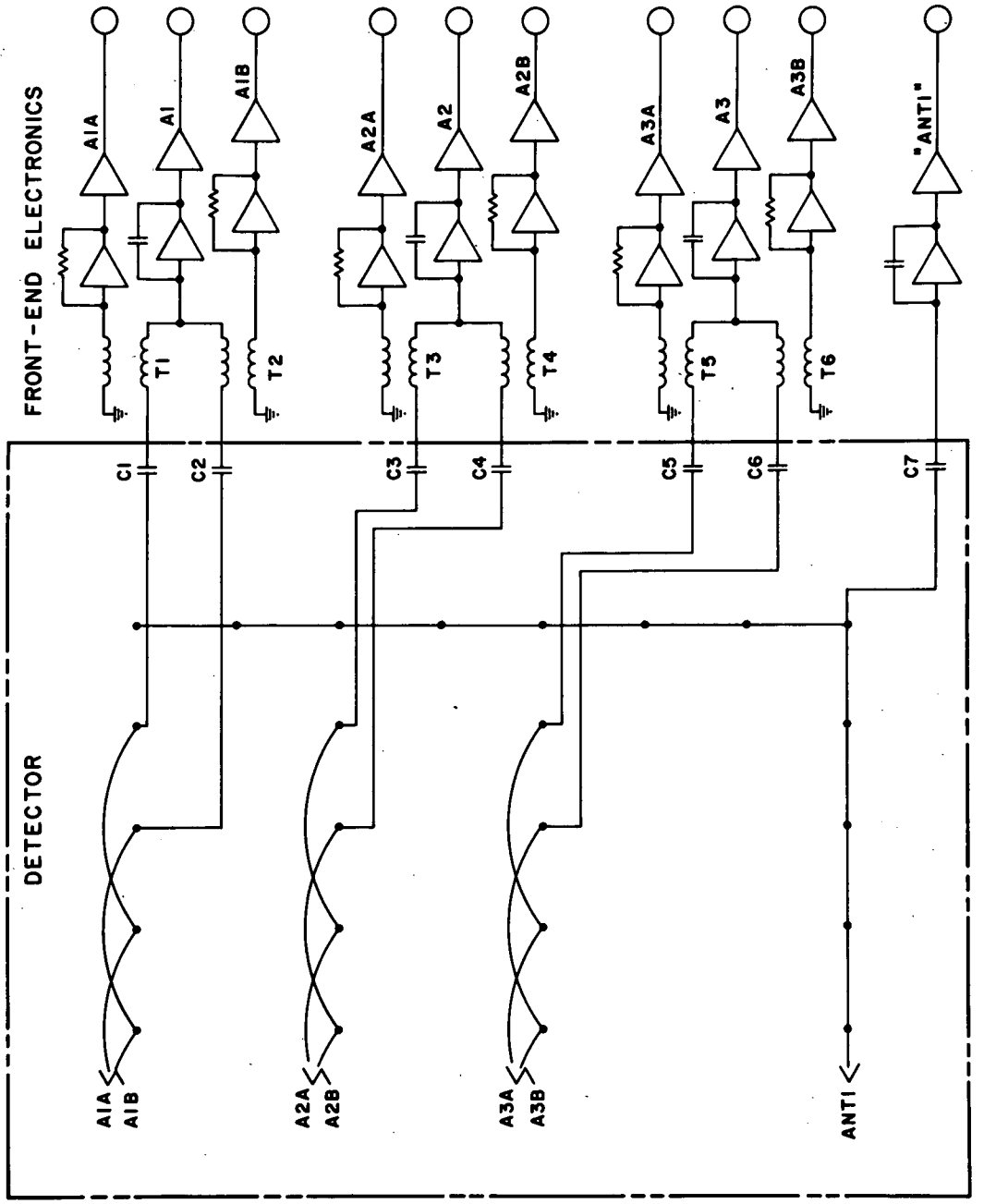

FIGURE 9 - Signal handling techniques through the use of pulse transformers and charge-sensitive preamplifiers.

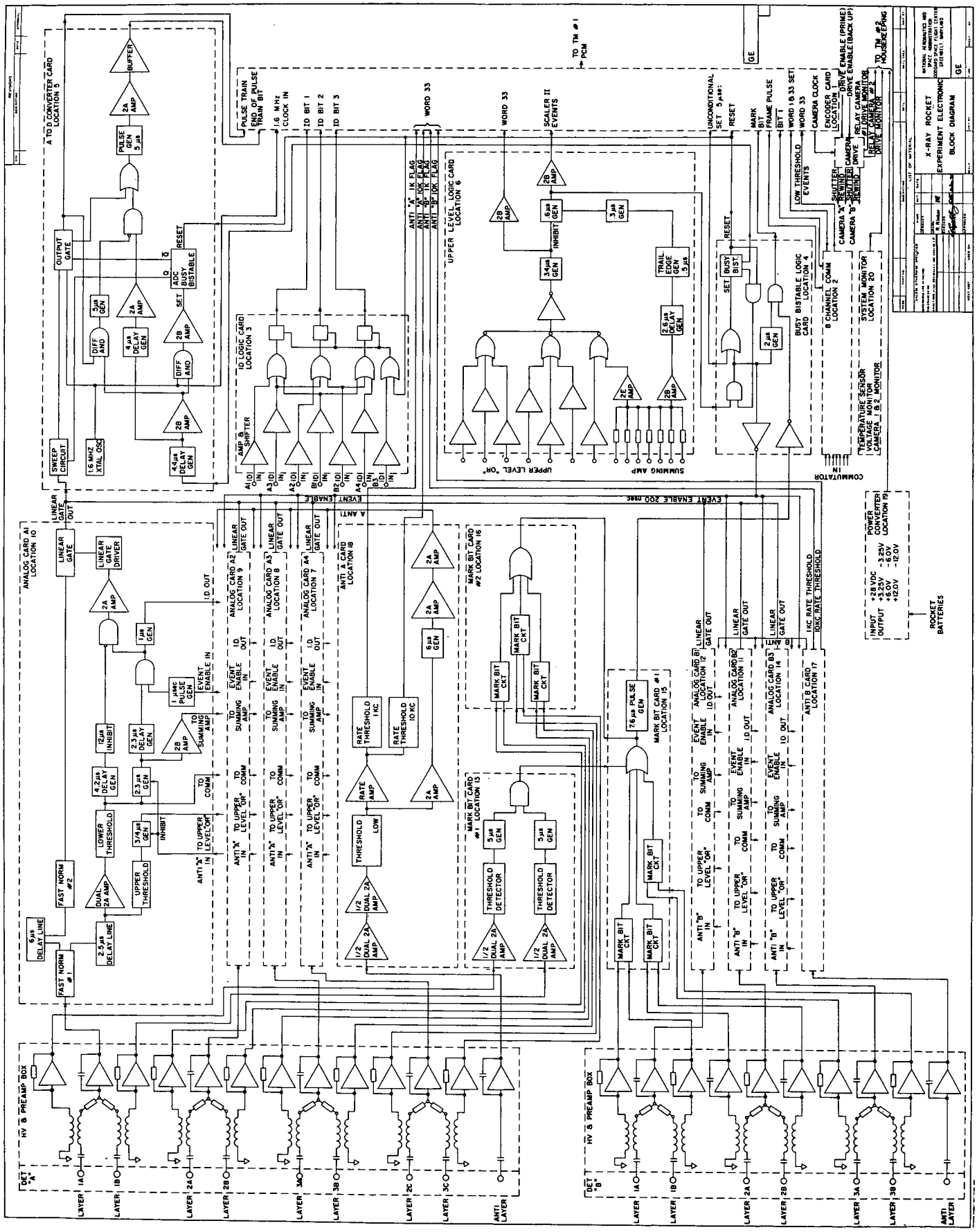

FIGURE 10 - Block diagram of the electronics

TELEMETRY READOUT FORMAT

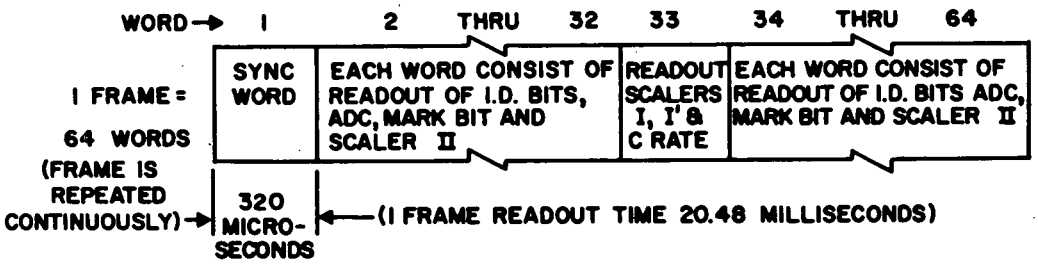

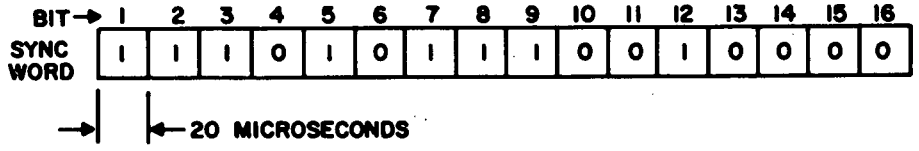

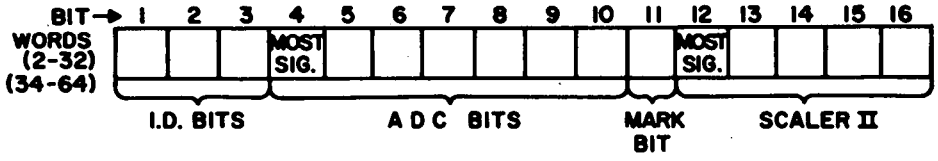

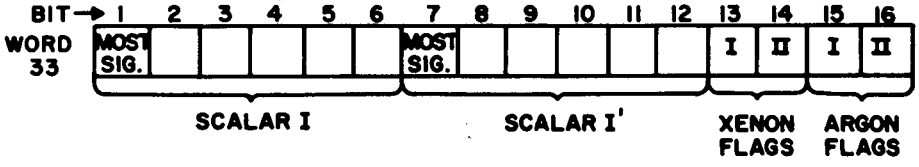

ID BIT CODE			
BITS	1	2	3
DET.			
A1	1	0	0
A2	0	1	0
A3	0	0	1
A4	1	1	0
B1	1	0	1
B2	0	1	1
B3	0	0	0

FIGURE 11 - Telemetry readout format

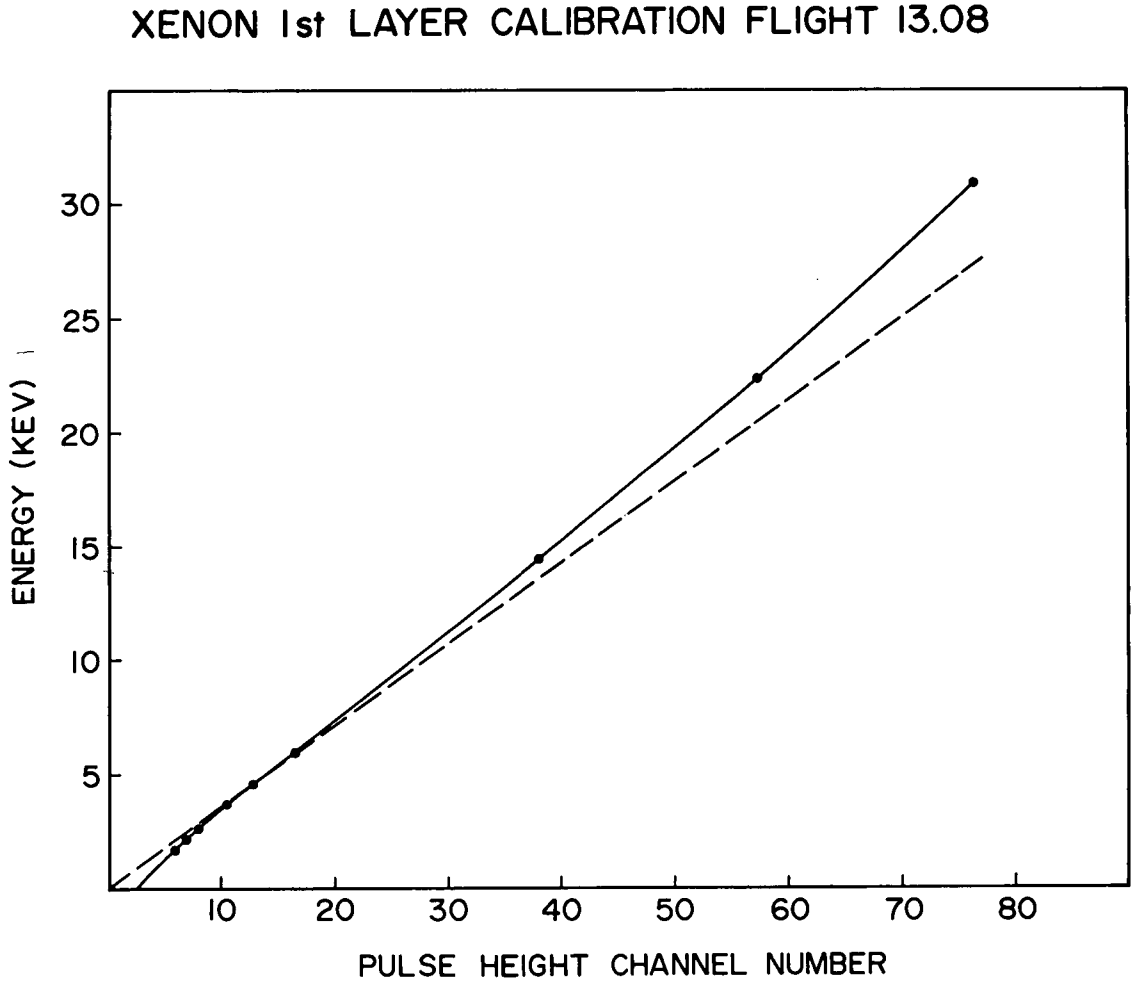

FIGURE 12 - Energy calibration for xenon 1st layer in flight 13.08 showing non-linearities. Dots represent data and the dashed line is the best fit to a linear response.

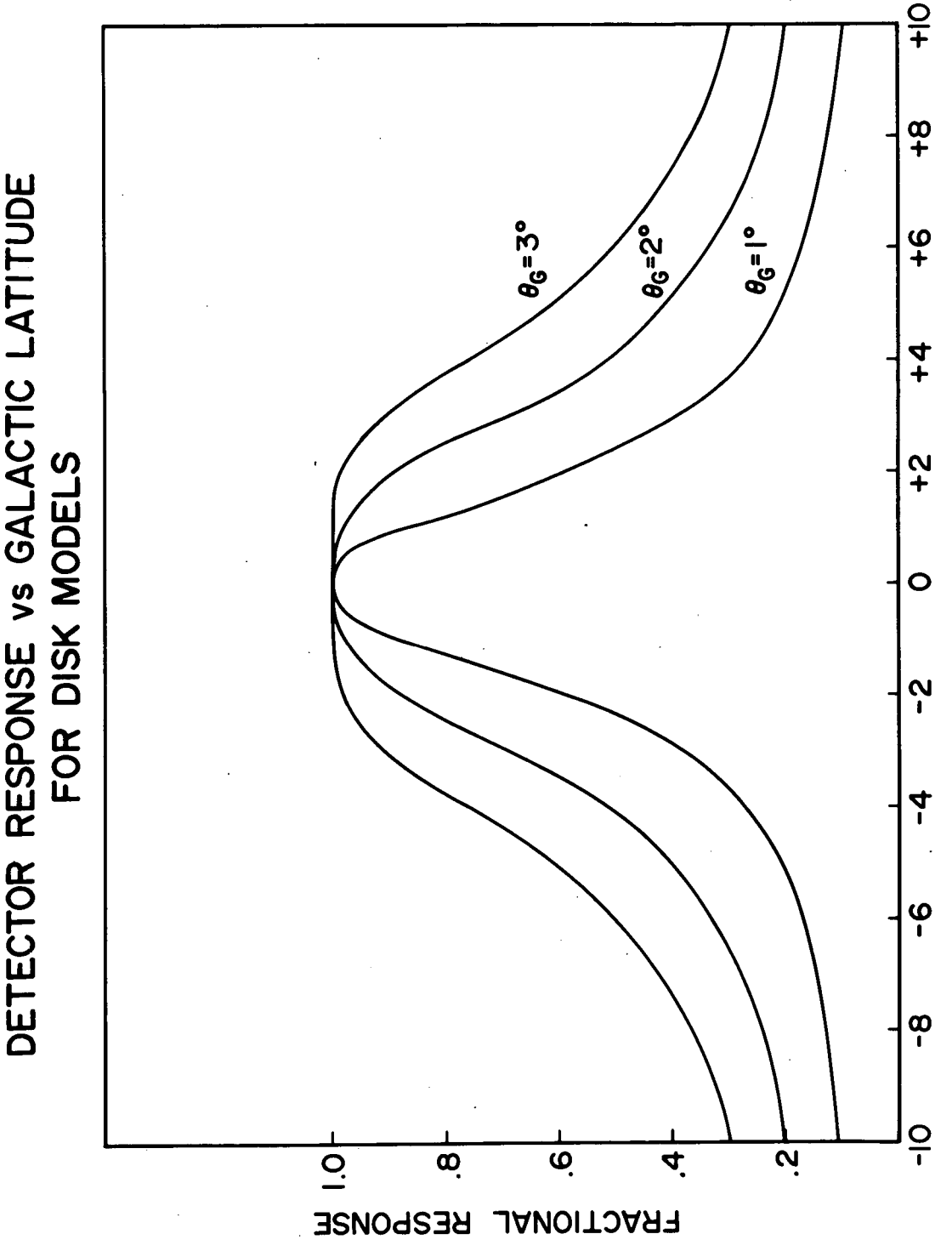

FIGURE 13 - Detector response with 1.8° FWHM collimation scanning perpendicular to the galactic plane for disk models with angular thickness θ_g

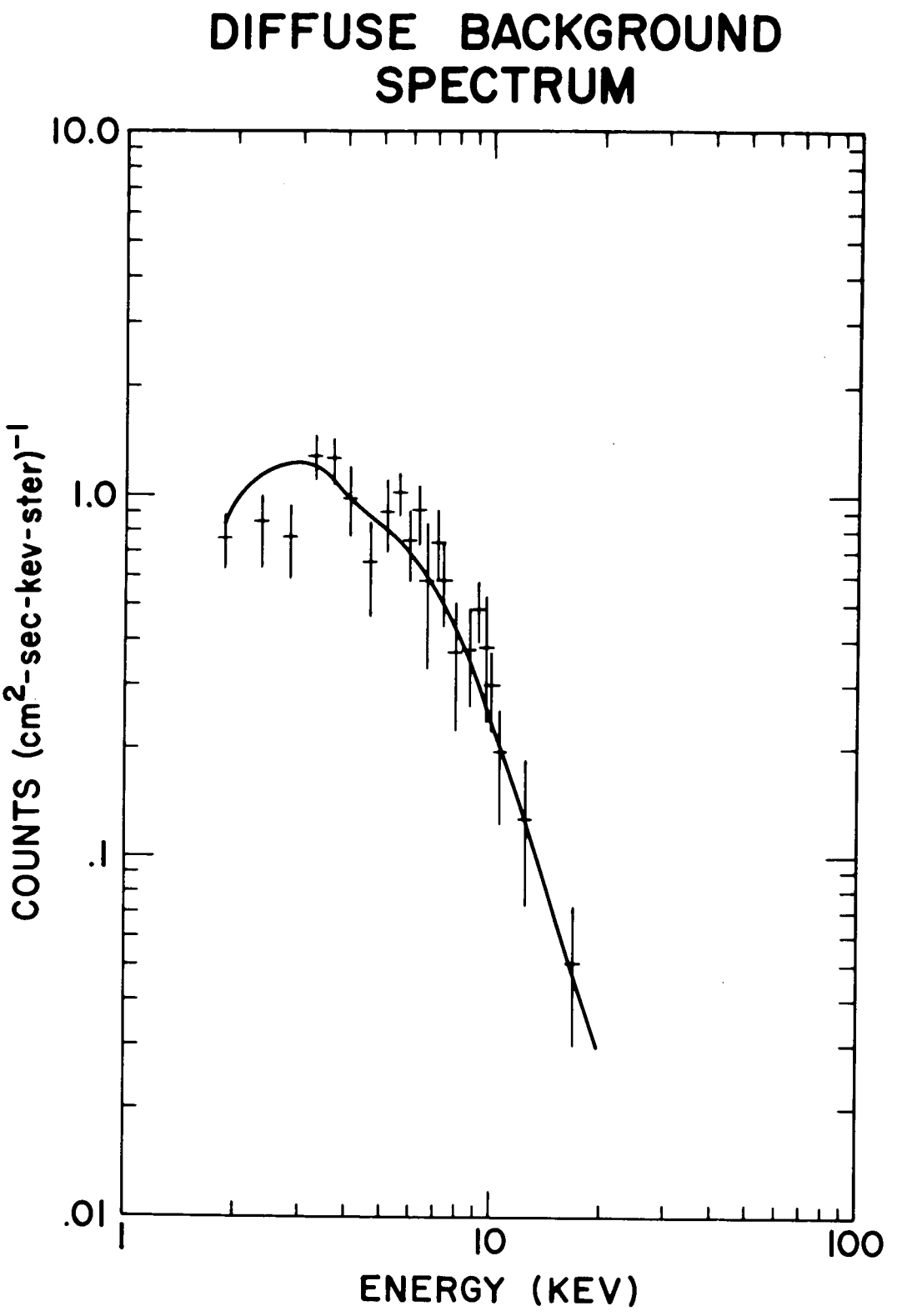

FIGURE 14 - Diffuse background spectrum from the xenon 1st layer for $|b| > 3.5°$ in flight 13.08. The solid line represents the best fit spectrum $8.2\ E^{-1.4}$ photons $(cm^2\text{-sec-ster-keV})^{-1}$ folded through the detector response. No efficiency corrections were made to the displayed data.

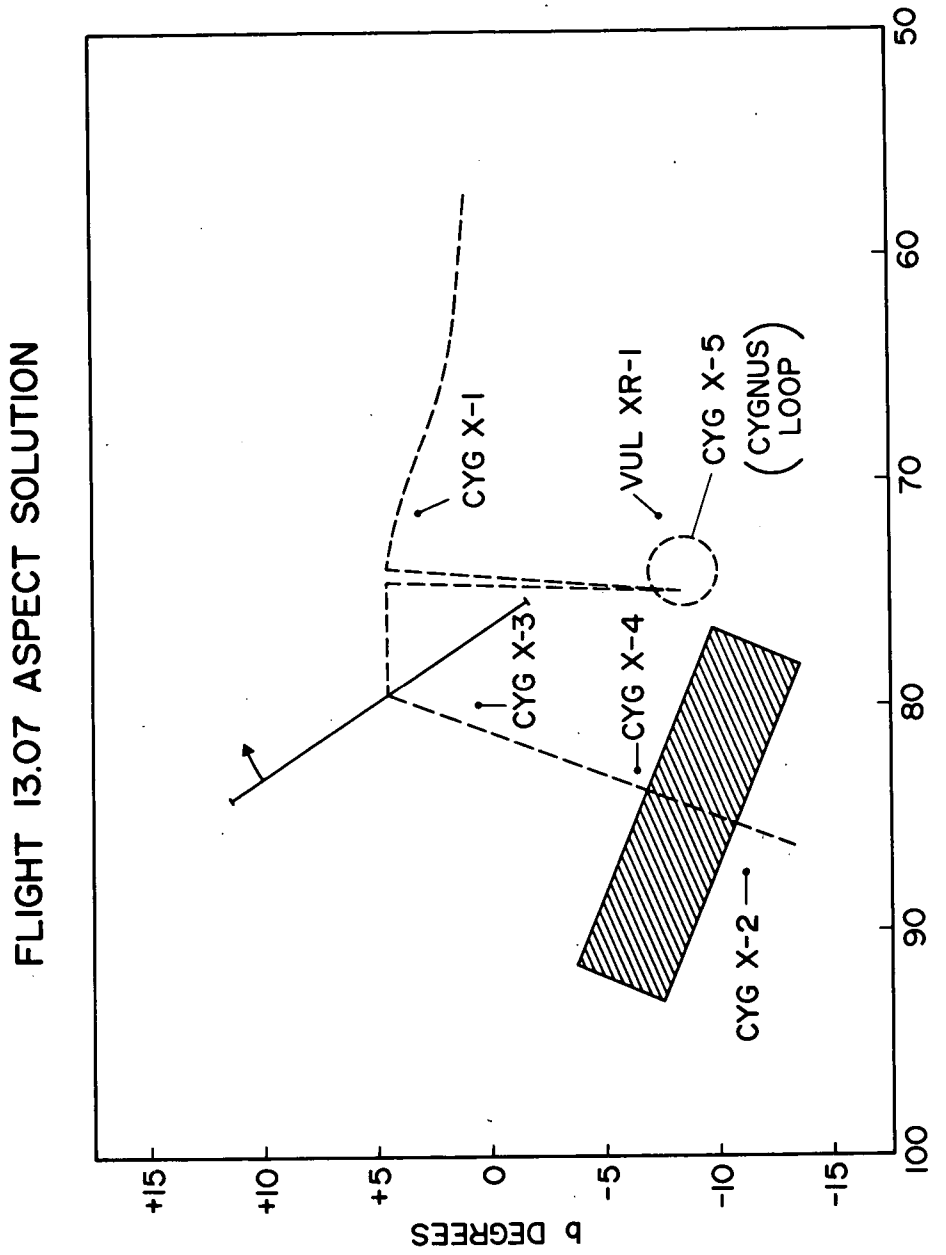

FIGURE 15 - Aspect solution for flight 13.07. Shaded rectangle and solid line represent total collimator response and orientation. Dashed line is the track of the center of the collimators.

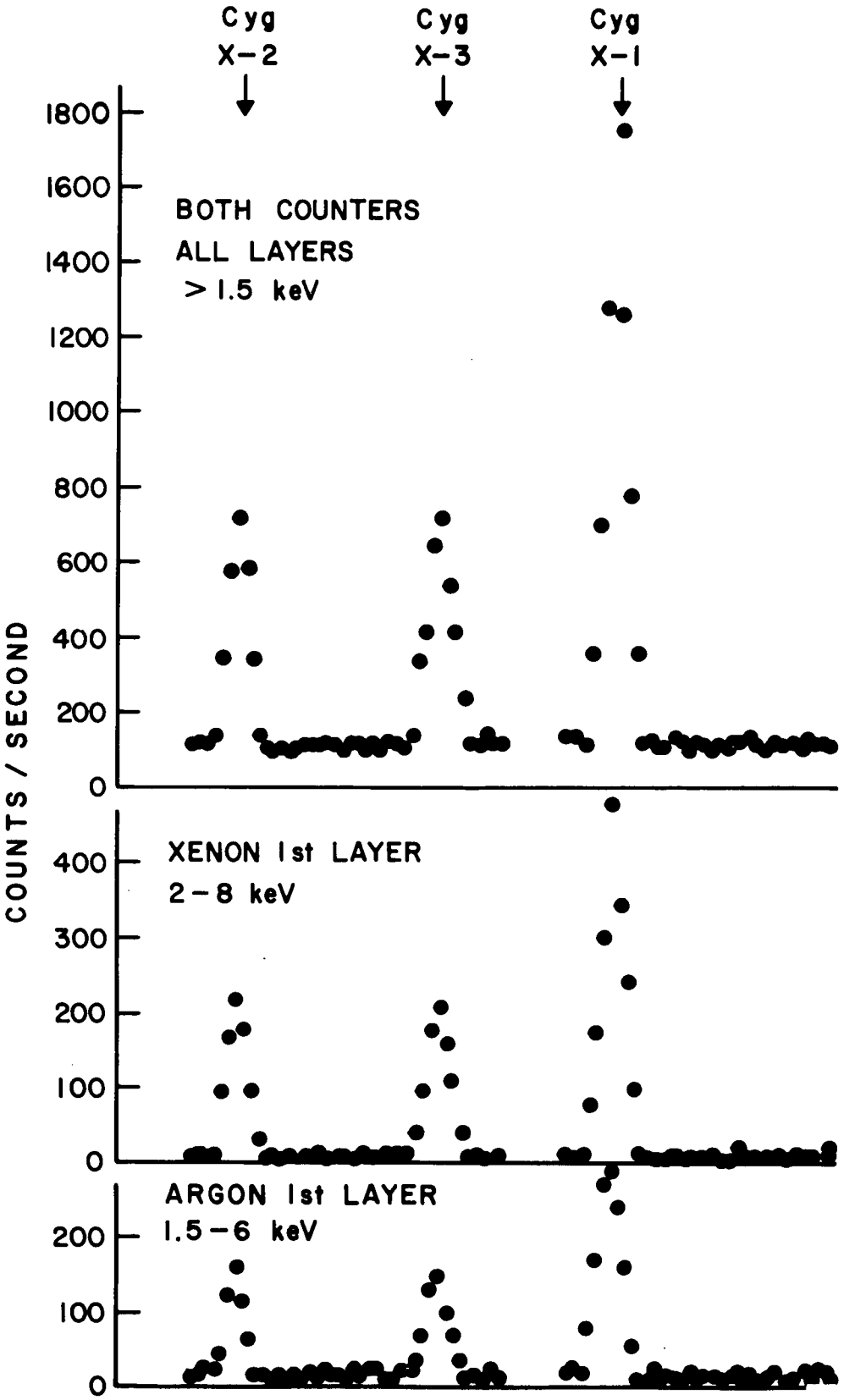

FIGURE 16 - Count rate profiles for flight 13.07
top) both counters, middle) xenon 1st layer,
bottom) argon 1st layer.

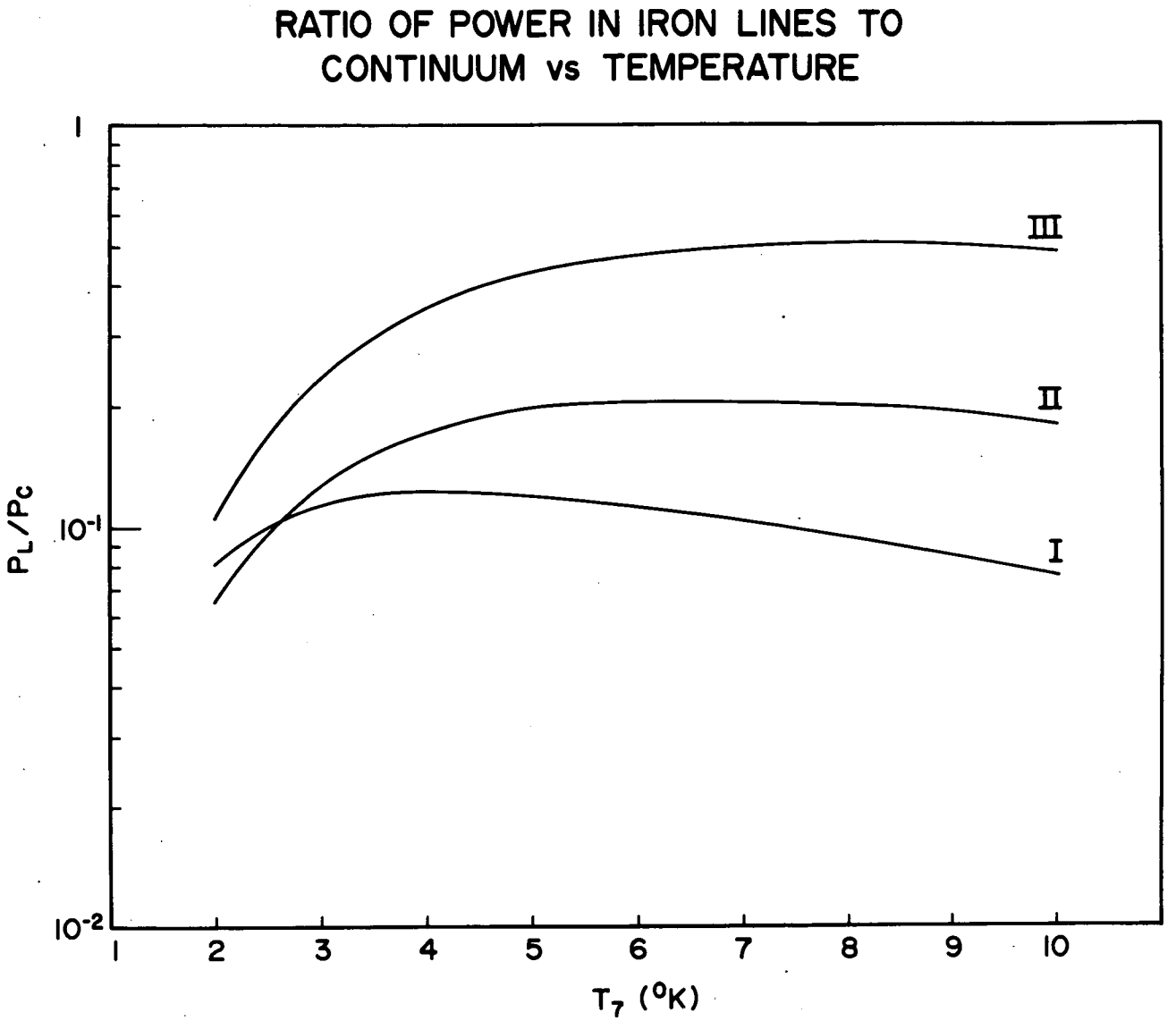

FIGURE 17 - Ratio of power emitted by FeXXV and FeXXVI Kα lines to power emitted in the continuum (bremsstrahlung plus recombination radiation) in a 1 keV bin centered at 7.0 keV as a function of temperature. The trace I represents Brown and Gould (1970) abundances with the addition of iron in an abundance determined by Nussbaumer and Swings (1970). Traces II and III refer to models 2 and 3 of Tucker (1966).

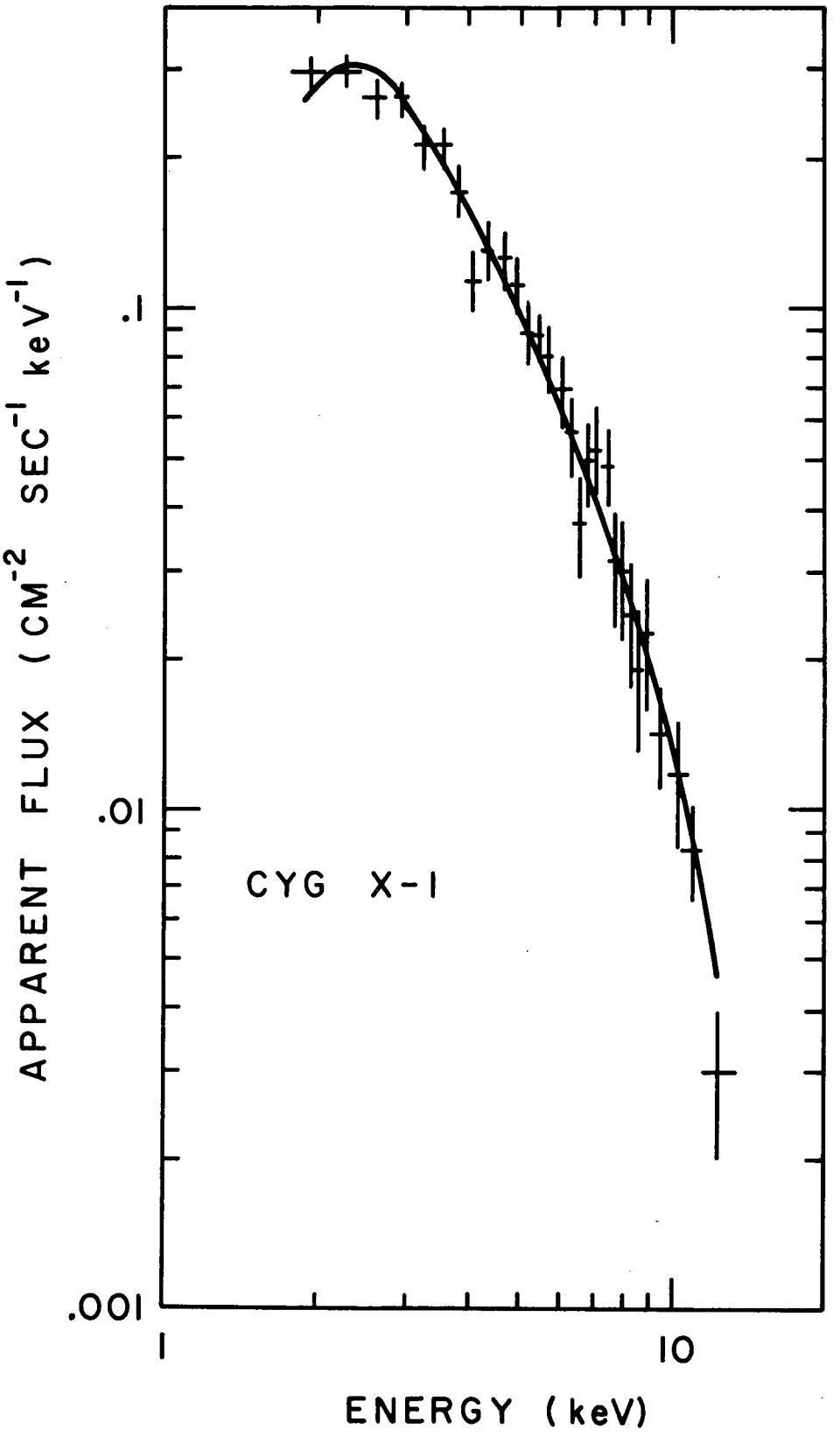

FIGURE 18 - Apparent flux observed from Cygnus X-1. The data points represent the observed count rate divided by the nominal exposure and energy range for the first layer of the xenon filled counter. No efficiency corrections are made to the displayed data. The solid line represents the best-fit spectrum $7.4E^{-2.6}$ photons $(cm^2\text{-sec-keV})^{-1}$ folded through the detector response.

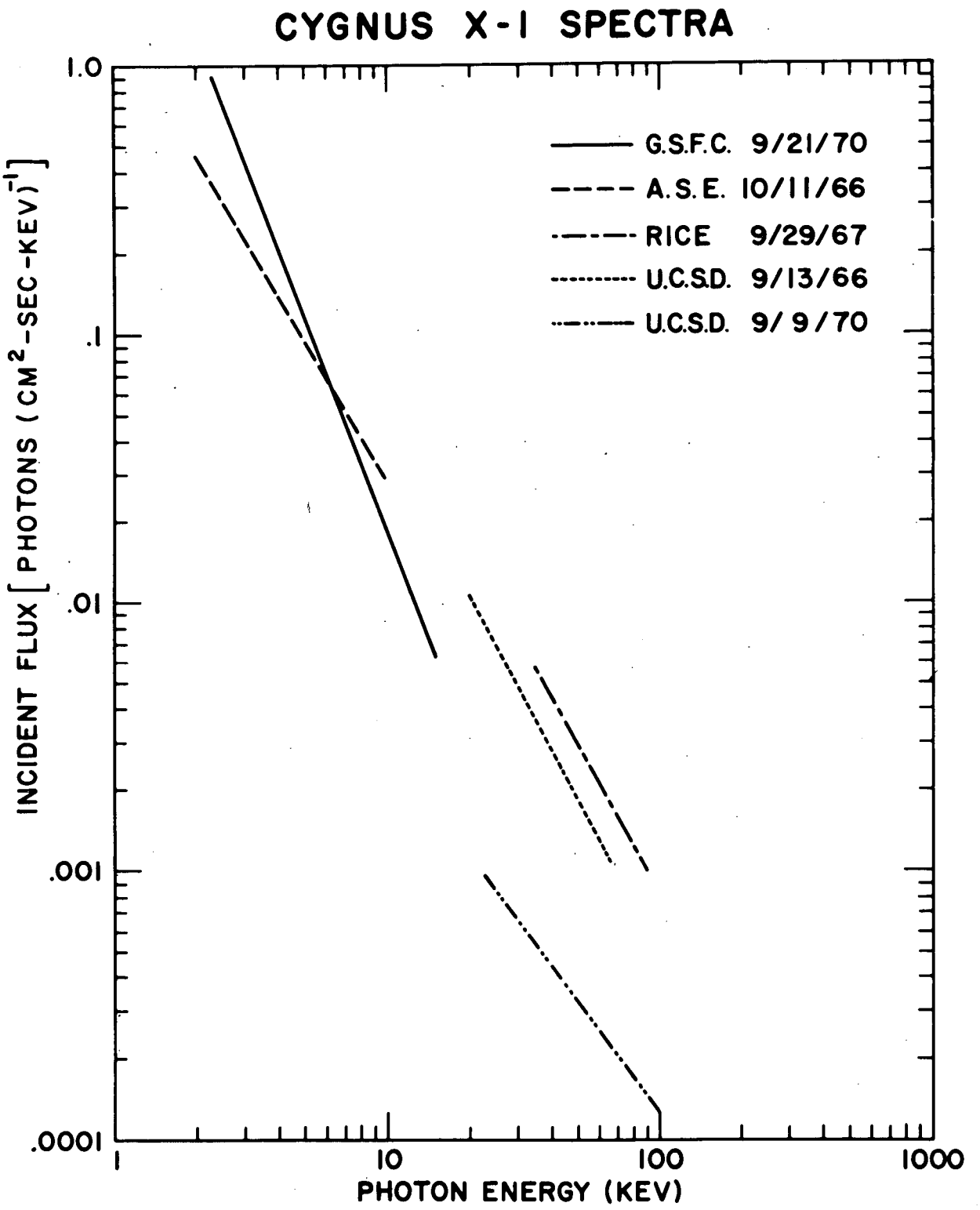

FIGURE 19 - Comparison of spectral measurements of Cygnus X-1. The best-fits are (A.S.E.) 1.50 $E^{-1.7}$, (RICE) 3.42 $E^{-1.8}$, (UCSD, 1966) 3.58 $E^{-1.93}$, (GSFC) 7.4 $E^{-2.6}$, (UCSD, 1970) .125 $E^{-1.5}$.

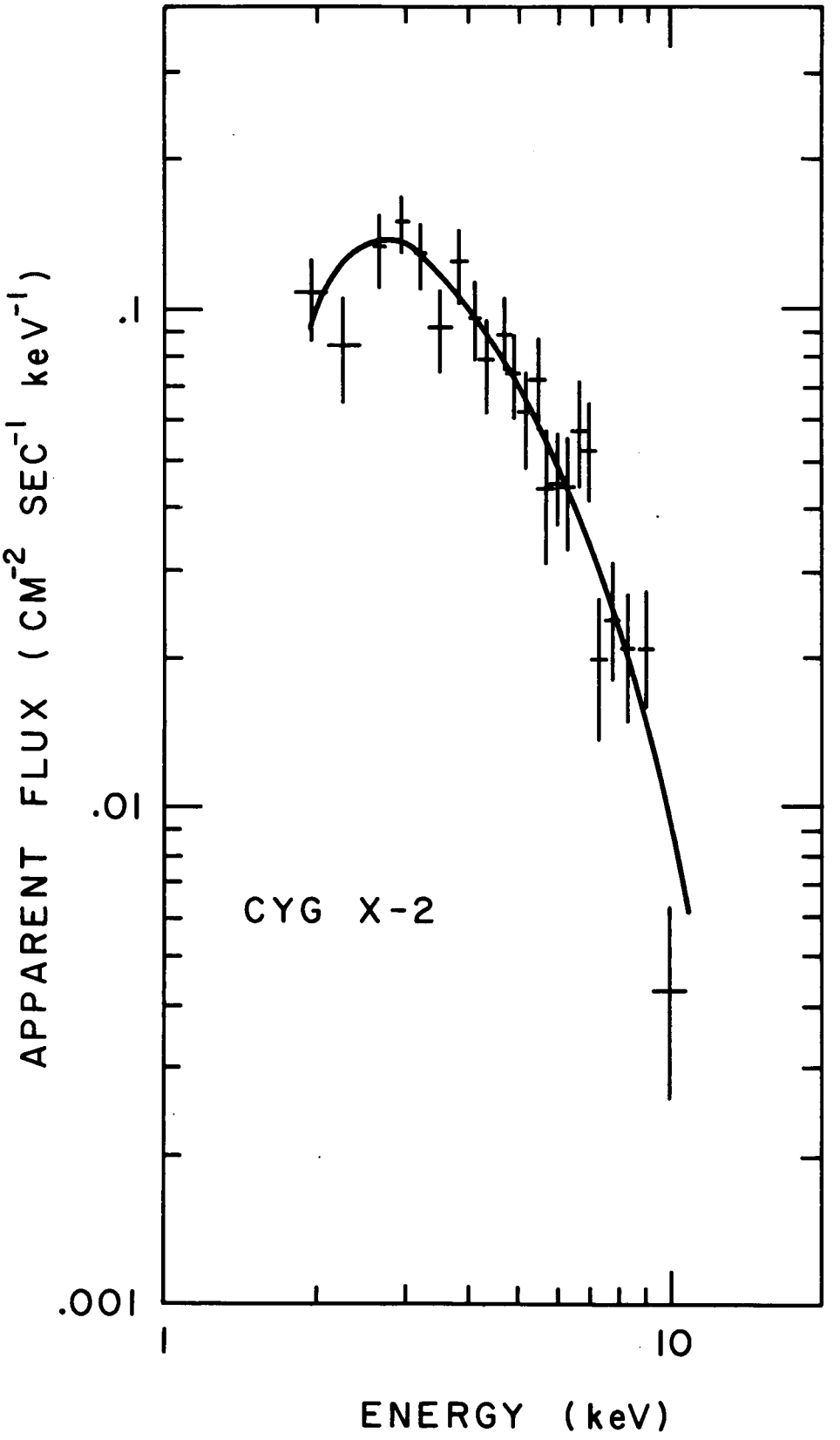

FIGURE 20 - Apparent flux observed from Cygnus X-2 using xenon 1st layer. The solid line represents the best-fit spectrum $\frac{1.4}{E} \exp(-\frac{E}{4.5})$ folded through the detector response.

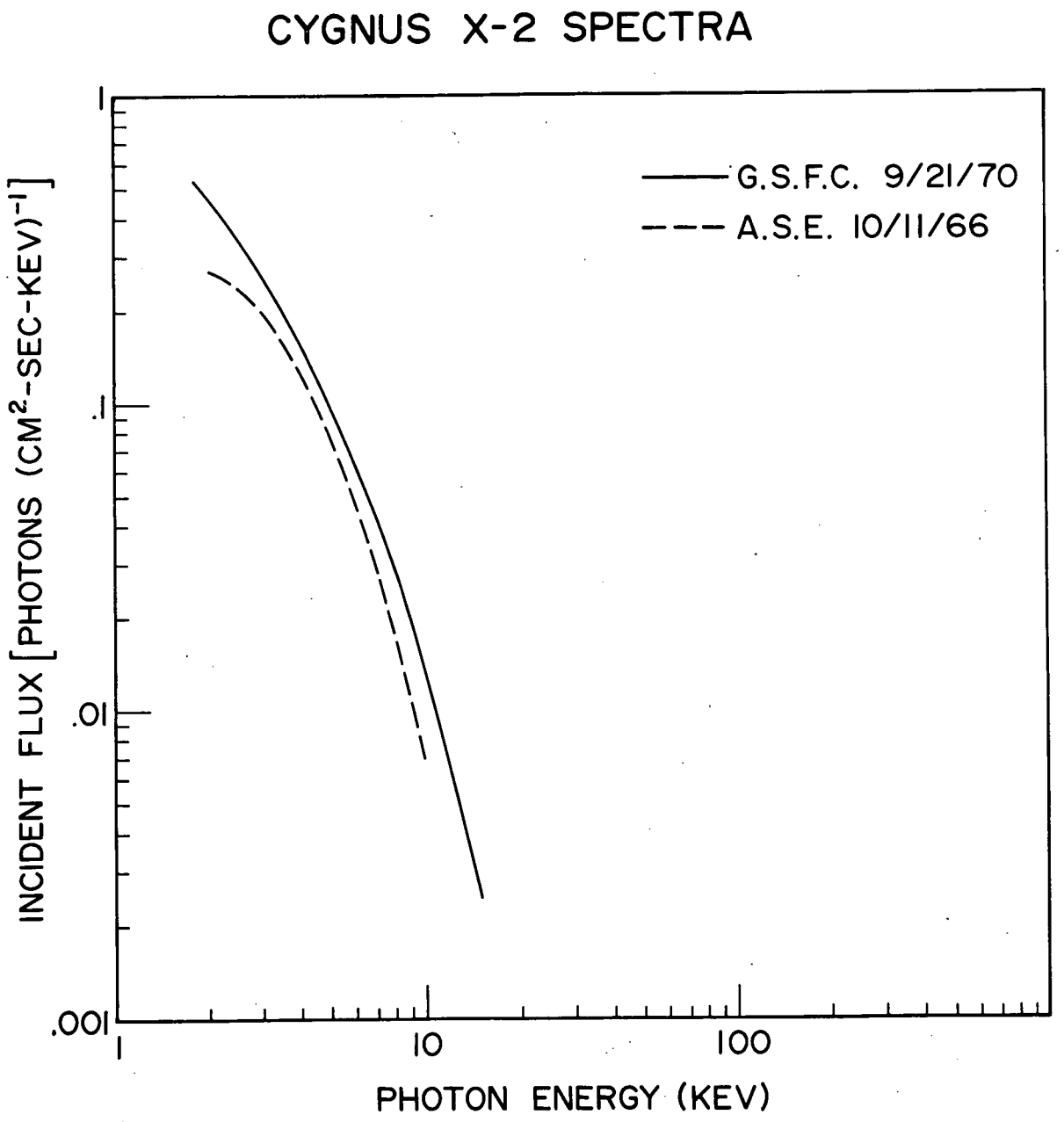

FIGURE 21 - Comparison of spectral measurements of Cygnus X-2. The best fits are:

(A.S.E.) $\frac{1.96}{E} \exp(-(\frac{1.67}{E})^{8/3} - \frac{E}{3.1})$;

(GSFC) $\frac{1.4}{E} (-\frac{E}{4.5})$.

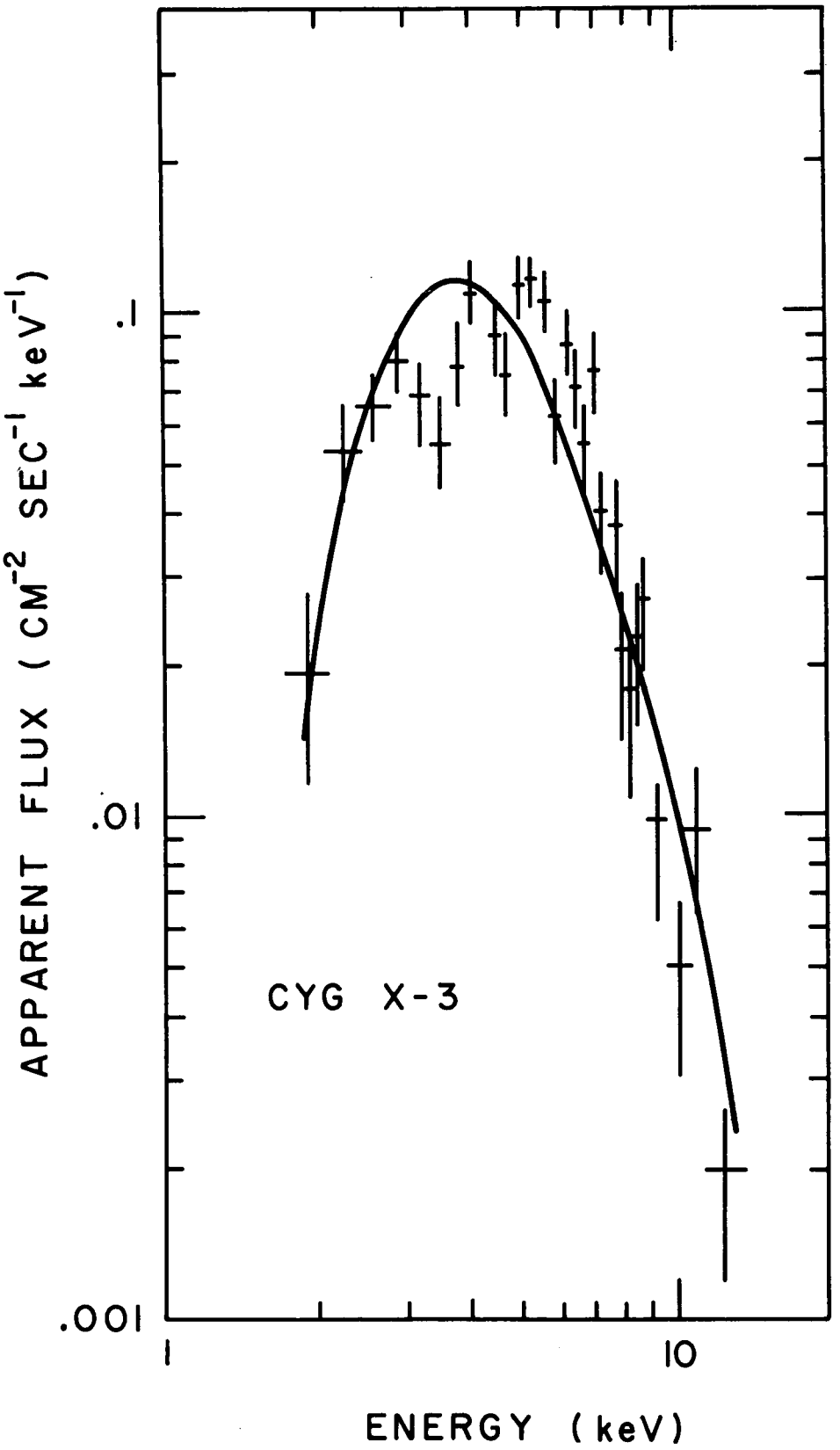

FIGURE 22 - Apparent flux observed from Cygnus X-3. The solid line represents the best-fit spectrum 87 f(E, EO) $E^{-3.9}$ folded through the detector response, where f(E, EO) denotes the Brown and Gould (1970) interstellar opacity at a characteristic energy EO of 4.0 keV. This best-fit was not acceptable at the 90% confidence level.

C.3

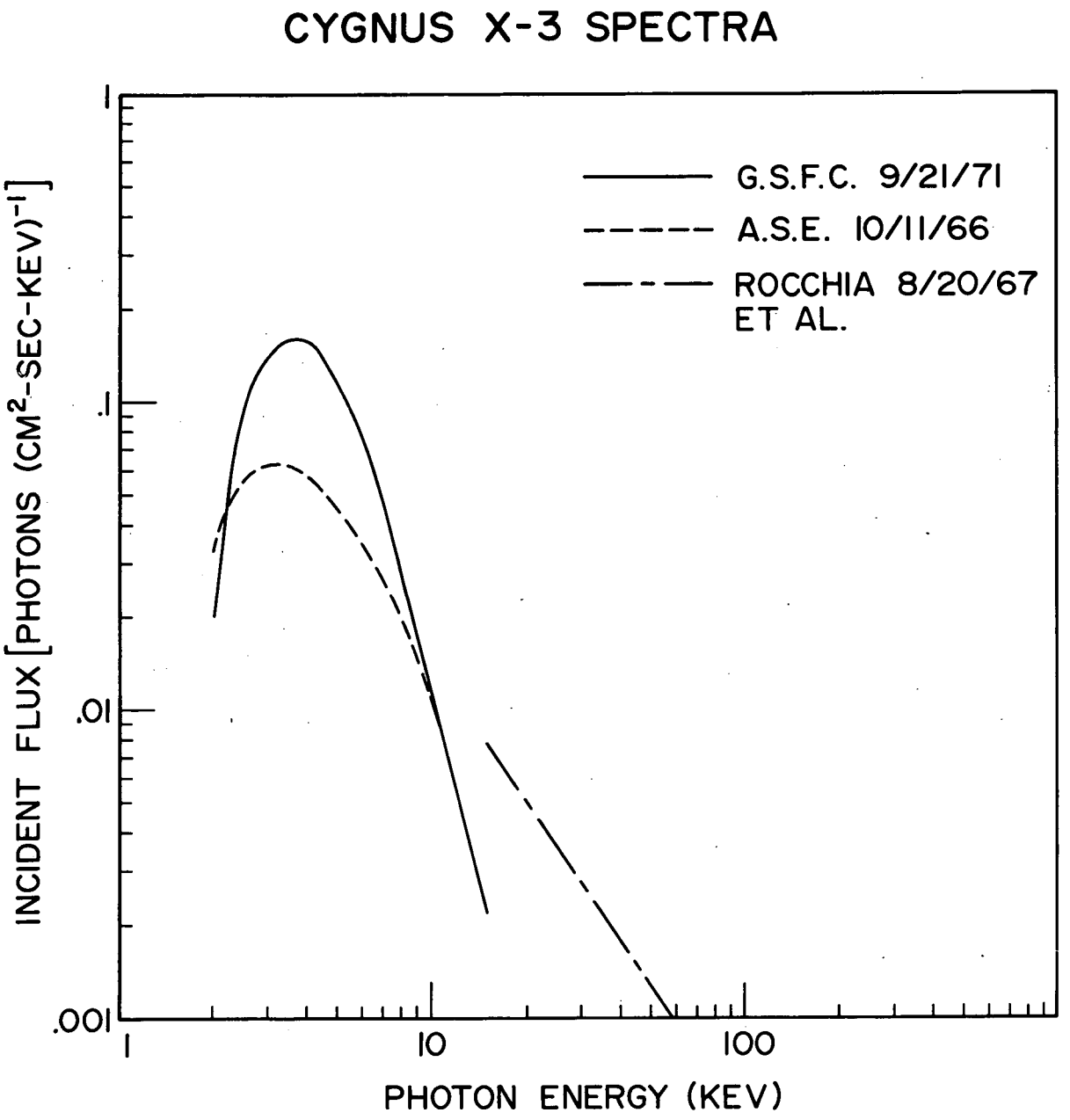

FIGURE 23 - Comparison of spectral measurements of Cygnus X-3. The best-fits are:

(A.S.E.) $\frac{.58}{E}\exp(-(\frac{2.54}{E})^{8/3} - \frac{E}{6.38})$;

(GSFC) 87 $f(E,EO)E^{-3.9}$ (see Figure 22);

(Rocchia et al., 1969) .45 $E^{-1.5}$.

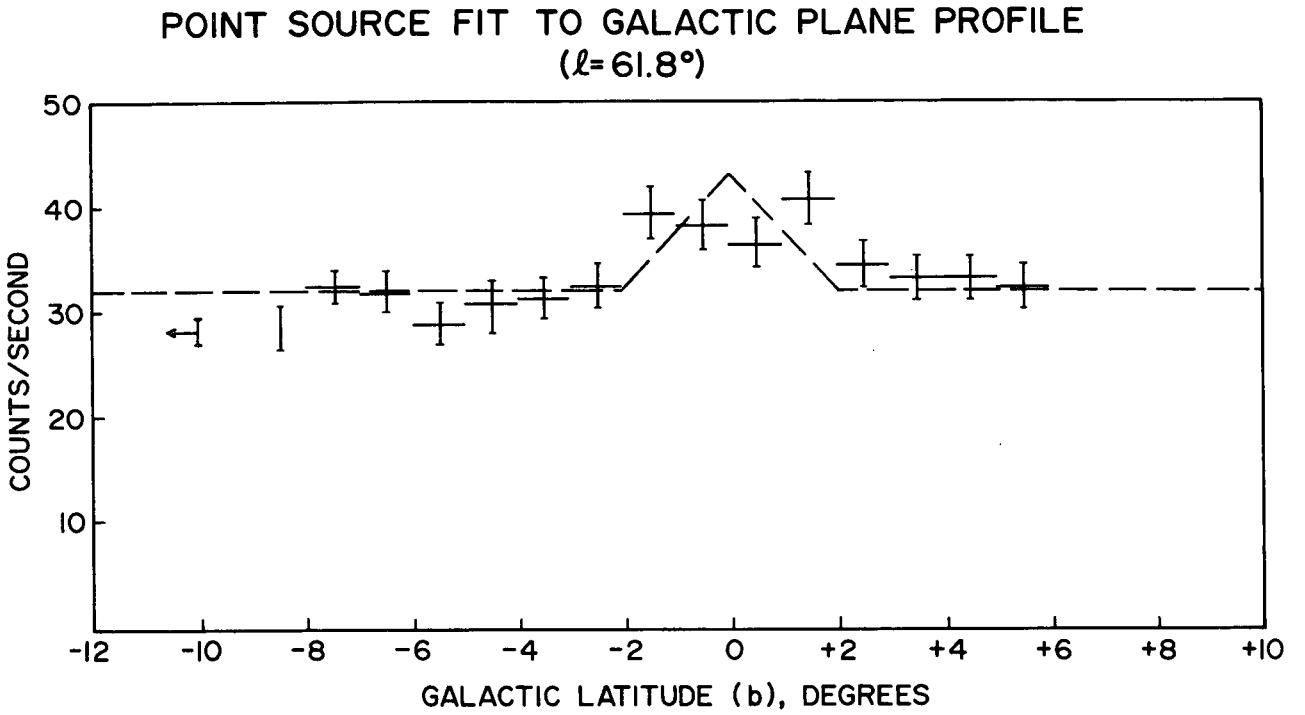

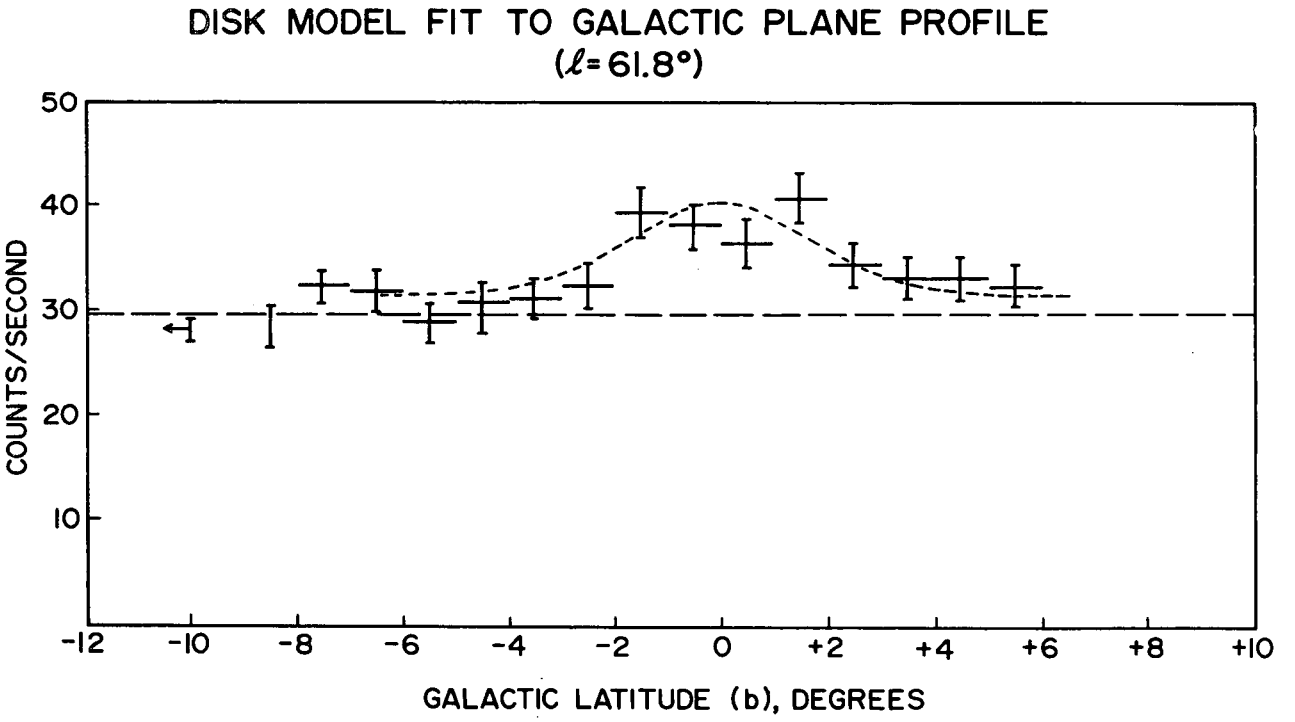

FIGURE 24 - top) Spatial profile of the galactic disk (4 scans summed) plus 2 data points from galactic latitude greater than -8°. These data were obtained from 2-8 keV range in xenon 1st layer, 2-9 keV range in argon 1st layer, and 2-4 keV range in argon 2nd, 3rd, and 4th layers. The dashed line represents the best-fit to point sources at b=0° plus background. This model was not acceptable at a confidence level of 92%. bottom) Spatial profile of galactic disk (same as top) showing best-fit to a disk model plus background.

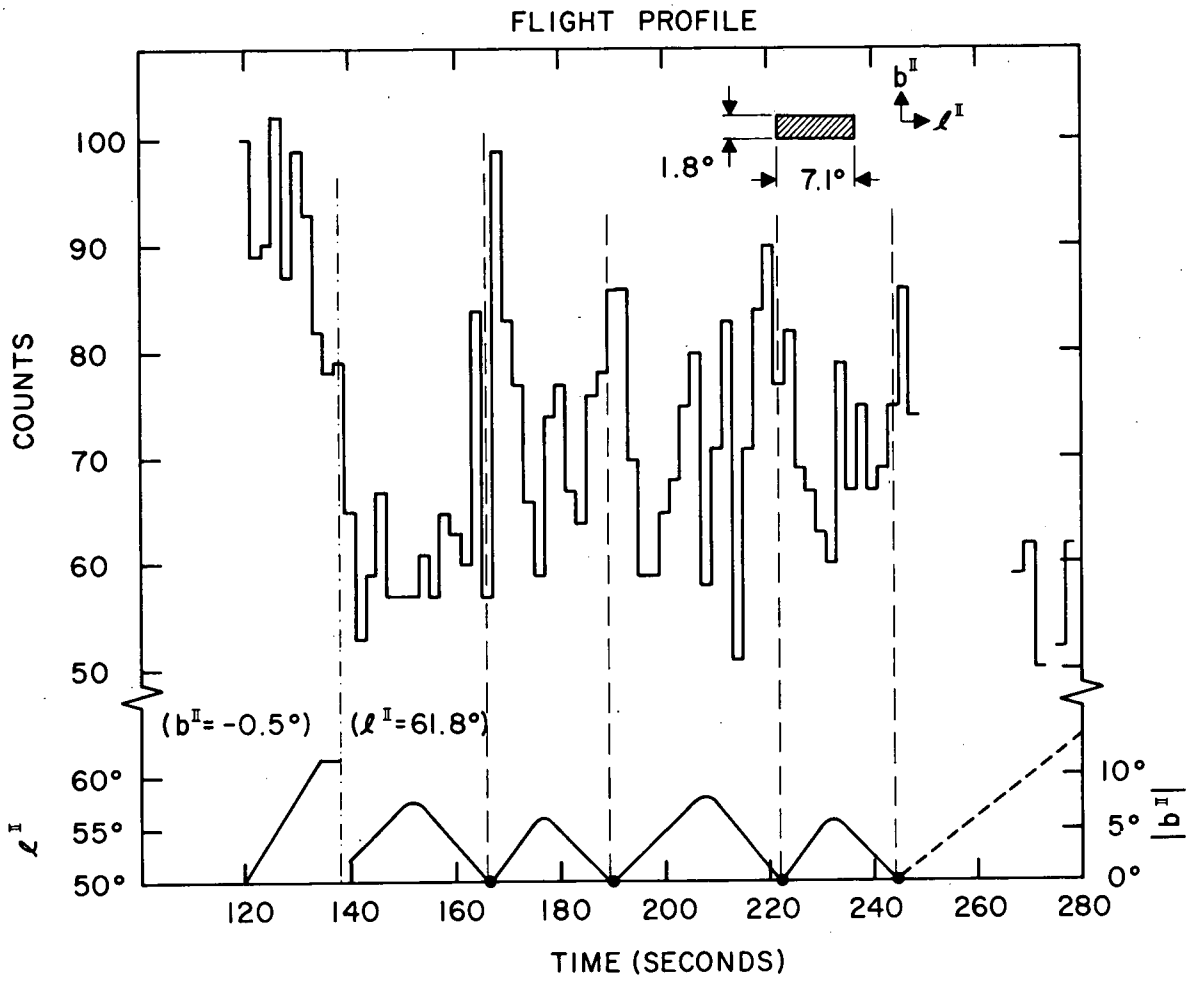

FIGURE 25 - Count rate profile for both counters in flight 13.08. Galactic longitude vs. time is shown (scale on left) up to about 138 seconds after launch and absolute magnitude of galactic latitude is shown (scale on right) for 4 scans of the galactic plane at $\ell = 61.8°$ plus later portions of the flight (dashed line).

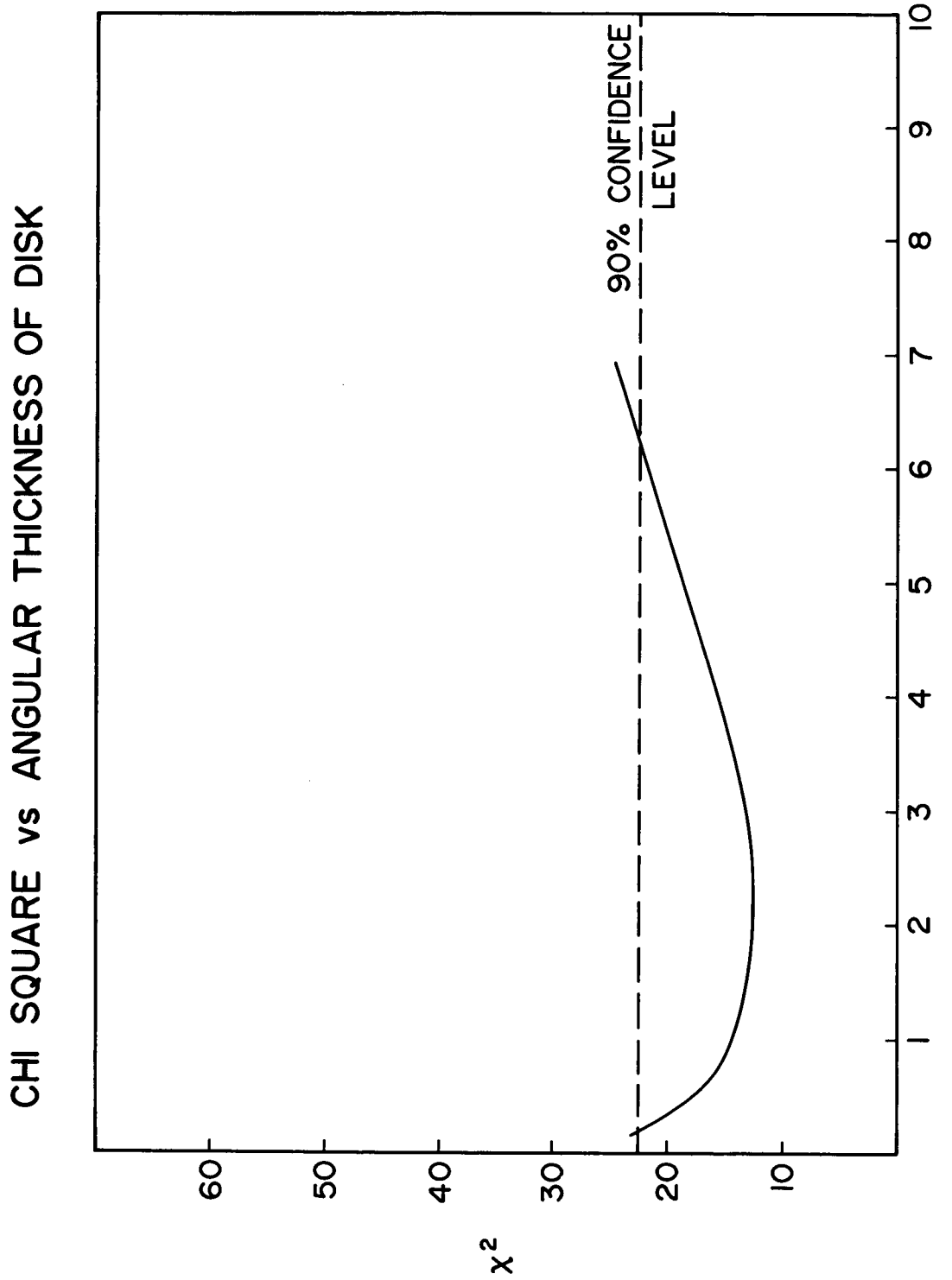

FIGURE 26 - Chi square vs. angular thickness θ_g of disk model. Dashed line represents 90% confidence limit.

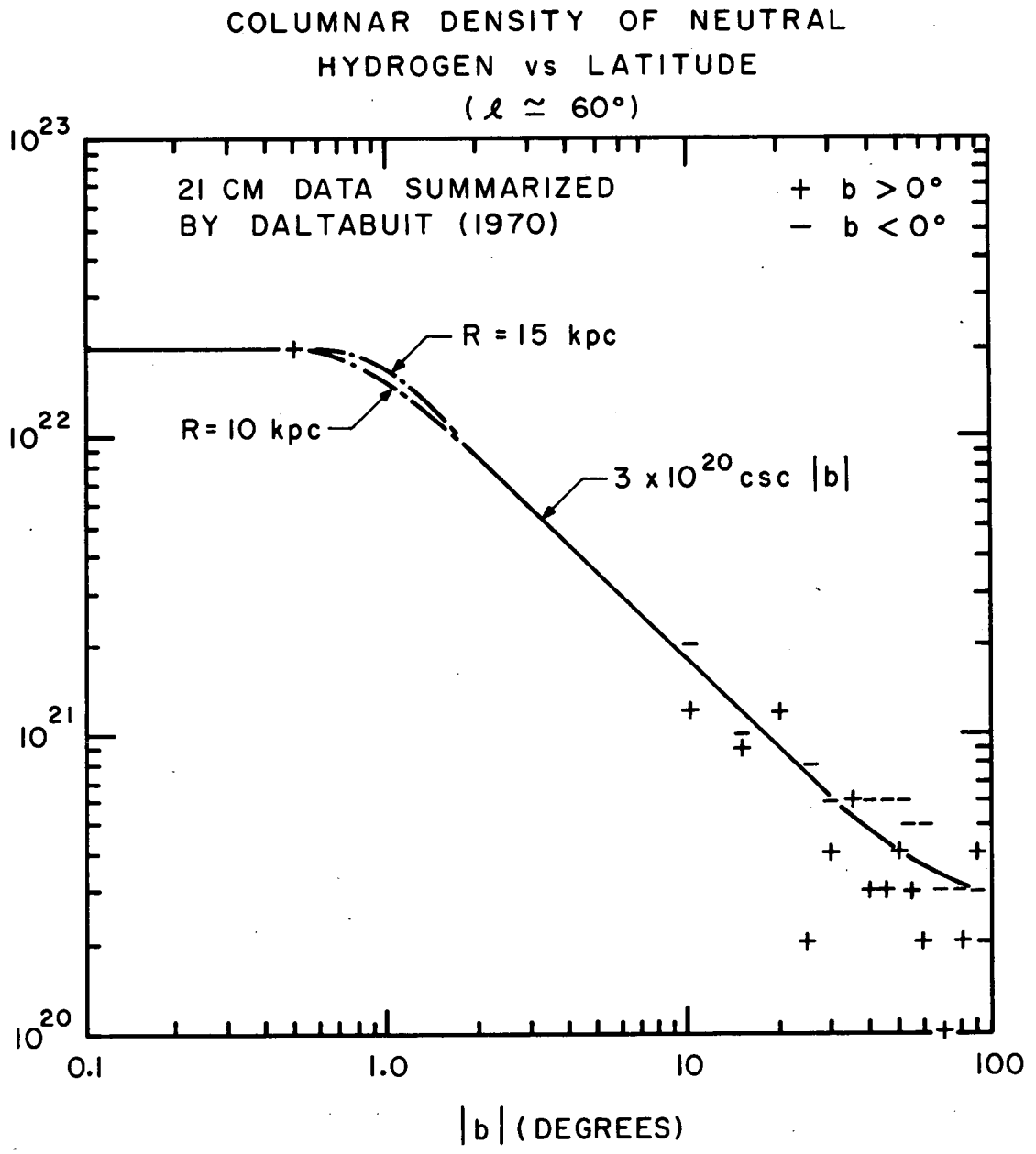

FIGURE 27 - Distribution of neutral hydrogen vs. galactic latitude at galactic longitude 60°. Solid line represents $N_H = I(z)n_o \csc|b|$ where I(z) is taken from Gould (1969), z = R tan b, and n_o = .7 H atoms/cm^3.

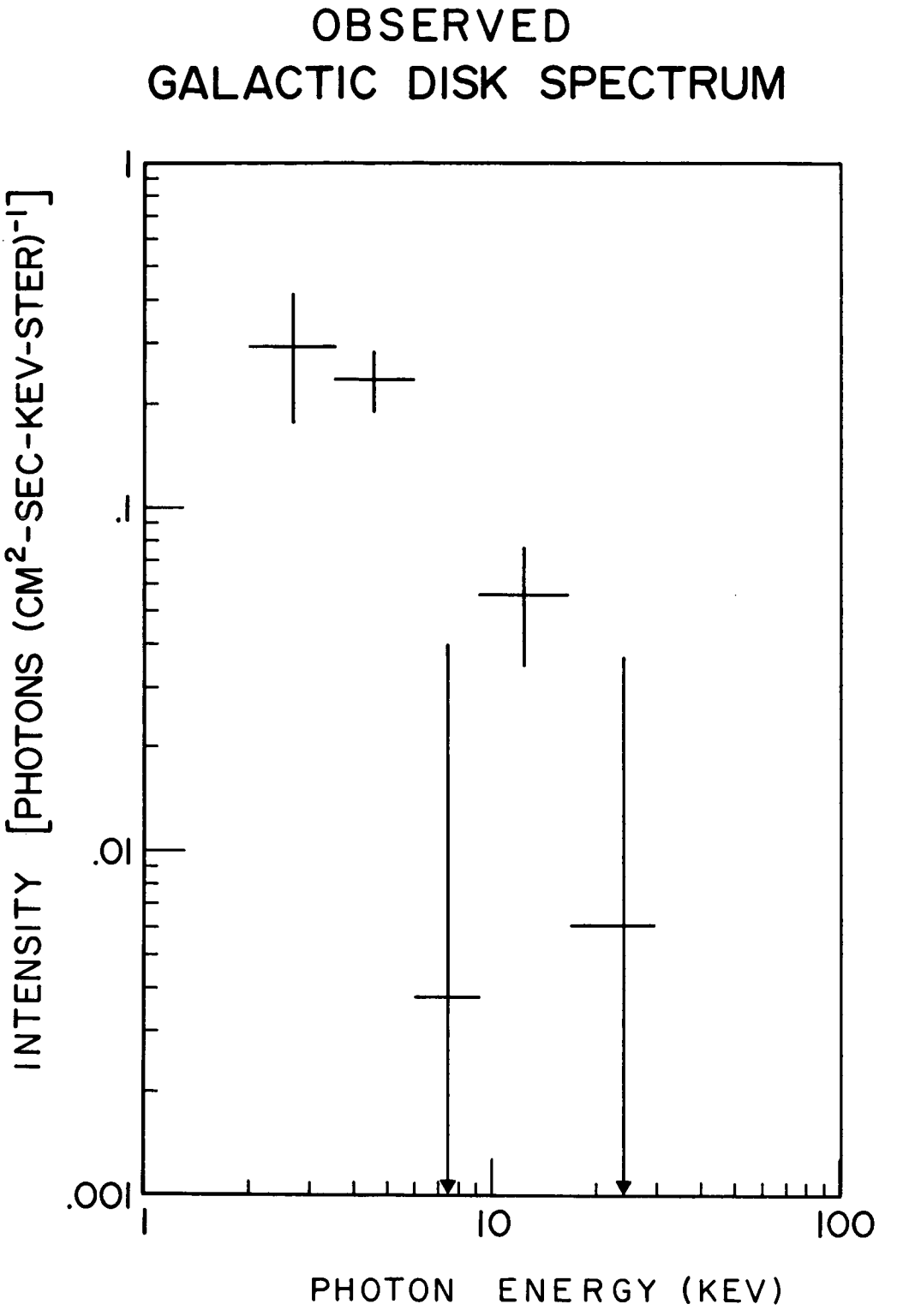

FIGURE 28 - Observed galactic disk spectrum at b=0° corrected for efficiency according to spectral analysis procedure 2.

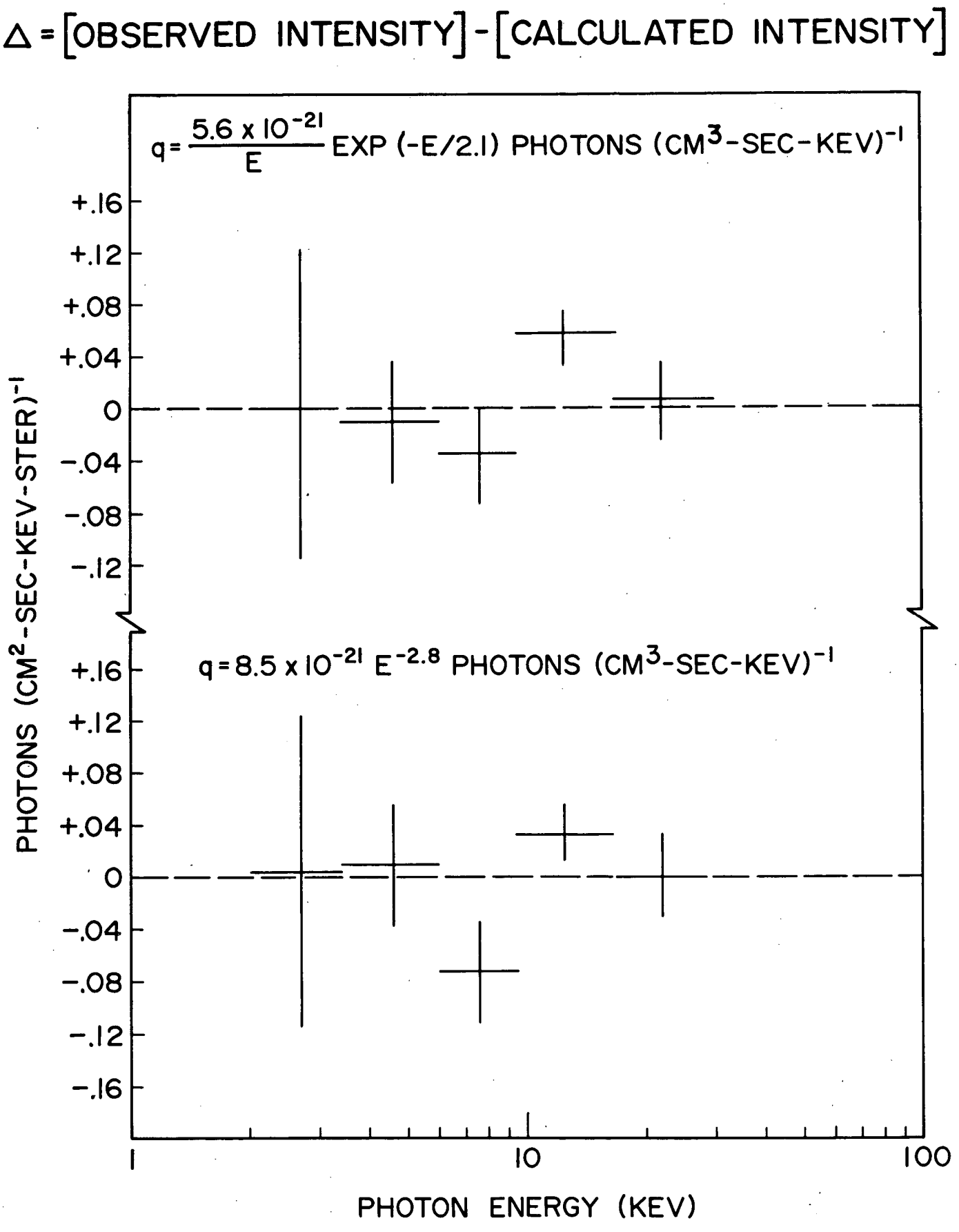

FIGURE 29 - Difference in observed and calculated best-fit source function (q) for exponential and power law models.

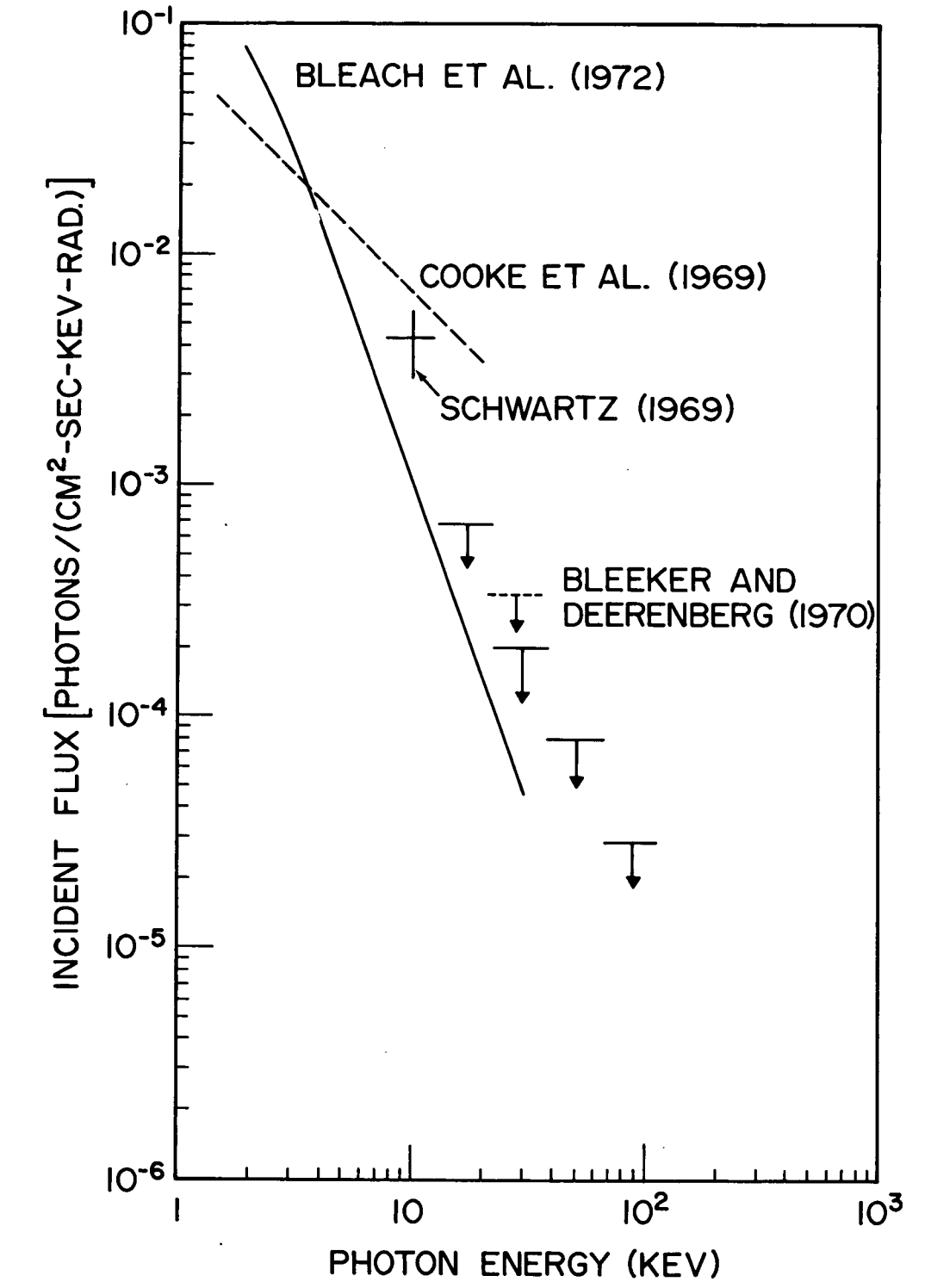

FIGURE 30 - Comparison of spectral measurements of the galactic disk. All results have been renormalized on the basis of a disk with angular thickness 2° by dividing observer's results by the factor $[1+\ell n(\frac{\theta_d}{2^\circ})]$ where θ_d = FWHM response in galactic latitude of observer's detector.

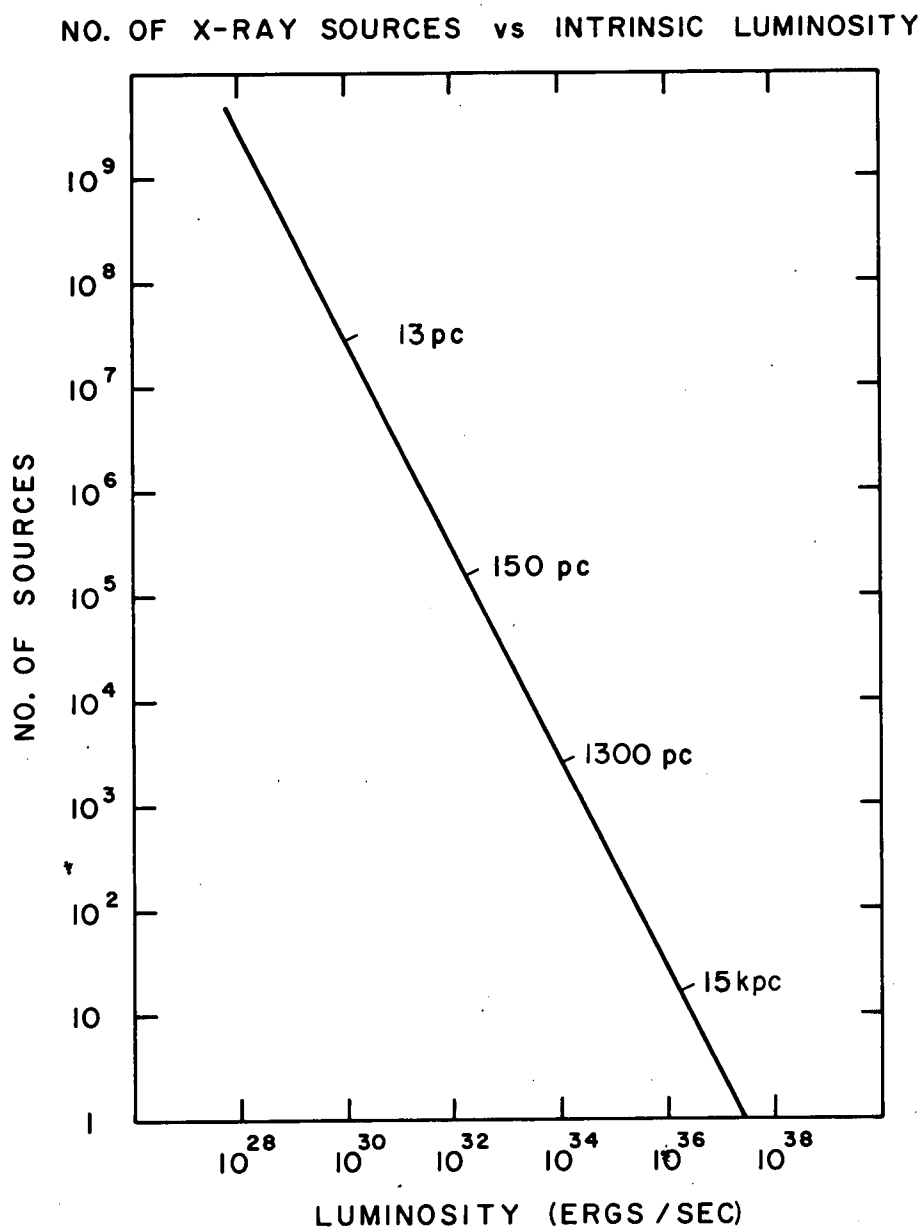

FIGURE 31 - Number of discrete sources in the disk vs. intrinsic luminosity per source based on the integral photon source function $q=7\times10^{-30}$ ergs/cm^3-sec(2-10 keV) and a disk volume of 4×10^{66}cm^3. Reference marks represent the distance to which UHURU can resolve discrete sources of that luminosity assuming a limiting sensitivity of 5×10^{-11}ergs/cm^2-sec.

THIN TARGET BREMSSTRAHLUNG EXPERIMENT

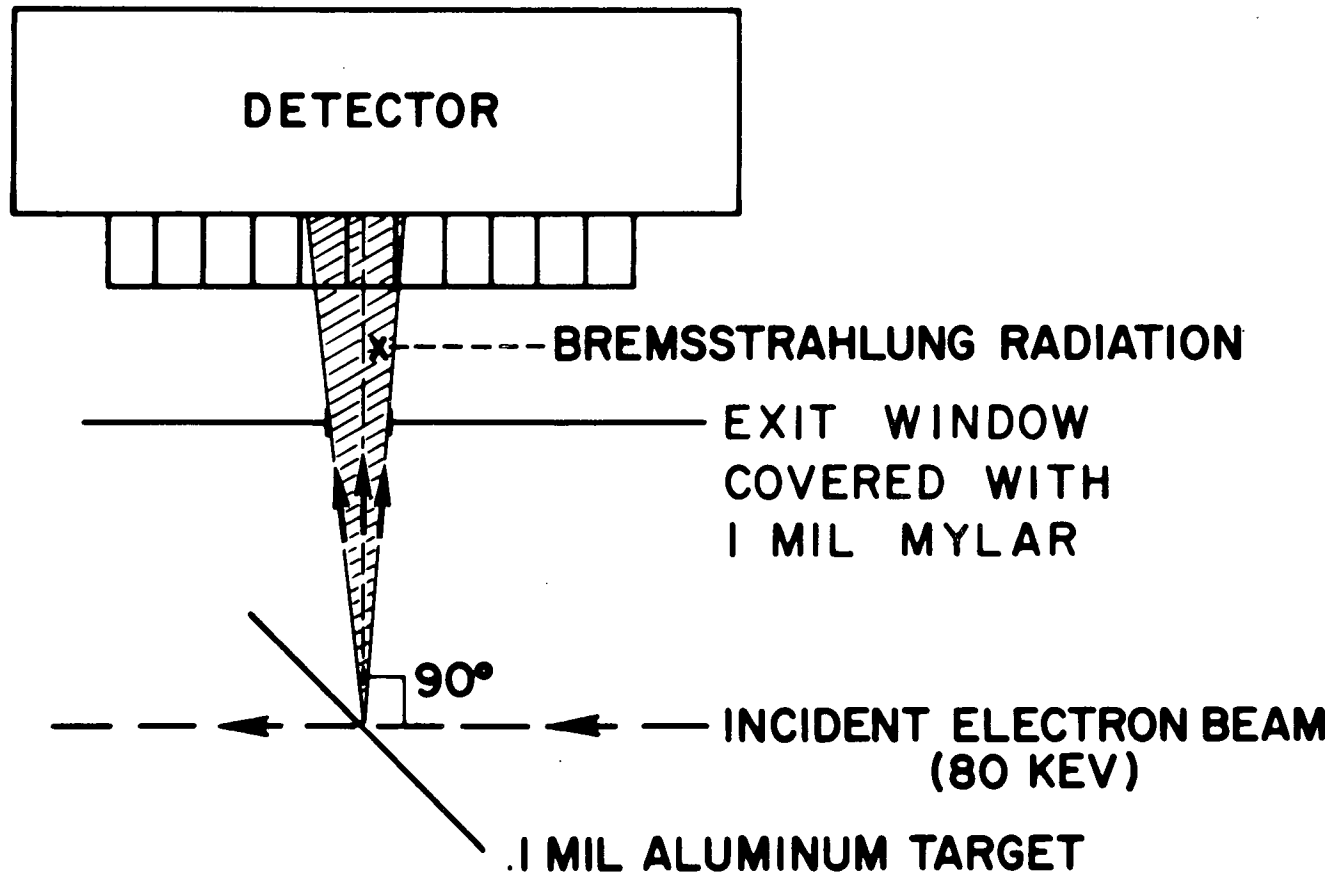

FIGURE 32 - Experimental configuration for producing thin-target bremsstrahlung. The entire system is enclosed in a vacuum.

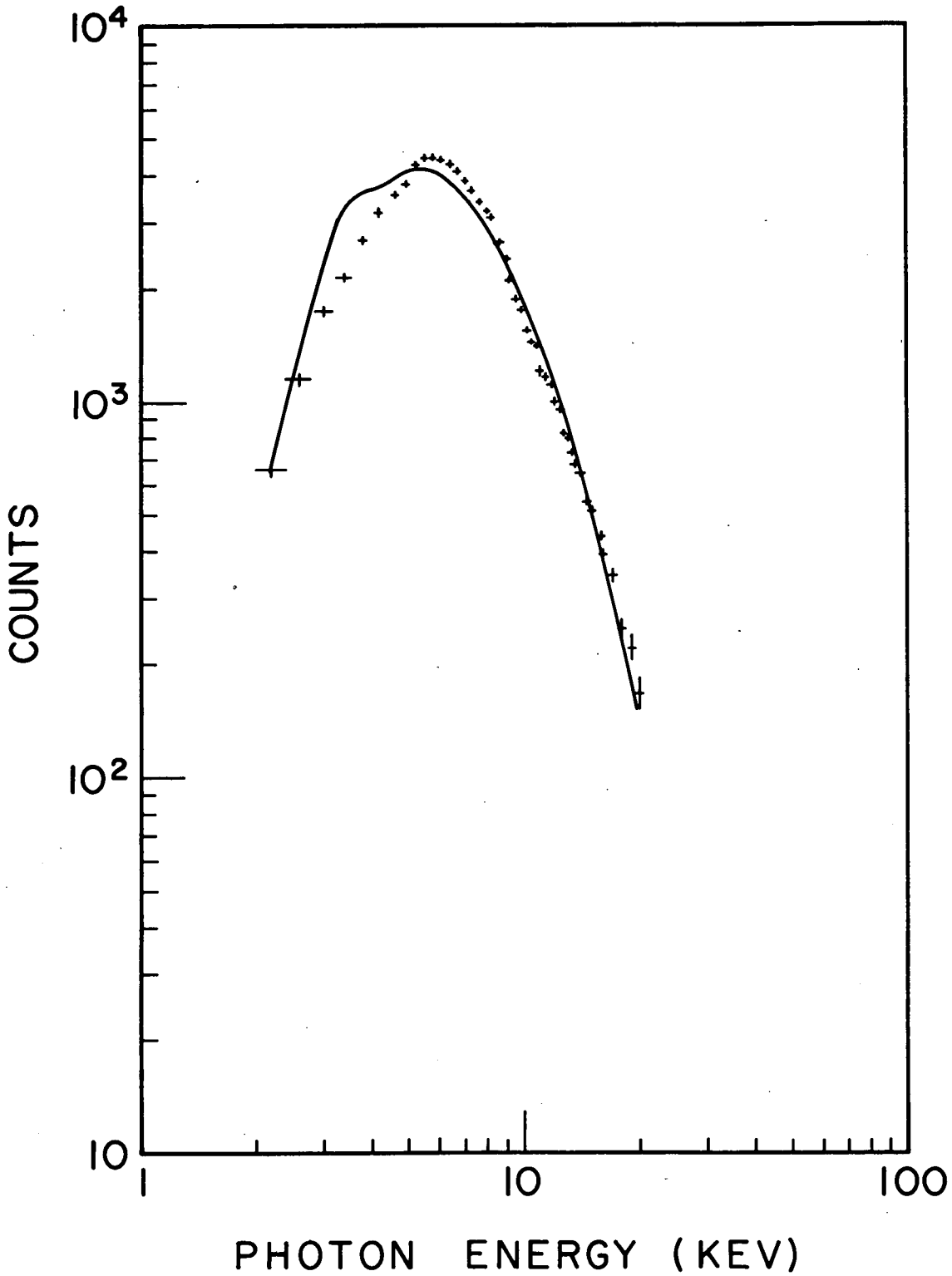

FIGURE 33 - Observed spectrum from .1 mil aluminum thin-target bremsstrahlung using 80 keV electrons. Solid line represents the best-fit Kirkpatrick-Wiedmann (1945) cross section as modified by Motz and Placious (1958) folded through the detector response.